UNIVERSITY OF CALIFORNIA
RIVERSIDE

Investigation of the Composition and Preservation Potential of Precambrian Sedimentary Organic Matter and Lipid Biosignatures

A Dissertation submitted in partial satisfaction
of the requirements for the degree of

Doctor of Philosophy

in

Geological Sciences

by

Kelden Pehr

June 2020

Dissertation Committee:
Dr. Gordon D. Love, Chairperson
Dr. Andrey Bekker
Dr. Marilyn Fogel

The Dissertation of Kelden Pehr is approved:

_____

_____

_____

Committee Chairperson

University of California, Riverside

ACKNOWLEDGMENTS

This research was made possible through funding and support from the NASA Earth and Space Science Fellowship (17-PLANET17R-0019), the Earle C Anthony Award and the UCR Dissertation Year Fellowship.

I am very grateful to my advisor Gordon Love, whose support and guidance has been invaluable over these past years. I would like to thank my qualifying exams and defense committee members as follows: Andrey Bekker for the many opportunities and great conversations; Marilyn Fogel for the encouragement and excellent discussions on all things biogeochemical; Mary Dorser for welcoming me as an honorary member of the Droser lab; and Francesca Hopkins for asking the big questions.

Rose Bisquera, Carina Lee, Alex Zumberge, JP Duda, Adam Hoffman, Nathan Marshall, and Adriana Rizzo were all wonderful lab mentors and mates. Steven Bates and Laurie Graham provided much needed support in the dark hours of instrument failure. Aaron Martinez deserves a special shout out for the awesome adventures, fantastic food, and long hours of laughter.

I have had the pleasure to work with an amazing cast of collaborators, without whom, this research presented here would not have been possible. Anton Kuznetsov, Victor Podkovyrov, Leonid Shumlyanskyy, Tetyana Sokur, Andrew Bishop, Frantz Ossa Ossa, and William Meredith provided samples. Christopher K. Junium, Allison A Baczynski,

and Kate Freeman conducted the isotope analysis and Simon Poulton performed the iron speciation analysis. The text of this dissertation is in part a reprint of the material as it appears in Pehr, K., Love, G.D., Kuznetsov, A., Podkovyrov, V., Junium, C. K., Shumlyanskyy, L., Sokur, T., Bekker, A. 2018.. Ediacara biota flourished in oligotrophic and bacterially dominated marine environments across Baltica. *Nature Communications*, 9, 1807. The coauthor Gordon. D. Love listed in that publication directed and supervised the research which forms the basis for this dissertation.

And last but not least, my family, who have always believed in me.

Mom, Dad, and Nick

<3

ABSTRACT OF THE DISSERTATION

Investigation of the Composition and Preservation Potential of Precambrian Sedimentary Organic Matter and Lipid Biosignatures

by

Kelden Pehr

Doctor of Philosophy, Graduate Program in Geological Sciences
University of California, Riverside, June 2020
Dr. Gordon D. Love, Chairperson

The preservation of organic matter in the sedimentary rock record is strongly controlled by thermal maturity. This poses a problem when investigating Precambrian or extraterrestrial samples as they are typically heavily altered. In order to preform detailed biomarker analysis on very ancient samples, one must either scour for unusually well preserved specimens or develop new organic matter parameters suitable at high thermal maturities. Presented here are two such studies, the first is a detailed investigation of exceptionally preserved Ediacaran rocks while the second is a broad study of preservation of polycyclic aromatic compounds (PAH) bound in kerogen.

In the first study I perform a lipid biomarker, stable isotope ($\delta^{15}N_{total}$ and $\delta^{13}C_{TOC}$) and compound specific $\delta^{13}C$ investigation of exceptionally immature late Ediacaran strata from across Baltica. The biomarker assemblages encompass an exceptionally wide range of high hopane/sterane ratios (1.6–119), which is a broad measure of bacterial/eukaryotic source organism inputs. A high contribution of bacteria to the overall low productivity was most likely the result of persistent oligotrophic conditions. Total organic carbon (C_{TOC}) isotope values range from –23.0‰ to –33.9‰, with the largest differences observed between the different drill-core locations. Pico-CSIA suggests the cause of these site-varying $\delta^{13}C_{TOC}$ was regional environmental heterogeneity and a microbial populations shift between the Redkino and Kotlin horizons.

In the second study I report the distribution of bound PAHs in biogenic kerogens and in a selection of insoluble organic matter (IOM) from carbonaceous residues. The degree of thermal maturity of the sedimentary organic matter exerts the primary control on the preservation and distributions of the major 5-ring and 6-ring PAH compounds generated by catalytic hydropyrolysis (HyPy) from kerogens. All ancient biogenic kerogens analyzed contain detectable amounts of perylene, even for the most thermally transformed samples. A suite of PAH abundance ratios were identified which succeeded in separating biogenic kerogens (including highly overmature samples) versus abiogenic IOM formed from high temperature thermal cracking reactions. While not a definitive biosignature, the ability to recognize aromatics formed from low-temperature processing

of organic material will aid in the search for past and extant life on extraterrestrial bodies such as Mars.

TABLE OF CONTENTS

Chapter Four: What can the Last Remaining Organic Molecules Tell Us? Investigating the Preservation of Covalently Bound Polyaromatic Hydrocarbons in Ancient Biogenic Kerogens and Insoluble Organic Macromolecules (IOM)

LIST OF FIGURES

LIST OF TABLES

CHAPTER ONE

Introduction

1.1. Organic molecules as biosignatures

Hydrocarbons derived from biochemicals or produced by abiotic means can be preserved within the rock record for billions of years, providing clues to Earth's past. Lipid biomarkers are fossil biolipids detected in the geological record whose basic skeletal features have been sufficiently preserved to allow unambiguous links to known, contemporary natural product precursors (Peters et al., 2005). Biomarker molecules that are both thermodynamically-stable and have only a limited number of well-defined biological sources provide the specific information about their source organism across a large range of samples. For example, polycyclic terpenoids, such as hopanoids and steroids, meet both of these requirements. They are extremely resistant to degradation, surviving hundreds of millions of years or more in sedimentary rocks and petroleum products (Brocks et al., 2005; Brocks and Schaeffer, 2008).

Steranes are tetracyclic triterpenes derived from sterol precursors, which are produced by eukaryotes (Moldowan et al., 1990; Brocks et al., 1999; Kodner et al., 2008). Hopanes are pentacyclic triterpenes derived from hopanoids, which are cell membrane lipids synthesized by a wide variety of bacterial groups (Rohmer et al., 1984; Pearson et al., 2007). Select hopane and sterane compounds are derived from precurors produced by only select organisms such as C_{29} steranes that represent contributions by green algae and

higher plants (Kodner et al., 2008). Additional lipid biomarkers used throughout this thesis include include straight and branched alkanes, acyclic isoprenoids such as pristane and phytane, and aryl isoprenoids.

1.2. Temperature controls on organic matter preservation

Thermal maturity is the single most important factor influencing the preservation of ancient sedimentary biomarkers as organic molecules are susceptible to structural and stereochemical alteration during progressive burial and with increasing thermal stress (Peters et al., 2005; Tissot and Welte, 1984). The level of thermal maturity of sedimentary organic matter is primarily controlled by both the peak and duration of temperature experienced through the burial history of the host strata (Killops and Killops, 2005). Sedimentarry organic matter is divided into three phases based on the thermal maturity: diagenesis, catagenesis, and metagenesis (Tissot and Welte, 1984).

During the first stage, diagenesis, which begins during deposition, samples have only undergone low temperature alteration and have usually not experienced maximum burial temperatures in excess of 50°C. These samples are defined as immature with respect to the oil window and can preserve a wide range of compounds. Microbial activity and degradation can significantly transform organic matter at this stage.

Samples within the second stage, catagenesis, have undergone some degree of covalent bond cleavage of the sedimentary organic matter, resulting in the structural modification

of organic compounds and macromolecules and generation of fragments. These samples are defined as mature with respect to the oil window and typically correspond to burial temperatures of 50°C to 150°C; however, these boundaries are gradual and are not strictly fixed at these exact values (Killops and Killops, 2005; Tissot and Welte, 1984).

The last stage, metagenesis, corresponds to early metamorphism in rocks. These samples have been heated to much higher sedimentary temperatures (typically >150°) over protracted geologic time such that the main residual organic component is aromatic-rich kerogen. A significant proportion of the original sedimentary organic matter has been lost as hydrocarbon fragments (i.e., as oil and then gas) generated by thermal cracking.

1.3. Types of preserved organic matter

The total organic content (TOC) of a sediment, rock, or meteorite sample consists of organic molecules preserved in two different arrangements: bound and unbound. In the unbound state, called ‘bitumen’ or ‘free organic matter’, the molecules are freely existing as individuals independent of each other. In the bound state, the molecules bind together to form a complex macromolecular insoluble organic matter known as ‘kerogen’ or ‘insoluble organic matter’ (IOM). Polycyclic organics can become covalently linked to form kerogen within tens to hundreds of years (Huc and Durand, 1977; Burdige, 2007; Lee et al., 2019). The term IOM will be used in this thesis when referring to insoluble organic matter from extraterrestrial samples and carbonaceous residues produced by hydrocarbon cracking, whereas the term kerogen will be used for all other terrestrial

samples. Their general structure is similar in terms of complexity, however, and the terms have been used interchangeably throughout past literature. Due to the difficulties of extracting insoluble organic matter, the majority of organic carbon studies are limited to studying bitumen, even though kerogen and IOM account for the vast majority of TOC retained in sedimentary rocks on Earth as well as in meteorites (Smith and Kaplan. 1970; Tissot and Welte, 1984; Killops and Killops, 2005; Alexander et al., 2017). In addition, organic molecules bound within insoluble organic matter experience less alteration than bitumen at equal temperature and pressures (Love et al., 1995; Peters et al., 2005).

1.4. Stable carbon isotopes

Biological and physical processes discriminate in favor of either 'light carbon' ^{12}C which accounts for 98.93% of all carbon or ^{13}C (1.07% abundance) (Hoefs, 2018). The ratio of these two isotopes is commonly expressed in delta notation as follow:

$$\delta^{13}C = \left(\left(\frac{^{13}C\text{sample}/^{12}C\text{sample}}{^{13}C\text{standard}/^{12}C\text{standard}} \right) - 1 \right) \times 1000 \qquad \textit{(Equation 1)}$$

Bulk organic carbon isotope ($\delta^{13}C_{TOC}$) ratios of ancient sedimentary rocks reflect the balance of the many isotopic fractionations resulting from the biological and physical transformations of organic matter. While broad changes in $\delta^{13}C_{TOC}$ over geological time represent global perturbations to the carbon cycle, including changes to total organic carbon burial and pCO_2, regional ecological and environmental changes are important determinants of isotopic and chemical composition. Compound-specific carbon isotopic analysis (CSIA) can help disentangle this complex web of sources and effects on $\delta^{13}C_{TOC}$

by restricting taxonomic influences on $\delta^{13}C_{TOC}$ and revealing changes in the carbon sources of the organisms.

1.4. Overview of thesis

This thesis is split into two separate foci. Chapters 2 and 3 focus on a select time period at the end of the Precambrian, known as the Ediacaran. The Ediacaran Period (~635 - 541 ± 1.0 Ma) was part of an era of extreme tectonic, geochemical and evolutionary changes, which fundamentally reorganized marine ecosystems. Middle to late Ediacaran (575-541 Ma) marine sedimentary rocks record the first appearance of macroscopic, multicellular body fossils known as the *Ediacaran Biota*, thought to represent stem and crown group metazoans (animals) as well as potentially extinct clades leading up to the Cambrian explosion (Narbonne, 2005; Droser and Gehling, 2015). In Chapter 2, I present lipid biomarker assemblages from the most thermally well-preserved rocks of the Ediacaran (and Precambrian), which come from Baltica. Baltica was an isolated paleocontinent at this time period, inundated by epicontinental seas (Bogdanova et al., 2008). Lipid biomarker identification is used to address the state of the both bacterial and eukaryotic microbial populations during the appearance of the Ediacaran Biota. The majority of Chapter 2 was published in the peer-reviewed journal *Nature Communications* (Pehr et al., 2018). In Chapter 3, I continued to investigate the microbial environments of Ediacaran Baltica with the addition of compound specific carbon isotope analysis. I also utilized iron speciation to determine the heterogeneity of ocean redox across Baltica at this time.

Chapter 4 is dedicated to a broader study of organic matter in samples of wide ranging thermal maturities. Recent missions to Mars have detected simple aromatic and other stable organic compounds in surface rocks and sediments. These highly derived organic compounds are not necessarily biogenic in origin, but are convincingly not Earth contamination (Freissinet et al., 2015; Eigenbrode et al., 2018; Szopa et al., 2019). I am attempting to better understand the distributions and systematics of preservation of organic compounds that persist in the accessible Martian sedimentary record specifically, polycyclic hydrocarbons (PAHs), as both free hydrocarbons and bound in insoluble macromolecules. To carry out my study, I investigated the PAH distributions in samples ranging from immature to overmature thermal maturity, as well as carbonaceaous residues from pyrobitumens and coke residue from hydrocracking experiments, in order to determine how PAHs are altered during preseration.

Chapter 5 contains a synthesis and summary of the main data and conclusions presented in this thesis.

REFERENCES

Alexander, C.M.O., Cody, G.D., Gregorio, B.T.D., Nittler, L.R., Stroud, R.M., 2017. The nature, origin and modification of insoluble organic matter in chondrites, the major source of Earth's C and N. *Geochemistry* 77, 227–256.

Bogdanova, S.V., Bingen, B., Gorbatschev, R., Kheraskova, T.N., Kozlov, V.I., Puchkov, V.N., and Volozh, Y.A., 2008, The East European Craton (Baltica) before and during the assembly of Rodinia: Precambrian Research, v. 160, no. 1-2, p. 23–45, doi: 10.1016/j.precamres.2007.04.024.

Brocks, J.J., Love, G.D., Summons, R.E., Knoll, A.H., Logan, G.A., Bowden, S.A., 2005. Biomarker evidence for green and purple sulphur bacteria in a stratified Palaeoproterozoic sea. *Nature* 437, 866–870.

Brocks, J.J., Schaeffer, P., 2008. Okenane, a biomarker for purple sulfur bacteria (Chromatiaceae), and other new carotenoid derivatives from the 1640Ma Barney Creek Formation. *Geochimica et Cosmochimica Acta* 72, 1396–1414.

Burdige, D.J., 2007. Preservation of Organic Matter in Marine Sediments: Controls, Mechanisms, and an Imbalance in Sediment Organic Carbon Budgets? *Chemical Reviews* 107, 467–485.

Droser, M.L., and Gehling, J.G., 2015. The advent of animals: The view from the Ediacaran: *Proceedings of the National Academy of Sciences*, 112, 4865–4870, doi: 10.1073/pnas.1403669112.

Eigenbrode, J.L., Summons, R.E., Steele, A., Freissinet, C., Millan, M., Navarro-González, R., Sutter, B., McAdam, A.C., Franz, H.B., Glavin, D.P., Archer, P.D., Jr., Mahaffy, P.R., Conrad, P.G., Hurowitz, J.A., et al. 2018. Organic matter preserved in 3-billion-year-old mudstones at Gale crater, Mars. *Science* 360, 1096–1101, doi: 10.1126/science.aas9185.

Freissinet, C., Glavin, D.P., Mahaffy, P.R., Miller, K.E., Eigenbrode, J.L., Summons, R.E., Brunner, A.E., Buch, A., Szopa, C., Archer, P.D., Jr., Franz, H.B., Atreya, S.K., Brinckerhoff, W.B., Cabane, M., et al. 2015. Organic molecules in the Sheepbed Mudstone, Gale Crater, Mars. J*ournal of Geophysical Research: Planets* 120, 495–514, doi: 10.1002/2014JE004737.

Hoefs, J., 2009. Stable Isotope Geochemistry. doi:10.1007/978-3-540-70708-0

Huc, A.Y., Durand, B.M., 1977. Occurrence and significance of humic acids in ancient sediments. *Fuel* 56, 73–80.

Killops, S and Killops, V. 2005.. Long-Term Fate of Organic Matter in the Geosphere. In Introduction to Organic Geochemistry, Blackwell Publishing, Malden, MA, pp. 117-165, doi:10.1002/9781118697214.

Lee, C., Love, G.D., Jahnke, L.L., Kubo, M.D., and Marais, Des, D.J. 2019. Early diagenetic sequestration of microbial mat lipid biomarkers through covalent binding into insoluble macromolecular organic matter (IMOM) as revealed by sequential chemolysis and catalytic hydropyrolysis. *Organic Geochemistry* 132, 11–22, doi: 10.1016/j.orggeochem.2019.04.002.

Love, G.D., Snape, C.E., Carr, A.D., Houghton, R.C., 1995. Release of covalently-bound alkane biomarkers in high yields from kerogen via catalytic hydropyrolysis. *Organic Geochemistry* 23, 981–986.

Narbonne, G.M., 2005. The Ediacara Biota: Neoproterozoic Origin of Animals and Their Ecosystems: *Annual Review of Earth and Planetary Sciences*, 33, 421–442, doi: 10.1146/annurev.earth.33.092203.122519.

Pearson, A., Page, S.R.F., Jorgenson, T.L., Fischer, W.W., Higgins, M.B., 2007. Novel hopanoid cyclases from the environment. *Environmental Microbiology* 9, 2175–2188.

Pehr, K., Love, G.D., Kuznetsov, A., Podkovyrov, V., Junium, C. K., Shumlyanskyy, L., Sokur, T., Bekker, A. 2018.. Ediacara biota flourished in oligotrophic and bacterially dominated marine environments across Baltica. *Nature Communications*, 9, 1807, doi:10.1038/s41467-018-04195-8

Peters, K.E., Walters, C.C., Moldowan, J.M. 2005.. The Biomarker Guide. Cambridge University Press, Cambridge, UK.

Rohmer, M., Knani, M., Simonin, P., Sutter, B., Sahm, H., 1993. Isoprenoid biosynthesis in bacteria: a novel pathway for the early steps leading to isopentenyl diphosphate. *Biochemical Journal* 295, 517–524.

Smith, J.W., Kaplan, I.R., 1970. Endogenous Carbon in Carbonaceous Meteorites. *Science* 167, 1367–1370.

Szopa, C., Freissinet, C., Glavin, D.P., Millan, M., Buch, A., Franz, H.B.., Summons, R.E., Sumner, D., Sutter B., Eigenbrode, J.L., Williams, R., Navarro-González, R., Guzman, R., Malespin, C., Teinturier, S., Mahaffy, P.R., Cabane, M., 2020. First Detections of Dichlorobenzene Isomers and Trichloromethylpropane from Organic Matter Indigenous to Mars Mudstone in Gale Crater, Mars: Results from the Sample Analysis at Mars Instrument Onboard the Curiosity Rover. *Astrobiology* 20, 292-306 doi: 10.1089/ast.2018.1908

Tissot, B.P. and Welte, D.H. (1984) Petroleum Formation and Occurrence. 2nd Edition, Springer-Verlag, Berlin.

CHAPTER TWO

Ediacara biota flourished in oligotrophic and bacterially dominated marine environments across Baltica

ABSTRACT

Middle-to-late Ediacaran (575–541 Ma) marine sedimentary rocks record the first appearance of macroscopic, multicellular body fossils, yet little is known about the environments and food sources that sustained this enigmatic fauna. Here, we perform a lipid biomarker and stable isotope ($\delta^{15}N_{total}$ and $\delta^{13}C_{TOC}$) investigation of exceptionally immature late Ediacaran strata (<560 Ma) from multiple locations across Baltica. Our results show that the biomarker assemblages encompass an exceptionally wide range of hopane/sterane ratios (1.6–119), which is a broad measure of bacterial/eukaryotic source organism inputs. These include some unusually high hopane/sterane ratios (22–119), particularly during the peak in diversity and abundance of the Ediacara biota. A high contribution of bacteria to the overall low productivity may have bolstered a microbial loop, locally sustaining dissolved organic matter as an important organic nutrient. These oligotrophic, shallow-marine conditions extended over hundreds of kilometers across Baltica and persisted for more than 10 million years.

1. INTRODUCTION

The Ediacaran Period (~635–541 Ma) was part of an era of extreme tectonic, geochemical, and evolutionary changes, which fundamentally reorganized marine ecosystems. Oxygen has often been proposed as an enabler, if not the driver, of the rise and evolution of multicellular biota and metazoans. Trace-metal and isotope redox proxies place an atmospheric and ocean surface oxygenation event at ~850 Ma (Planavsky et al., 2014; Turner and Bekker, 2016), and numerous settings of oxygenated shallow waters have been identified throughout the Ediacaran (Fike et al., 2006; Wood et al., 2015; Sahoo et al., 2016). The Ediacaran is known for its wide variety of fossils, notably body and trace fossils, left by soft-bodied multicellular fauna unique to the middle and late Ediacaran ca. 575–541 Ma (Narbonne, 2005; Droser and Gehling, 2015). While there are also anoxic, and even euxinic, productive marine settings identified at this time (Li et al., 2015; Sahoo et al., 2016), redox proxies in the majority of units containing the diverse and large Ediacara biota indicate predominantly oxic conditions (Bowyer et al., 2017). The emergence of metazoan fauna at that time has thus often been ascribed to increasing oxygenation of the oceans. This interpretation has been challenged on the basis that anatomically simple metazoans, particularly sponges, could survive under very low dissolved oxygen levels, which may have been sustained in shallow waters prior to the Ediacaran (Sperling et al., 2013). However, detailed geochemical studies, in some cases across a range of ecosystems, do show a correlation between oxygen stability and fossil diversity and size (Wood et al., 2015; Bowyer et al., 2017). It seems most likely that while metazoans might have initially evolved in low-oxygen

environments, it was not until oxygen level increased enough to support persistent oxygenation of shallow waters that the macroscopic Ediacara biota began to flourish (Johnston et al., 2012; Sperling et al., 2015).

However, oxygen was likely not the only control on metazoan early evolution and diversification. Nutrient availability, usually of nitrogen or phosphorus, limits the productivity and composition of microbial communities and would have imposed an important selective pressure on the Ediacara biota. It has been proposed that marine anoxia in the Proterozoic Era prior to the late Ediacaran could have favored nitrogen limitation in the oceans by supporting denitrification and anammox reactions and thus limited metazoan evolution and expansion (Olson et al., 2016). However, as oxygenated surface waters expanded globally in the late Neoproterozoic (Tostevin et al., 2016; Sahoo et al., 2016; Johnston et al., 2012), nitrogen limitation would have become less persistent, and productivity on shelves became increasingly controlled by advection of nutrients, resulting in productivity patterns more similar to those in Phanerozoic oceans (Brocks et al., 2017). Ferruginous deep waters in the Archean and early Proterozoic likely also limited bioavailable phosphorous (Reinhard et al., 2017). While seawater phosphate concentration probably increased substantially due to a fundamental shift in the phosphorus cycle during the Cryogenian period associated with the glaciations and their aftermaths, (Reinhard et al., 2017; Planavsky et al., 2010) the temporal trajectory of phosphate marine availability through the late Ediacaran is not readily deciphered and was likely variable from location to location. The role that essential nutrients and food

sources, including carbon, nitrogen, and phosphorus, played in the early evolution and diversification of metazoans during the Ediacaran remains open for debate and deserves further study.

On the basis of their morphology, some of the earlier Ediacara biota are thought to have used osmotrophy, which is the uptake of dissolved organic compounds by diffusion, while other types of the Ediacara biota are thought to show evidence of suspension feeding and active (motile) heterotrophy (Laflamme et al., 2009; Gehling et al., 2014; Droser et al., 2017). The Ediacara biota is traditionally divided into three groups on the basis of their age, diversity, and unique biological and ecological capabilities (Droser et al., 2017). Exact age constraints are however scarce, and the fossil records of these groups seem to overlap in some locations. The oldest, Avalon assemblage is usually associated with deep-water settings and high body surface area to volume ratios, characteristic of osmotrophy (Liu et al., 2015). The second group, the White Sea assemblage, is notable for morphologies that suggest increased mobility, bilaterian forms, and evidence of burrowing and skeletonization (Gehling and Rigby, 1996; Fedonkin and Waggoner, 1997; Seilacher and Pflüger, 1994; Grazhdankin, 2014),. The third group, the Nama assemblage, maintained many of the evolutionary innovations observed in the White Sea assemblage, but is characterized by a sharp decrease in diversity. Lack of taphonomically suitable environments and changes in environmental conditions, as well as increased competition from evolving predators have been proposed as a cause for the disappearance of many forms of the Ediacara biota present in the White Sea assemblage

from the Nama assemblage (Laflamme et al., 2013; Kolesnikov et al., 2015). Near the end of the Ediacaran, the first calcified metazoans appeared, which has been suggested to result in a positive feedback between more oxygenated oceans and the rate of organic matter export due to their higher density (Lenton et al., 2014).

Paleomagnetic data track Baltica moving from high to low latitudes in the southern hemisphere between 615 and 550 Ma (Klein et al., 2015). Starting at ~620 Ma, Baltica began rifting from Laurentia and, potentially, Amazonia as part of the breakup of the supercontinent Rodinia. Rifting took place along the modern western edge of Baltica, resulting in the opening of the Iapetus Ocean by 570 Ma. Meanwhile, the eastern margin of Baltica transitioned from a long-lived passive margin to a foreland basin (Sliaupa et al., 2006; Pease et al., 2008). Throughout the Ediacaran, deposition across Baltica occurred along the passive margins and in the epicontinental basins, and, at a later stage, in the pro-foreland basin developed along the eastern margin. Study of the Ediacaran strata indicates an extremely low degree of thermal maturation across Baltica, from clay mineralogy (Aksenov and Volkova, 1969) and Rock-Eval pyrolysis (Table 2.3).The late Ediacaran strata of Baltica is traditionally divided into two regional biostratigraphic horizons based on extensive study of microfossil records from drillcores across Baltica: Redkino, and Kotlin, whereas the two lowermost horizons of the Early Cambrian (starting with the first appearance of *Treptichnus pedum*) are Rivno and Lontova, in order of oldest to youngest. Extensively developed over Baltica, Redkino is characterized by diverse assemblage of carbonaceous compression macrofossils and soft-bodied biota

deposited in marine basins. The younger Kotlin horizon is marked by decreasing diversity and abundance of the soft-bodied biota (although coincidental with the first appearance of *Psammocorallia*) accompanied by emergence of diverse ichnofossils, associated with shallow burrowing organisms, and macroscopic algal assemblages (Burzin, 1996; Martin et al., 2000; Veis et al., 2006; Vorob'eva et al., 2009; Marusin et al., 2011; Kolesnikov et al., 2015). This sudden shift in diversity and abundance of soft-bodied biota has been called the "Kotlin Crisis" and has been interpreted as either an extinction event or a migration of soft-bodied biota to distributary channel system caused by the competitive pressure from bilaterians (Kolesnikov et al., 2015). Recently, this two-fold stratigraphic scheme has been challenged with the proposal of an additional short interval of geological time placed between Redkino and Kotlin and tentatively named Belomorian, which would encompass the highest diversity of soft-bodied biota (Grazhdankin and Maslov, 2015). In this study we will use the traditional stratigraphy based on the Redkino and Kotlin horizons. Widespread and abundant occurrences of macroscopic soft-bodied fossils (see Fig. 2.1) are found in the Ediacaran strata from the Mezen Basin, White Sea region, the South and Central Urals of Russia as well as Podillya of Ukraine, and although these were not described from the Moscow Basin (Laflamme et al., 2013; Grazhdankin, 2014) and Baltic monocline (Podkovyrov et al., 2017), this might reflect a lack of outcrop with only drill cores available for investigation in the latter areas providing less opportunities to find fossils. Ediacaran strata from the Redkino Horizon contain select Avalon-type fossils, diverse White Sea type fossils, and even some Nama-type biota (Podkovyrov et al., 2017). The Kotlin horizon hosts Nama-

type fossils (Grazhdankin, 2014; Grazhdankin and Maslov, 2015). Noteworthy are abundant occurrences of White Sea-type fossil assemblages from the Redkino Horizon in Podillya outcrops (Ivantsov et al., 2015), close to where our own Podillya samples came from.

In addition to the body fossil record, lipid biomarker assemblages consisting of molecular fossils derived from cell membrane lipids and other recalcitrant organic molecules can be used to investigate source organism inputs and local paleoenvironmental redox conditions (Peters et al., 2005). Organic-matter-rich deposits are typically targeted for biomarker analysis due to their high potential of preserving sufficient extractable material for detection, however, organic-matter-lean deposits can also preserve abundant biomarkers if they have undergone only a mild thermal alteration. Diverse and abundant lipid biomarker assemblages have been previously reported from a variety of Ediacaran, eutrophic marine environments from rocks and/or oils of appropriate thermal maturity from South Oman (Grosjean et al., 2009; Lee et al., 2013), India (Dutta et al., 2013), eastern Siberia (Kelly et al., 2011; Duda et al., 2016) Australia (McKirdy et al., 2006), and Russia (Bazhenova and Arefiev, 1996).

Here, we present the lipid biomarker and nitrogen and carbon isotopic data obtained from exceptionally immature Ediacaran strata from seven drill cores and three outcrops spanning Baltica. Two of the drill cores, Utkina Zavod and Lugovoe, were located near St. Petersburg in the northeastern part of the Baltic mono-cline. Gavrilov-Yam-1 was

drilled in the Moscow Basin, the 4504, 4529, and 4592 drill cores were recovered from the Volyn region of Ukraine, while the 3628 drill core and 16PL outcrops of Podillya Basin were sampled in southwestern Ukraine and Moldova, respectively (see Fig. 2.1 and Table 2.1). Ediacara biota fossils have been described extensively across Baltica, as shown in Fig. 2.1, including abundant occurrences of White Sea-type fossil assemblages from the Redkino Horizon in Podillya outcrops (Ivantsov et al., 2015), close to where our own Podillya samples were collected. We studied fine-grained sedimentary rocks (mudstones and siltstones) of the Redkino and Kotlin Horizons from these sites; in addition, the Lontova Horizon (*Platysolenites antiquissimus* Zone) of the early Cambrian age was sampled in the Gavrilov-Yam-1 drill core.

2. SAMPLE SELECTION AND PROCESSING

A total of 29 thermally immature Ediacaran sedimentary rock samples from Russia, Ukraine, and Moldova, encompassing strata from the Redkino, Kotlin, and Lontova horizons, were selected for investigation from the Baltic monocline, Moscow, and Volyn-Podillya Basins. This provided sampling across a wide paleogeographic transect for late Ediacaran marine paleoenvironments of Baltica (Table 2.1). All our samples are younger than 560 Ma based on established correlations with the well-dated strata of White Sea and Ural Mountains, Russia and Podillya, Ukraine (Grazhdankin, 2014; Grazhdankin and Maslov, 2015) and thus were deposited during the time interval when shallow-marine waters in the surface mixed layer were redox-stabilized and predominantly oxic (Johnston et al., 2012a), despite evidence for redox instability and anoxic conditions in

deeper ocean settings (Sperling et al., 2015) and in some lower-energy, shallow-marine settings (Marusin et al., 2011).

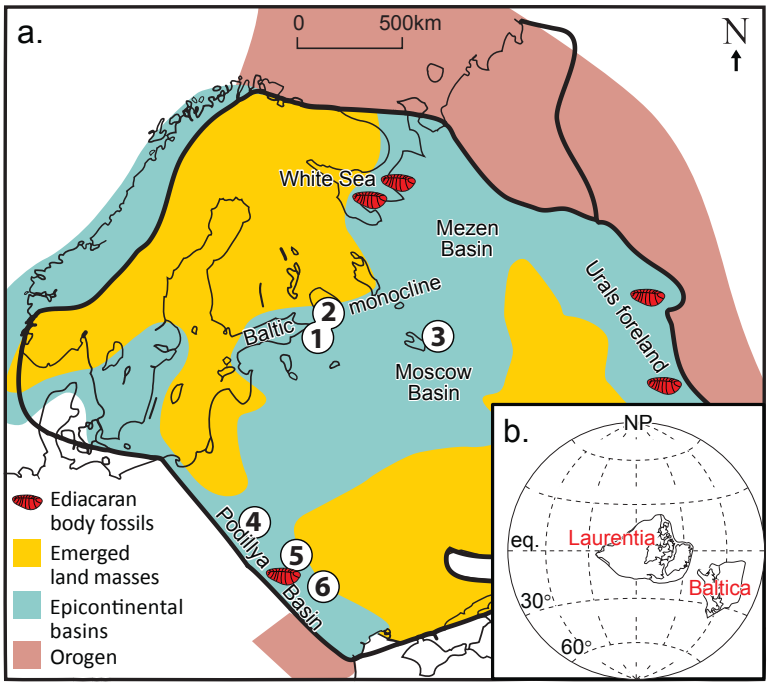

Figure 2.1. Paleogeography and known Ediacara biota fossil occurrences across Baltica. (a) Paleogeographic reconstruction of Baltica during the late Ediacaran (modified from Sliaupa et al. 2006) with studied drill cores and outcrops shown (1—Utkina Zavod; 2—Lugovoe; 3—Gavrilov-Yam-1 in Russia; 4—4504, 4529, and 4592 cores from the Volyn Basin, Ukraine; 5— 3628 core from the Podillya Basin, Ukraine; and 6—outcrops 16PL from the Podillya Basin, Moldova). (b) Global reconstruction of Laurentia and Baltica at ~550 Ma, modified from Fedorova et al. 2013

2.1. Geology of the studied units

Sedimentary rock sample details are given in Table 2.1. In the St. Petersburg area of Russia, the Redkino Horizon is represented by the locally developed Staraya Russa Formation, which averages 50m in thickness. It consists of mudstones and siltstones. The Staraya Russa Formation records a full transgressive-regressive cycle, potentially formed in a submarine, delta-fan setting and low-energy environment of sea shoals. The overlying Vasileostrovskaya Formation of the Kotlin Horizon has a basal unconformity

in the Utkina Zavod drill core, but not in the Lugovoe drill core (Podkovyrov et al., 2017). Its lower part consists of silty mudstones, while its upper part is composed of laminated mudstones with fine, horizontal, and wavy bedding. These sediments are interpreted to have been deposited under generally oxic conditions along the coast with weak currents and in stagnant depressions in the sublittoral environments (Podkovyrov et al., 2017). In the Gavrilov Yam-1 drill core of the Moscow Basin of Russia, siltstones of the Reshminskaya Formation that belong to the Kotlin Horizon and the lower part of the Early Cambrian Lezhskaya Formation that belongs to the Lontova Horizon were sampled (Vinogradov et al., 2005). The sediments were accumulated in epicontinental seaways with depths straddling the storm wave base under predominantly oxic conditions. In the Volyn area of the northwestern Ukraine (Volyn-Polissye Basin), the drill cores 4504 and 4529 containing mainly siltstones of the Kanyliv Group (undivided in this area, but correlated to the Upper Kotlin Horizon) were sampled. Mudstones of the Roznychi Formation of the Mohyliv-Podilsky Group that belong to the Upper Redkino Horizon were sampled in the drill core 4592.The presently separate Volyn-Polissya Basin and Podillya Basin, developed in the western part of Ukraine and extending across its border to Moldova, belonged to the same Late Ediacaran Volyn-Podillya epicontinental basin extending to the continental margin to the south. They are now separated by the older Precambrian crystalline basement, uplifted during the orogenic event along the southern margin of Baltica in the earliest Paleozoic. In the Podillya Basin, the drill core 3628 from the northernmost part of the Podillya Basin, Ukraine and outcrops in Moldova near the border with Ukraine were sampled. The samples from the drill core 3628 are from the

Lomozov Beds of the Mohyliv Formation, the Lyadova Beds of the Yaryshiv Formation, and the Kalyus Beds of the Nagoryany Formation, which belong to the lower, middle, and upper intervals of the Redkino Horizon, respectively. The outcrop samples from Moldova are from the upper Redkino Kalyus Beds of the Nagoryany Formation. The 20m-thick Lomozov Beds contain thin, interbedded dark-grey mudstones and fine-grained sandstones; in middle part of the beds thick intervals of arkosic gravelites occur. The Lomozov Beds constitute the oldest strata hosting Ediacara Biota macrofossils within the succession; they have the highest macrofossil diversity through the Ediacaran succession of the Volyn-Podillya Basin (Ivantsov et al., 2015).The 25m-thick Lyadova Beds contain greenish-grey and brown thin-bedded micaceous mudstones with a gradual lower contact. The beds contain films of algal (or, possibly, fungal) origin and an assemblage of microphytofossils, typical for the Mohyliv Formation (Velikanov et al., 1983). The 50m-thick Kalyus Beds are represented by homogeneous, dark-grey thin-bedded mudstones. The beds contain in the middle part up to 15 levels of phosphorite concretions and have gradual lower contact, marked by lenses and interbeds of fine-grained calcareous sandstone. The beds include two 4-and 5.5m-thick levels, at the top and bottom, rich in Vendotaenian algae.

2.2. Sample preparation

Standardized procedures were employed to prevent contamination during the cutting and crushing stages. Rock chips were first trimmed with a clean water-cooled rock saw to remove the outer surfaces. The obtained solid inner portion was sonicated in a sequence

of ultrapure water, methanol (MeOH), and dichloromethane (DCM). The cleaned inner-rock fragments were powdered in a zirconia ceramic puck mill using a SPEX 8515 shatterbox, treated between successive samples by powdering two batches of combusted sand (at 850 °C overnight) and rinsing with methanol, DCM, and hexane. As an important control, combusted quartz sand blanks were run parallel with the samples as full analytical procedural blanks. This procedure yielded pristine rock powders for subsequent solvent extraction (see below). TOC determination and Rock-Eval pyrolysis. TOC contents were determined at GeoMark Research in Houston, TX. Samples were decarbonated with 5 M HCl for at least 2 h, rinsed through a filtration apparatus to remove the acid, dried at low temperature, and weighed to obtain percent carbonate based on weight loss. They were then combusted on a LECO C230 instrument to measure TOC content. The LECO C230 instrument was calibrated with standards having known carbon contents. Standards were combusted by heating to 1200 °C in the presence of oxygen; both carbon monoxide and carbon dioxide were generated and carbon monoxide was converted to carbon dioxide by a catalyst. The carbon dioxide yield was measured using an IR cell. Combustion of unknowns followed the same procedure and the response per mass unit of unknown was compared to that of the calibration standard. Standards were analyzed every ten samples to check stability and calibrate the analysis. Standard deviation for TOC was 3% from the established value. Approximately 100 mg of washed, ground (to 60-mesh) whole-rock samples were analyzed with a Rock-Eval II instrument. Measurements include S1: free bitumen content (mg HC/g rock); S2: remaining generation potential (mg HC/g rock); T_{max}: temperature at maximum evolution of S2

hydrocarbons (°C); and S3: carbon dioxide yield from organic carbon (mg CO2/g rock). The data were generated by heating according to the following parameters: S1: 300 °C for 3 min; S2: 300–550 °C ramping at 25 °C/min, and then held at 550 °C for 1 min; S3: hold at a temperature between 300 and 390 °C. Instrument calibration was achieved using a rock standard with values determined based on a curve calibrated with pure hydrocarbons of varying concentrations. The low values of T_{max} (ranging from 417 to 443 °C, with mean = 426 °C, n = 22) indicate that these rocks are all thermally immature and most of them are at a low thermal maturity stage that is a pre-oil window or (for 16PL outcrop samples only) at an early-to-middle stage within the oil window prior to peak oil generation (Table 2.3).

2.3. Lipid biomarker analysis

The following methods outlined in (Haddad et al 2016), solvent extractions of rock bitumens were performed on 5–20 g of rock powder per sample using a 9:1 (v/v) DCM:MeOH mixture in a CEM Microwave Accelerated Reaction System (MARS) at 100 °C for 15 min. The total bitumen extract was separated into aliphatic hydrocarbons, aromatics, and polar fractions on a silica gel column, eluting with hexane, a 1:1 (v/v) mixture of DCM and hexane, and a 4:1 (v/v) DCM to MeOH mixture, respectively. Aliphatic and aromatic hydrocarbon fractions were analyzed to generate total ion chromatograms (Fig. 2.2) in full-scan mode using a gas chromatography–mass spectrometry (GC–MS) with an Agilent 7890A GC system coupled to an Agilent 5975C inert MSD mass spectrometer. The GC temperature program for full-scan analysis was

60 °C (held for 2 min), heated to 150 °C at 20 °C/min, then to 325 °C at2 °C/min, and held at 325 °C for 20 min. The GC was equipped with a DB1-MScapillary column (60 m × 0.32 mm, 0.25-μmfilm thickness) and helium was used as a carrier gas. To determine accurate molecular biomarker ratios (Table 2.3 and 2.4), aliphatic hydrocarbons were also analyzed by metastable reaction monitoring (MRM)–GC–MS on a Waters Autospec Premier mass spectrometer equipped with an Agilent 7890A gas chromatograph and DB-1MS coated capillary column (60m × 0.25 mm, 0.25-μmfilm) using He as a carrier gas to look at polycyclic biomarker stereoisomer patterns in more detail. The GC temperature was programmed with an initial hold at 60 °C for 2 min, then heating to 150 °C at 10 °C/min rate, followed by heating to 320 °C at 3 °C/min rate, and a final hold for 22min; analyses were performed via splitless injection in an electron-impact mode, with an ionization energy of 70 eV and an accelerating voltage of 8 kV. MRM ion-pair transitions were used for a suite of biomarker compounds (C_{27}–C_{35} hopanes, C_{31}–C_{36} methylhopanes, C_{19}–C_{26} tricyclic terpanes, C_{24} tetracyclic terpanes, C_{21}–C_{22} and C_{26}–C_{30} steranes, and C_{30} methylsteranes), which were identified by retention time and published mass spectra and were quantified by comparison of their peak area with that of an added deuterated C_{29} sterane standard [d4-ααα-24-ethylcholestane (20R)]. Individual analyte peaks in rock extract hydrocarbon fractions were quantified and found to constitute at least three orders of magnitude larger signal than any peak detected in full-laboratory blank using combusted sand. Procedural blanks with pre-combusted sand typically yielded less than 0.1 ng of individual hopane and sterane compounds per gram of combusted sand. In addition to the rock bitumen extraction, catalytic hydropyrolysis

(HyPy, Love et al., 1995) was used as an important self-consistency check for testing biomarker syngenicity. HyPy was performed on a subset of pre-extracted rock powders (Utkina Zavod 111.6 m, Lugovoe 41 m, and Lugovoe 73 m). This technique involves temperature-programmed heating of samples gradually up to 520 °C in a continuous-flow configuration under high hydrogen gas pressure (15 MPa) to cleave covalent bonds and release the bound molecular constituents, while preserving their structural and stereochemical integrity to a high degree. Because the kerogen is insoluble and immobile, it yields primary biomarker signals immune from contamination due to oil migration or with drilling fluids and represents a key strategy to identify any significant biomarker contaminant in the extractable bitumen phase (Love et al., 1995). Fig. 2.3 and 2.4 show that both the bitumen and kerogen-bound hopanes from the Utkina Zavod (111.6-m) sample exhibit a very immature profile as is the case for the steranes. The bound hopanes yield a slightly less-mature diastereoisomer distribution than the free hopanes due to protection of the bound biomarker pool by covalent binding, which is consistent with the expected bound versus free patterns found for sedimentary rocks of all geological ages (Love et al., 1995). Thus, we are confident that the exceptionally immature polycyclic alkanes found in our bitumen extracts are primary and genuine Ediacaran biomarkers consistent with immature biomarker stereoisomer ratios (Table 2.3) and with the expected maturity profiles from Rock-Eval pyrolysis parameters (particularly T_{max}).

2.4. Organic carbon and nitrogen isotope ratios

Nitrogen isotopic analysis of sediments was performed in the Syracuse University GAPP Lab using an automated "nano-EA" that is similar to that described in (Polissar et al. 2008). Nano-EA allows for the analysis of small sample sizes that is essential for reliable measurements of N-lean materials or samples for which complete combustion is difficult to achieve. The Syracuse University nano-EA comprises an Elementar Isotope Cube elemental analyzer coupled to an Isoprime Trace Gas analyzer. The Trace Gas analyzer is used for N_2 trapping and chromatographic focusing prior to the introduction of gas into the Isoprime 100 stable-isotope mass spectrometer. Sample powders were loaded into tin capsules, evacuated, and purged with argon prior to introduction into the EA to remove contamination from atmospheric N_2. EA conditions were the following: helium purge was set for 45 s, oxidation and reduction reactor temperatures were 1100 °C and 650 °C, respectively, helium carrier gas flow was150 ml/min, and the O_2 pulse was set for 60s. During sample analysis, the full flow of the EA is diverted to automated silica gel-filled cryotrap that is immersed in liquid nitrogen over the duration that N_2 gas was generated during sample combustion. The N_2 trap is switched to a low-flow He carrier gas (2 ml/min) via an automated Vici 6-port Valco valve and released to the IRMS through an Agilent CarboBond column (25 m × 0.53 mm × 5 μm). CO_2 generated during sample combustion was retained in a molecular sieve trap that is integral to the Elementar Isotope Cube EA, which is heated and released to waste after each sample. This eliminates the potential of carryover of CO_2 and generation of CO in the ion source that would interfere with nitrogen isotope analysis. Samples were run in triplicate using

sequentially larger samples (i.e., 6, 8, and10 mg) and blank-corrected using Keeling-style plots. International (IAEA N1ammonium sulfate [0.4 weight‰ N], N_2 ammonium sulfate [20.3 weight‰ N], and NIST 1547 peach leaves [2.0 weight‰ N]) and in-house (Messel Oil Shale [7.0weight‰ N]) reference materials were also run in a similar manner, and in nitrogen quantities that bracketed the N-content of the sample materials. The resulting blank-corrected sample and standard data were calibrated using accepted values for the reference materials applying the scheme described in (Coplen et al., 2006). Reproducibility for samples and standards (±0.25‰) approaches that for the reported nitrogen isotope composition of the reference materials (±0.2‰) and is similar to standard EA-IRMS techniques for samples of similar nitrogen content. Carbon isotope analysis was performed on acidified rock powder residuals using an Elementar Isotope Cube elemental analyzer coupled to an Isoprime 100 stable-isotope mass spectrometer in a conventional format. EA conditions were the following: helium purge was set for 30 s, oxidation and reduction reactor temperatures were 1100 °C and 650 °C, respectively, helium carrier gas flow was 230 ml/min, O_2 pulse was set for 60 s, and CO_2 trap was heated to 230 °C to release trapped sample CO2. International reference materials (ANU sucrose [−10.4‰] and NIST 1547 peach leaves [−26.0‰]) were used to develop the correction scheme for sample data as described previously (Coplen et al., 2006). Reproducibility for samples and standards was better than ±0.1‰.

3. RESULTS AND DISCUSSION

3.1. Exceptionally low thermal maturity of the strata.

Thermal maturity is the single most important factor influencing the preservation of ancient sedimentary biomarkers as organic molecules are susceptible to structural and stereochemical alteration during progressive burial and with increasing thermal stress (Peters et al., 2005). Precambrian rocks of appropriate thermal maturity (oil window maturity or lower) are prerequisites for preserving robust and primary biomarker lipid assemblages. Multiple hopane and sterane biomarker stereoisomer ratios, along with independent evidence from low Tmax values (mostly within a 417–433 °C range, with a mean of 426 °C) from Rock-Eval pyrolysis, indicate that the rocks in this study represent by far the most thermally immature Ediacaran rocks analyzed to date using the state-of-the art organic geochemical methods (Table 2.3 and 2.4). Although our rocks have undergone sedimentary diagenesis, they did not pass significantly into the oil window apart from the slightly more mature 16PL outcrop samples from Podillya Basin in Moldova, which are still suitable for analysis (early-to-middle oil window maturity and no obvious sign of organic contaminants). The majority of the set then had not likely been exposed to burial temperatures exceeding 50 °C, thus our samples are highly immature. Other lines of molecular evidence, which support low thermal maturity and syngenicity, include (i) a dominance of polycyclic biomarker alkanes over n-alkanes in rock extracts (Fig. 2.2), (ii) survival of detectable amounts of 17β,21β(H)-hopanes resolvable from the more abundant hopanes possessing stable 17β,21α(H)- and 17α,21β(H)-stereochemical configurations (Table 2.3, Fig. 2.3 and 2.4), (iii) a discernible

odd-over-even preference among then-alkanes in the $C_{22}$to C_{27} range (Fig. 2.2), as n-alkanes show a carbon-number preference only prior to catagenesis(Scalan and Smith, 1970, and (iv) generation of thermally immature hopane and sterane biomarkers from the (insoluble) kerogen phase using catalytic hydropyrolysis (Fig. 2.3). The low thermal maturity of sedimentary organic matter in our samples is consistent with previously published indicators of sedimentary alteration, including conodont and acritarch alteration indices, and previous Rock-Eval pyrolysis and biomarker studies of the Ediacaran and Paleozoic sedimentary rocks in Baltica (Bazhenova and Arefiev, 1996; Nehring-Lefeld et al., 1997; Talyzina et al., 1998), as well as clay mineralogy (Aksenov and Volkova, 1969). Critically, in settings where thermal maturity is this low, the mechanisms for significant alteration of primary $\delta^{15}N$ and $\delta^{13}C$ signals are largely absent (Robinson et al., 2012).

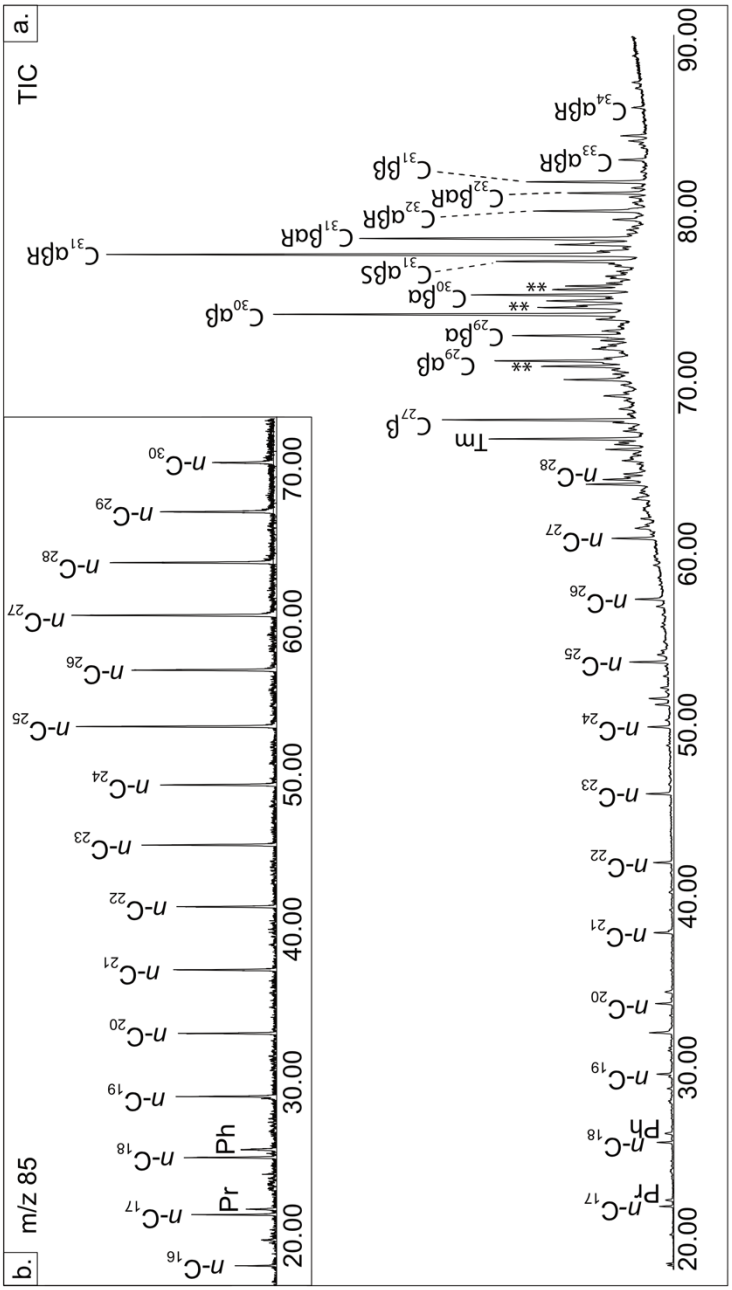

Figure 2.2. Distribution of extractable aliphatic hydrocarbons for a representative sample. (a) Total ion chromatogram (TIC) for extractable aliphatic hydrocarbons for Lugovoe #13–73 m from the Redkino Horizon. The n-alkane series, pristane (Pr), phytane (Ph), and C_{27}–C_{34} hopanes (denoted by their total carbon number and stereochemistry at C-17, C-21, and C-22, e.g., $C_{31}\alpha\beta R$) are labeled; ** denotes C_{29} and C_{30} hopenes. Note the hopane abundance dominance over other alkane compound classes. (b) Partial 85-Da ion chromatogram shows dominance of the n-alkane series, exhibiting a discernible odd-over-even carbon-number preference in the C_{22}–C_{27} range, over methylalkanes

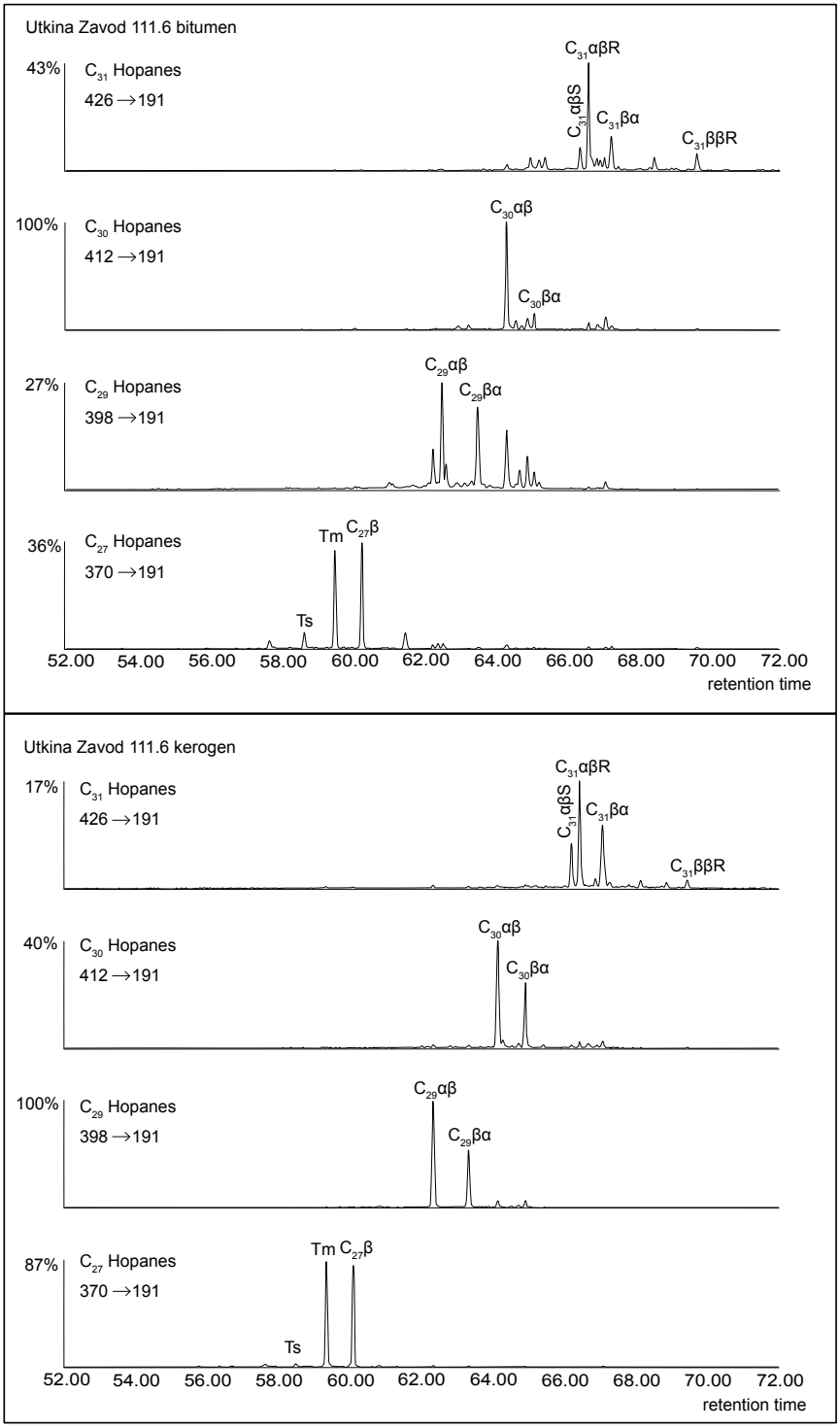

Figure 2.3. MRM-GC-MS chromatograms for the free and kerogen-bound aliphatic hydrocarbon fractions generated from sample Utkina Zavod (111.6m depth) with C_{27}–C_{31}hopanes labeled. Top traces show free hopane distributions from bitumen extraction; bottom chromatograms show bound hopanes generated from the insoluble organic matter (kerogen) using catalytic hydropyrolysis (HyPy).

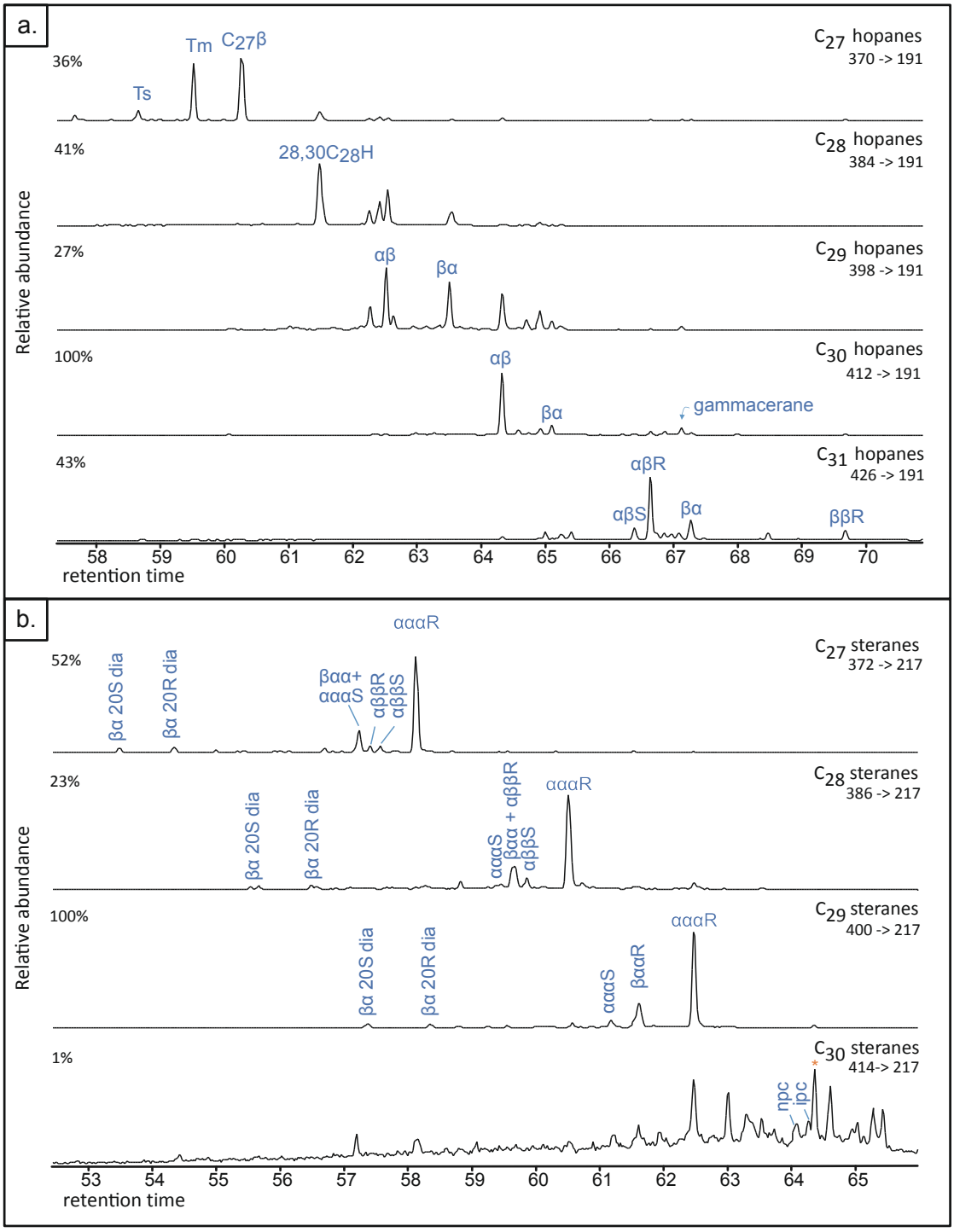

Figure 2.4. MRM-GC-MS chromatograms for the extractable aliphatic hydrocarbon fraction for sample Utkina Zavod (111.6m depth).Top chromatograms show C_{27}–C_{31}hopanes labeled; bottom chromatograms show C_{27}–C_{30} steranes labeled.

3.2. Lipid biomarker assemblage patterns

An abundance ratio of the major (C_{27}–C_{35}) hopanes to major (C_{27}–C_{29}) steranes is often used to assess the balance of bacterial versus eukaryotic source organism inputs to the ancient aquatic ecosystem. Hopanes are molecular fossils derived from hopanoids, which are cell membrane lipids synthesized by a wide variety of bacterial groups. Similarly, steranes are derived from sterol precursors, which are produced almost exclusively by eukaryotes (Summons et al., 2006). Hopane/sterane (H/St) ratios for our samples cover a strikingly large range of values from 1.6 to 119.2 (Table 2.4). For context, H/St ratios from organic-rich Neoproterozoic rocks and oils typically fall in a narrow range from 0.5 to 2.0 (Grosjean et al., 2009; Kelly et al., 2011; Dutta et al., 2013; Lee et al., 2013). While there is a clear difference in the values from the younger Kotlin Horizon (average H/St of 8.9) and the older Redkino Horizon (average H/St of 42.9), the values for most samples are unusually high and suggest anomalously elevated contributions of bacteria.

By the late Neoproterozoic, eukaryotic algae were an ecologically significant component and major producers in many marine ecosystems (Brocks et al., 2017; Duda et al., 2016; Knoll et al., 2007). The discrepancy between the globally important contribution of eukaryotic algae in the late Neoproterozoic and yet the low levels of sterane biomarkers in these samples indicates that there must be some local determinant on eukaryotic abundance. The most parsimonious explanation for the extremely elevated hopane/sterane ratios alongside low total organic carbon (TOC) contents and low hydrogen indices (HI) found for our samples (Table 2.2 and 2.3) is that these strata were

deposited in oligotrophic (i.e., strongly nutrient-limited) settings, in which bacteria outcompeted algae. While modern analogs for ancient epicratonic seas developed during high sea-level stand are hard to find, parallel observations of higher hopane/sterane ratios (by up to an order of magnitude) have been found previously for organic-lean versus organic-rich sedimentary rocks deposited in Ordovician–Silurian epicontinental seaways (Rohrssen et al., 2013).

Typically, low TOC content can be caused by limited deposition of organic matter in low-productivity settings, low preservational potential of organic matter in the water column or sediments, or dilution with a high siliciclastic flux. In modern oceans, productivity is most commonly limited by low levels of the essential nutrients: nitrogen, phosphorus, silicon, and iron (Pease et al., 2008). Nitrogen, phosphorus, and iron are limited in open-ocean regions where upwelling, dust input, and coastal runoff do not supply sufficient amounts of nutrients. In modern oligotrophic settings, the ratio of bacterial to eukaryotic biomass is higher than in eutrophic or mesotrophic settings. Interestingly, the Podillya 16PL outcrop samples from the Redkino horizon of Moldova are phosphorite-containing mudstones and yield significantly lower hopane/sterane ratios (8.1:11.5) than the other Redkino samples in Table 2.4 (though still significantly higher than those found in South Oman Salt Basin or in organic-rich Phanerozoic sediments, which typically fall within a narrow, 0.5–2.0 range), possibly suggesting that increased phosphate availability could have favorably influenced the eukaryotic-to-bacterial ratio found locally (given that the nitrogen isotopic signatures are largely invariant, see the

next section). Phosphorus (P) contents, as well as P/Fe_{total} and P/Al ratios, are otherwise generally low for the late Ediacaran sediments of Podillya, Ukraine, and Estonia (Pirrus, 1992) with the exception of this stratigraphic level marked with phosphorite nodules. Similarly, low (~0.01 to ~0.1 wt%) levels of P in Kotlin and Redkino siliciclastic rocks were reported from a drill core from the northeastern margin of the East European Platform (Johnston et al., 2012a).

The broad and shallow topography in the epicontinental seas across Baltica could have sustained phosphorus or other nutrient limitations in marginal settings, due to authigenic precipitation of phosphate with iron minerals in the oxic surface waters and sequestration of a range of elements by shelfal sediments (Ozaki and Tajika, 2013). If phosphate was a limiting nutrient, increasing bioavailable phosphorus would have enhanced local primary production and provided more favorable growth conditions for larger-sized unicellular phytoplankton (Marañón et al., 2001; Biddanda et al., 2001; Ward et al., 2014). With respect to the modern ocean system, the marine picocyanobacteria, Prochlorococcus and Synechococcus, are recognized to dominate phytoplankton cell counts and biomass in the oligotrophic tropical and subtropical ocean settings, including phosphate-limited oligotrophic regions of ocean-surface waters (Casey et al., 2016). Prochlorococcus and the heterotrophic SAR11 (Pelagibacter) flourish due to a variety of adaptations, including low-energy costs by virtue of small genomes and low replication rates, a higher surface-area-to-volume ratio through smaller cell sizes, and additional cell uptake functions to maximize nutrient utilization (Giovannoni, 2017). Many bacteria are also able to

substitute low-abundance nutrients, e.g., by utilizing sulfolipids instead of phosphorus-bearing lipids in P-deficient settings (Carini et al., 2015), or by use of alternative substrates, e.g., sourcing nitrogen from atmospheric N_2 via nitrogen fixation (Gruber and Sarmiento, 1997), to alleviate nutrient stress. A recent study regarding survival of marine bacterioplankton in oligotrophic environments (Temperton et al., 2011), where available phosphate is limited, suggests an important role for polyphosphate metabolism in marine oligotrophs. The select eukaryotes that compete in oligotrophic settings are typically small picoeukaryotes, which may supplement their nutritional requirements through mixotrophy (Rii et al., 2016). Picoeukaryote-to-cyanobacteria biomass ratio tends to increase under enhanced nutrient supply (Marañón et al., 2001). The possible influence of phosphorus, and other biolimiting nutrients, in moderating primary productivity and marine community structure in Ediacaran epeiric seaways requires further investigation.

Without exception, the abundance of C_{29} steranes is greater than the corresponding C_{27} or C_{28} steranes for all our locations (Table 2.4). A predominance of C_{29} over C_{27} and C_{28} steranes likely indicates a green-algae dominance within the eukaryotic phytoplankton community (Knoll et al., 2007 Kodner et al., 2008). This feature has been observed in most previous Ediacaran biomarker studies (Brocks et al., 2017; Grosjean et al., 2009; Kelly et al., 2011; Dutta et al., 2013; Lee et al., 2013 Duda et al., 2016; McKirdy et al., 2006; Bazhenova and Arefiev, 1996; Knoll et al., 2007). Notably, the C_{30} sterane distribution in several samples from each drill core in the Kotlin Horizon contains low, but detectable, amounts of the demosponge sterane biomarker known as 24-

isopropylcholestane (24-ipc) (Love et al., 2009; Love and Summons, 2015). In total, 24-ipc steranes have been reported in rock and oil samples dating as far back as the Cryogenian (>635 Ma ago) in the South Oman Salt Basin and represent the oldest lipid biomarker evidence for metazoans (Love et al., 2009 Love and Summons 2015).The 24-ipc biomarkers in our samples were either around one order of magnitude lower in abundance (relative to the total C_{27} to C_{30} sterane ratios, these were only 0.06–0.61%; mean=0.22%) compared with Ediacaran rocks and oils from South Oman (1.7% on average, (Love et al., 2009) or were below detection limits due to negligible abundance for the majority of samples.

3.3. Nitrogen and organic carbon isotope ratios

Nitrogen isotopes can help discern the relative balance in the nitrogen cycle, and the degree to which either nitrogen fixation or incomplete denitrification were significant pathways to influence the nutrient balance available for marine communities. When diazotrophic bacteria fix molecular nitrogen due to a lack of fixed nitrogen in the water column, this can yield sedimentary bulk nitrogen isotope values near 0‰ (Bauersachs et al., 2009). This is in contrast to the positive nitrogen isotope signatures (in the range of +2 to +10‰) with a mode of +4 to +6‰ found for the Neoproterozoic marine sediments deposited under what are thought to be nitrate-replete conditions where nitrate has only undergone partial denitrification (Ader et al., 2014). Nitrogen isotope values for all of our samples bar one outlier (Table 2.4) cover a limited positive range from +3.5 to +6.5‰, which overlaps with the mode for late Neoproterozoic organic-matter-rich sedimentary

rocks (Ader et al., 2014). Constrained by redox proxies suggesting that oxic water-column conditions prevailed, our data imply that nitrate dominated the dissolved inorganic nitrogen pool. The range of $\delta^{15}N$ values also suggests that N_2-fixation was not the primary mode of nitrogen acquisition for primary producers. Rather, the nitrogen cycle was likely dominated by water-column recycling, and organic N was subject to quantitative oxidation to nitrate as it is in modern, proximal marine settings. Benthic denitrification and organic N burial would have been the primary sinks for dissolved inorganic nitrogen, and the range of $\delta^{15}N$ values suggests only a limited role for incomplete water-column denitrification, which typically results in significant ^{15}N-enrichment (Sigman et al., 2009). The limited variability in $\delta^{15}N$ values therefore likely reflects $\delta^{15}N$ of nitrate advected onto the platform, with minor influence from limited water column nitrate reduction and N_2-fixation. Without strong $\delta^{15}N$ evidence for nitrogen fixation, we hypothesize that nitrogen was not the primary bio-limiting nutrient in the epicontinental basins of Baltica. Isolation from riverine and eolian sources of phosphorus, and oxic conditions in the broad, shallow-marine epicontinental basins may have enhanced the removal of authigenic phosphorite and trace-metal-bearing phases, resulting in nutrient limitation that con-strained eukaryotic cell growth and production.

Total organic carbon (C_{TOC}) isotope values range from –23.0 to –33.9‰, with the largest differences observed between the different drill-core locations. The relative ^{13}C-enrichment to isotope ratios higher than ca. –28‰ contrasts with data from contemporaneous strata deposited in the eutrophic, open-marine settings of Oman

(Grosjean et al., 2009; Lee et al., 2013). However, the range we report is generally consistent with the $\delta^{13}C_{TOC}$ range for other locations from Baltica deposited over the same time period (Johnston et al., 2012a). The difference between Baltica and Oman might highlight the fact that $\delta^{13}C_{TOC}$ values do not exclusively reflect a uniform secular change in the carbon cycle during this interval of time, (Lee et al., 2013; Johnston et al., 2012a). Rather, the $\delta^{13}C_{TOC}$ range from Baltica may, in part, reflect the bacterially dominated microbial ecology suggested by the unique lipid biomarker ratios. Small-cell size, high surface-area-to-volume ratios, and slow growth rates under oligotrophic conditions can increase the magnitude of the fractionation during autotrophy (ε_p) (Popp et al., 1998; Tolosa et al., 2008) resulting in low $\delta^{13}C$ values.

The mechanism for the more ^{13}C-enriched isotopic signatures within the range reported (Johnston et al., 2012a) for the late Ediacaran Baltica succession is less clear. The potential contribution of detrital, metamorphically altered organic matter to Precambrian low-TOC sedimentary successions is a possible mechanism for disparities between sites in $\delta^{13}C_{TOC}$ (Johnston et al., 2012b). However, the TOC content of our samples, while low, is generally greater than 0.10 wt%, revealing no relationships between TOC content and $\delta^{13}C$ values. Furthermore, our samples contain thermally immature organic matter and biomarker lipid patterns that are inconsistent with a mainly allochthonous carbon source. More ^{13}C-enriched $\delta^{13}C_{TOC}$ signatures may be the result of alternative mechanisms for carbon assimilation. Carbon-concentration mechanisms or active bicarbonate uptake by prokaryotes can result in smaller values for ε_p and higher $\delta^{13}C_{TOC}$

values (Hayes et al., 1993; Smith et al., 1999). The emergence of the Ediacaran biota may have significantly expanded marine food webs and stimulated new avenues of microbial heterotrophy, including possible contributions from complex carbon cycling within benthic microbial mats. With additional consideration for the potentially important role of dissolved organic matter (Sperling et al., 2011) as a carbon source, the breadth of $\delta^{13}C_{TOC}$ values likely reflects a range of biogeochemical carbon-cycling processes that might be unique to the evolving Ediacaran marine environment and may be related to a phenomenon for which we have no representative modern analogs.

Ancient lipid biomarker assemblages and stable isotope indicators for benthic, microbial mat production in tandem with fixed nitrogen limitation have been found in the early Triassic rocks from South China (Cao et al., 2009). In the aftermath of the end-Permian mass extinction at Meishan, there was a large spike in hopane/sterane ratios (up to ca. 60) accompanied by a strong shift in N_{org} isotope signature to values of 0 to–2‰, consistent with bacterial diazotrophy. This is associated with a high signal of 2-methylhopanes (2-methylhopane index up to 33%) and distinctive methylalkanes that point to the proliferation of benthic microbial mats. We do not observe a similar trend in nitrogen isotope signature or biomarker patterns that would obviously point to significant microbial mat input within our Ediacaran data set, although a singular ^{15}N-depleted value was found in our samples (Table 2.4). Therefore, the strong bacterial signal observed in our Baltica samples is likely not predominantly a signature of benthic microbial mats.

3.4. Paleoenvironmental sustenance of Ediacara biota vs. demosponges.

The apparent oligotrophic conditions across the epicratonic and continental margin basins of Baltica, as it drifted from high to low latitudes from the late Ediacaran to early Cambrian, might be associated with either limited advection of relatively nutrient-replete deep waters or nutrient depletion, resulting from assimilation and scavenging during transport and deposition across these broad, shallow-marine epicontinental basins (Fig. 2.5).These basins were episodically isolated from the oceans and developed hypersalinity (e.g., during the Redkino time) and brackish conditions (e.g., during the Kotlin time) (Bessonova et al., 1980). Long-term tectonic stability resulted in a low-relief topography of late Ediacaran Baltica, highly susceptible to flooding and inefficient supply of weathering-derived phosphorus. In contrast to Baltica, biomarker studies of the strata from the Huqf Supergroup in Oman revealed an eutrophic ecosystem, rich in microalgae (Love et al., 2009; Grosjean et al., 2009; Lee et al., 2013), but lacking Ediacara biota, even in extensive outcrops in the Oman Mountains and Huqf region, in the inner- to outer-shelf settings (Fike et al., 2006). The paleogeography of the South Oman Salt Basin has been reconstructed for the late Neoproterozoic at ~13° from the equator in the southern hemisphere, broadly similar to the Baltica (Kilner et al., 2005) paleolatitude.

We suggest that the oligotrophic conditions described here were caused by inefficient terrestrial and deep-water nutrient fluxes to these settings, broadly similar to those in oligotrophic environments in modern ocean systems. Indeed, a trace-element geochemical investigation of the Utkina Zavod and adjacent drill cores from the St.

Petersburg area suggests that our samples were deposited under oxic conditions (Grazhdankin and Maslov 2015). This interpretation is independently supported by our data from the extended hopane (C_{31}–C_{35}) distributions that tail off sharply in abundance above C_{31} compounds with increasing carbon number, which is characteristic of side-chain degradation of bacteriohopanepolyols during diagenesis under oxic conditions (Peters et al., 2005), and also by low-hydrogen indices, as measured by Rock-Eval pyrolysis (all lower than 230 mg/g TOC, and many are below 100 mg/g TOC) for these immature samples due to the formation of recalcitrant kerogen via oxidative degradation and recondensation of lipid-poor primary biomass in locally oxic environments (Table 2.2 and 2.3).The Ediacaran multicellular organisms that existed in these shallow-marine environments must have had sufficient organic substrates for heterotrophy to meet their feeding needs along with sufficient oxygen and other nutrients to sustain their metabolism. Epicontinental basins of Baltica were likely more persistently oxic than the highly productive settings that fringed oxygen-minimum zones, such as on the middle to the outer shelf of South Oman Salt Basin, where respiration of abundant planktonic biomass would have maintained lower dissolved oxygen below the photic zone.

Ediacara biota and other multicellular organisms living offshore of Baltica would have had to cope with changing food sources (bacterial vs. eukaryotic) as nutrient fluxes varied through time, including small cells and organic detritus in epicontinental basins where bacteria were the dominant primary producers (Fig. 2.5). Modern coral reef communities survive in tropical oligotrophic settings due to efficient recycling of nutrients, including

the generation of a dissolved organic matter (DOM) flux which helps sustain faunal heterotrophy within the reef ecosystem (de Goeij et al., 2008). The establishment of a marine trophic structure with eukaryotic multicellular organisms sustained by feeding on organic detritus had to postdate the global-scale environmental expansion of eukaryotes into diverse marine environments, which occurred through the Tonian–Cryogenian interval (ca. 800–635Ma), as gauged from biomarker records (Brocks et al., 2017). We might then expect to discern evidence for significant differences in marine community and trophic structure from locality to locality during the late Ediacaran period, with the local nutrient balance selecting for eukaryote-rich or eukaryote-lean microbial communities and with the progressive expansion of multicellular organisms adding another dimension of complexity at an organismal and community level. Significant regional contrast in phosphate and other nutrient availability in shelf environments is also an expected consequence of a heterogeneous global marine redox structure for the late Ediacaran, prior to the oxygenation of the deep ocean (Sperling et al., 2015).

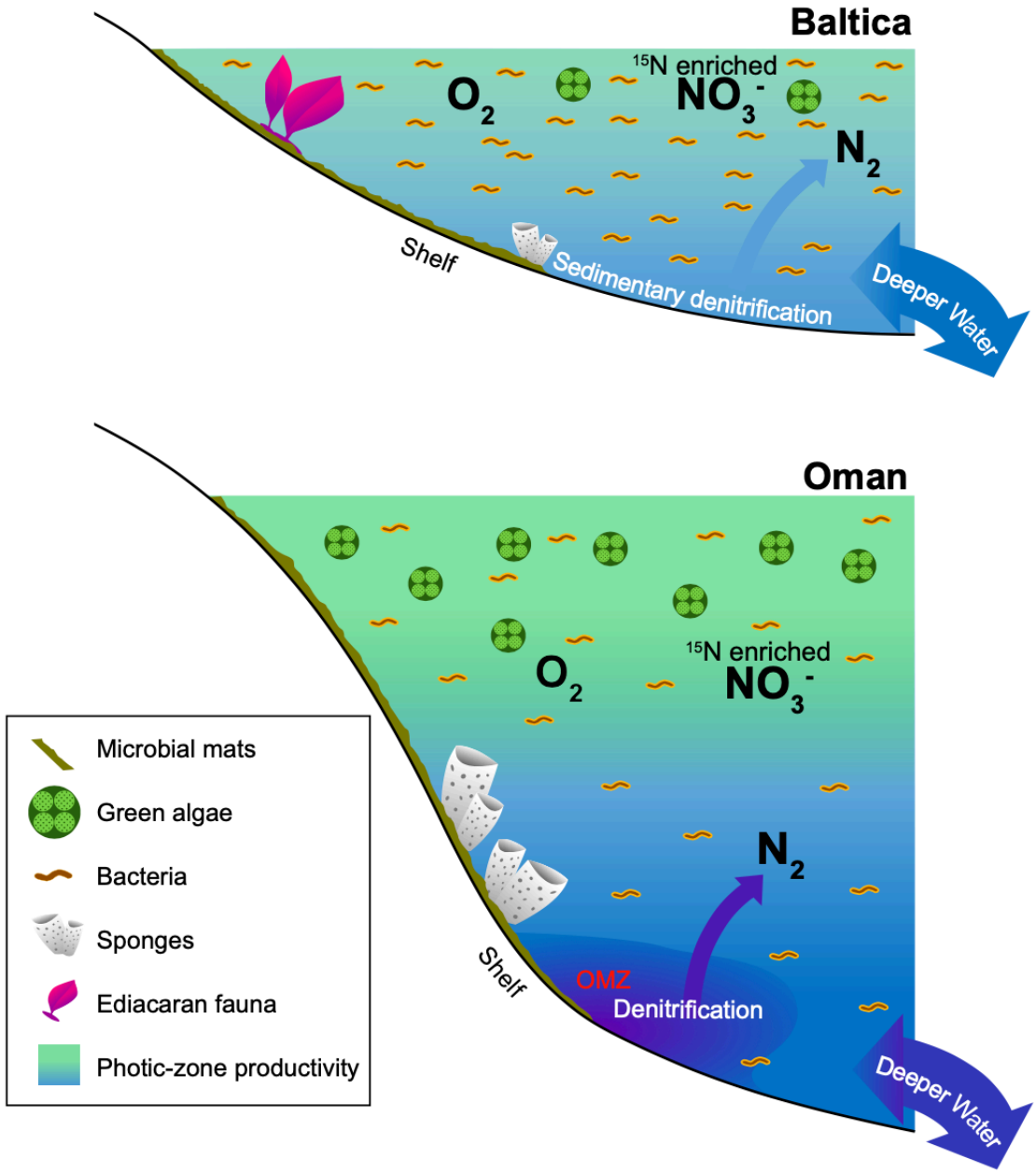

Figure 2.5. Major differences in low-productivity vs. productive Ediacaran marine environments. Schematic diagrams are shown for (a) extensive oligotrophic and shallow-marine epicontinental basin margins of Baltica often dominated by bacterial productivity where Ediacara soft-bodied fauna flourished and where denitrification and anammox likely were restricted to sediments; and (b) eutrophic and deeper-marine shelf settings of the South Oman Salt Basin, where green algae thrived as a primary producer and demosponges were abundant, but Ediacara soft-bodied fauna was not prominent (with Ediacara biota fossils also absent in correlative Ediacaran outcrops in northern Oman). On productive continental margins, denitrification and anammox likely occurred in both the water column and sediments

The dominance of picoplankton bacterial productivity and associated dissolved organic matter (DOM) degradation products in the Baltica epicontinental basins could have sustained amicrobial loop ecosystem in parallel with the conventional trophic structure based on around larger-sized planktonicproducers (Biddanda et al., 2001). This may have favored different modes of heterotrophy, including suspension feeding and, possibly, osmotrophy, as a viable feeding strategy for some rangeomorphs, sponges, and other late Ediacaran multicellular organisms (Laflamme et al., 2009) in conjunction with emerging active (motile) heterotrophy (Gehling et al., 2014; Droser et al., 2017). Nutrient-limited aquatic systems as a general rule are often dominated by small unicellular phytoplankton and heterotrophic plankton, with bacteria outcompeting eukaryotes, and sustaining low net biomass in oligotrophic marine settings of the modern ocean (Marañón et al., 2001; Ward et al., 2014). DOM is an important source of organic nutrients and often controls productivity and net biomass in modern oligotrophic tropical seas, but so is nitrogen and phosphorus colimitation (Mills et al., 2008). Similarly, DOM was also likely an important substrate for sustaining heterotrophic bacteria and a microbial loop in ancient oligotrophic settings. Benthic microbial mats may have been a component of this bacterially dominated food web, and matgrounds have been implicated to enhance the preservation of Ediacara biota in marine settings (Droser and Gehling, 2015). While moderate values of 2-methylhopane index were found for a subset of our samples (4–10%, Table 2.4), very low abundances of methylalkanes relative to n-alkanes (Fig. 2.1), and only trace and sporadic occurrences of carotenoids suggest that microbial mats did not dominate the primary productivity (Pawlowska et al., 2013), and that planktonic

bacteria and, correspondingly, their DOM breakdown products flourished. The generally low hydrogen-index values (Table 2.3; especially for Redkino samples), despite the low thermal maturity of the strata and biomarker assemblages, are also consistent with lipid-poor organic input in mainly oxic, shallow-marine marginal settings. Microbial mat occurrences as gauged only from sedimentological textures do not tell us about the balance of eukaryotes (microalgae) to bacteria in any case, nor can they constrain the relative contribution of microbial plankton to overall primary productivity and sustenance of food webs. Microbial mat communities that often contain abundant eukaryotes and the Ara Group carbonates from South Oman with prominent thrombolitic and crinkly laminite facies are a good example of late Neoproterozoic environments with significant microbial mat contribution, yielding abundant sterane signals due to a large contribution of microalgae (Grosjean et al., 2009 Love et al., 2009).

The extremely low level of 24-ipc biomarkers suggests that while demosponges were sometimes present, they were sparse in these environments. This could indicate fewer opportunities for smaller filter-feeding animals in competition with the Ediacara biota in these low-productivity settings, insufficient resilience of demosponges against more energetic shallow-marine conditions above the fair-weather wave base, or better adaptability of sponges to low-oxygen conditions dynamically maintained below the photic zone in eutrophic settings (Fig. 2.5). In total, 24-ipc was not detected in most of the samples of the Redkino Horizon, which also have generally the highest H/St ratios among our sample set, perhaps indicating an ecological change by the Kotlin Horizon

depositional time. Alternatively, it is also plausible that sponges did inhabit these settings, but did not produce these diagnostic steroid biomarkers in abundance, although this seems less likely as 24-ipc sterane is among the most commonly detected C_{30} sterane compounds in Ediacaran strata and oils (Grosjean et al., 2009; Lee et al., 2013; Kelly et al., 2011; Love et al., 2009; Love and Summons, 2015) and is also detectable in a subset of our samples (Table 2.4).

While the persistent oligotrophic marine environments suggested by our data represent localized conditions in the Ediacaran oceans, they were likely not uncommon for Precambrian shallow-marine seaways (Fig. 2.5). The vast majority of previous Ediacaran biomarker studies have been conducted on organic-rich sedimentary rocks deposited in eutrophic setting sand their petroleum products, which generally yield biomarker assemblages consistent with significant microalgal source contribution (Knoll et al., 2007). Our results highlight the importance of studying a wider variety of depositional environments, including organic-matter-lean strata of appropriate thermal maturity and different lithologies (Brocks et al., 2017; Grosjean et al., 2009; Duda et al., 2016; Love et al., 2009) in order to gain a more accurate picture for the scale of heterogeneity in marine chemistry and ecology from location to location. Despite progressive ocean ventilation and increased chemical weathering and nutrient supply during the breakup of Rodinia and throughout the Ediacaran Period (Peters and Gaines, 2012; McKenzie et al., 2014), ocean heterogeneity maintained a variety of marine chemical conditions, including nutrient-poor, but habitable environments that fostered metazoan adaptation, competition, and

evolution within the global ocean system (Fig. 2.5). While eutrophic marine shelves hosted demosponges, but often lacked the Ediacara biota, with the South Oman Salt Basin (and the correlative thick Ediacaran outcrops further north in Oman) being a prominent example; counterintuitively, shallow, oxic, and less-productive epicontinental seaways were colonized by the Ediacara biota in preference to demosponges despite DOM and other organic detritus being available locally for feeding. Whether metabolic requirements or environmental selective pressure restricted Ediacaran soft-bodied multicellular biota to these settings remains uncertain; however, our study highlights that Ediacaran oligotrophic settings played a potentially crucial role in the evolution of macroscopic multicellular organisms and marine community ecology.

Table 2.1. Sample details and locations for Ediacaran rocks used in this study

Sample	Drill Core/ Outcrop	Location	Formation/ Group	Regional Stratigraphic Horizon	Lithology
			Saint-Petersburg area, Baltic monocline, Russia		
UZ 1-9	Utkina Zavod	59.852778 N, 30.507222 E	Vasileostrovskaya Fm.	Kotlin	Green, silty mudstone
UZ 1-10	Utkina Zavod	59.852778 N, 30.507222 E	Vasileostrovskaya Fm.	Kotlin	Green/grey, silty mudstone with siderite
UZ 1-14	Utkina Zavod	59.852778 N, 30.507222 E	Vasileostrovskaya Fm.	Kotlin	Green, silty mudstone
UZ 1-20	Utkina Zavod	59.852778 N, 30.507222 E	Vasileostrovskaya Fm.	Kotlin	Green, silty mudstone
UZ 1-21	Utkina Zavod	59.852778 N, 30.507222 E	Vasileostrovskaya Fm.	Kotlin	Green to dark-grey, silty mudstone
UZ 1-22a	Utkina Zavod	59.852778 N, 30.507222 E	Vasileostrovskaya Fm.	Kotlin	Green, silty mudstone
UZ 1-22b	Utkina Zavod	59.852778 N, 30.507222 E	Vasileostrovskaya Fm.	Kotlin	Green, silty mudstone
UZ 1-26a	Utkina Zavod	59.852778 N, 30.507222 E	Vasileostrovskaya Fm.	Kotlin	Green, silty mudstone
UZ 1-26b	Utkina Zavod	59.852778 N, 30.507222 E	Vasileostrovskaya Fm.	Kotlin	Green to grey, silty mudstone
UZ 1-27	Utkina Zavod	59.852778 N, 30.507222 E	Vasileostrovskaya Fm.	Kotlin	Green, silty mudstone
UZ 1-28	Utkina Zavod	59.852778 N, 30.507222 E	Vasileostrovskaya Fm.	Kotlin	Green, silty mudstone
L-13-41	Lugovoe #13	60.695000 N, 30.195833 E	Vasileostrovskaya Fm.	Kotlin	Green, silty mudstone
L-13-44	Lugovoe #13	60.695000 N, 30.195833 E	Vasileostrovskaya Fm.	Kotlin	Green, silty mudstone
L-13-47	Lugovoe #13	60.695000 N, 30.195833 E	Vasileostrovskaya Fm.	Kotlin	Green, silty mudstone
L-13-71	Lugovoe #13	60.695000 N, 30.195833 E	Staraya Russa Fm.	Redkino	Green mudstone/siltstone
L-13-73	Lugovoe #13	60.695000 N, 30.195833 E	Staraya Russa Fm.	Redkino	Green, silty mudstone
L-13-75	Lugovoe #13	60.695000 N, 30.195833 E	Staraya Russa Fm.	Redkino	Green, silty mudstone
			Moscow Basin, Russia		
87-13	Gavrilov Yam -1	57.31111111 N, 39.91361111 E	Lezhskaya Fm.	Lontova	Grey siltstone
87- 25	Gavrilov Yam -1	57.31111111 N, 39.91361111 E	Reshminskaya Fm.	Kotlin	Grey siltstone
			Northwestern part of the Volyn area (close to city Kovel), Ukraine		
4-13	4529	Village Poliske; 51.477429 N, 24.514081 E	Kanyliv Gr.	Upper Kotlin	Grey siltstones interlayered with sandstones and mudstones
4-24	4529	Village Poliske; 51.477429 N, 24.514081 E	Kanyliv Gr.	Upper Kotlin	Grey siltstone interlayered with sandstone and mudstone
4-15	4504	Village Tur, next to Lake Tur; 51.680686 N, 24.282324 E	Kanyliv Gr.	Upper Kotlin	Mica-rich, chocolate-brown siltstones
3-13	4592	Village Kamianukha; 51.237161 N, 25.718928 E	Roznychi Fm.; Mohyliv-Podilsky Gr.	Upper Redkino	Dark-brown mudstones with mica-rich siltstones

Table 2.1. continued

Northern part of the Podillya Basin, between the cities of Khmelnitsky and Rivne, Ukraine					
226.5	3628	Village Denysivka, River Semenivka; 49.921217 N, 26.458906 E	Mohyliv-Podilsky	Uppermost Redkino	Light-brown mudstones with phosphorites
291	3628	Village Denysivka, River Semenivka; 49.921217 N, 26.458906 E	Mohyliv-Podilsky	Middle Redkino	Light-grey micaceous mudstone with interlayers of siltstone and sandstone
332	3628	Village Denysivka, River Semenivka; 49.921217 N, 26.458906 E	Mohyliv-Podilsky	Middle to low Redkino	Greenish-grey and grey mudstone with thin interlayers of siltstone
Southern part of the Podillya Basin, right bank of the Dniester river, Moldova					
16PL-22	16PL Outcrop	Village Naslavcea; 48.465779 N, 27.583773 E	Mohyliv-Podilsky	Upper Redkino	Dark-grey phosphorite-bearing mudstone
16PL-18	16PL Outcrop	Village Naslavcea, open pit near the Dniester river; 48.480442 N, 27.562998 E	Mohyliv-Podilsky	Upper Redkino	Dark-grey phosphorite-bearing mudstone
16PL-11	16PL Outcrop	Village Naslavcea, open pit near the Dniester river; 48.480442 N, 27.562998 E	Mohyliv-Podilsky	Upper Redkino	Dark-grey phosphorite-bearing mudstone

Table 2.2. Total organic content

Sample	Drill Core/ Outcrop	Location	Stage	Horizon	Depth (m)	Carbonate (wt %)	TOC (wt %)
UZ 1-9	Utkina Zavod	Baltic Monocline	Late Ediacaran	Kotlin	64.15	3.75	0.42
UZ 1-10	Utkina Zavod	Baltic Monocline	Late Ediacaran	Kotlin	71.67	4.96	0.34
UZ 1-14	Utkina Zavod	Baltic Monocline	Late Ediacaran	Kotlin	87	1.32	0.27
UZ 1-20	Utkina Zavod	Baltic Monocline	Late Ediacaran	Kotlin	111.6	14.37	0.67
UZ 1-21	Utkina Zavod	Baltic Monocline	Late Ediacaran	Kotlin	119.9	2.89	0.40
UZ 1-22a	Utkina Zavod	Baltic Monocline	Late Ediacaran	Kotlin	124.6	4.48	0.52
UZ 1-22b	Utkina Zavod	Baltic Monocline	Late Ediacaran	Kotlin	127.8	7.28	0.76
UZ 1-26a	Utkina Zavod	Baltic Monocline	Late Ediacaran	Kotlin	152.8	11.19	0.31
UZ 1-26b	Utkina Zavod	Baltic Monocline	Late Ediacaran	Kotlin	153.5	38.39	0.27
UZ 1-27	Utkina Zavod	Baltic Monocline	Late Ediacaran	Kotlin	162.1	2.33	0.44
UZ 1-28	Utkina Zavod	Baltic Monocline	Late Ediacaran	Kotlin	171.4	7.98	0.21
L-13-41	Lugovoe #13	Baltic Monocline	Late Ediacaran	Kotlin	41	5.22	0.48
L-13-44	Lugovoe #13	Baltic Monocline	Late Ediacaran	Kotlin	44	10.53	0.44
L-13-47	Lugovoe #13	Baltic Monocline	Late Ediacaran	Kotlin	47	7.63	0.51
L-13-71	Lugovoe #13	Baltic Monocline	Late Ediacaran	Redkino	71	9.34	1.06
L-13-73	Lugovoe #13	Baltic Monocline	Late Ediacaran	Redkino	73	8.43	0.85
L-13-75	Lugovoe #13	Baltic Monocline	Late Ediacaran	Redkino	75	10.17	0.49
87-13	Gavrilov Yam-1	Moscow Syneclise	Early Cambrian	Lontovan	1860	2.43	0.23
87-25	Gavrilov Yam-1	Moscow Syneclise	Late Ediacaran	Kotlin	2018	3.25	0.26
4-15	4529	Volyn Basin	Late Ediacaran	Kotlin	~195	56.53	0.12
4-13	4529	Volyn Basin	Late Ediacaran	Kotlin	~207	12.89	0.09
4-24	4504	Volyn Basin	Late Ediacaran	Kotlin	~200	10.47	0.13
3-13	4592	Volyn Basin	Late Ediacaran	Redkino	~166	19.16	0.47
226.5	3628	Podillya Basin	Late Ediacaran	Redkino	226.5	36.32	0.30
291	3628	Podillya Basin	Late Ediacaran	Redkino	291	8.01	0.43
332	3628	Podillya Basin	Late Ediacaran	Redkino	332	13.22	0.18
16PL-22	16PL	Podillya Basin	Late Ediacaran	Redkino	Surface Outcrop	9.51	0.50
16PL-18	16PL	Podillya Basin	Late Ediacaran	Redkino	Surface Outcrop	12.15	0.23
16PL-11	16PL	Podillya Basin	Late Ediacaran	Redkino	Surface Outcrop	20.96	0.21

Table 2.3. Select Rock-Eval parameters and lipid biomarker ratios for thermal maturity

Sample	Tmax (°C)	Hydrogen Index	C_{27}hop Ts/(Ts+Tm)	C_{31}hop αβ 22S/(S+R)	C_{31}hop ββ/ (ββ+αβ+βα)	C_{29}ster ααα 20S/(20S+20R)
UZ 1-9	431	143	0.09	0.13	0.110	0.06
UZ 1-10	428	131	0.14	0.15	0.113	0.06
UZ 1-14	427	219	0.16	0.19	0.054	0.07
UZ 1-20	419	199	0.15	0.16	0.099	0.06
UZ 1-21	425	172	0.13	0.15	0.061	0.06
UZ 1-22a	426	118	0.17	0.17	0.075	0.06
UZ 1-22b	428	221	0.15	0.15	0.069	0.07
UZ 1-26a	428	190	0.16	0.24	0.041	0.08
UZ 1-26b	426	170	0.15	0.25	0.037	0.05
UZ 1-27	427	195	0.11	0.21	0.047	0.06
UZ 1-28	426	157	0.08	0.22	0.056	0.08
L-13-41	424	76	0.09	0.20	0.040	0.10
L-13-44	427	95	0.09	0.19	0.021	0.07
L-13-47	425	80	0.09	0.17	0.033	0.09
L-13-71	417	85	0.08	0.17	0.041	0.12
L-13-73	417	112	0.09	0.18	0.037	0.15
L-13-75	n/a	28	0.13	0.27	0.032	0.11
87-13	433	217	0.02	0.47	0.009	0.13
87- 25	433	218	0.02	0.58	0.006	0.18
4-15	n/a	83	0.07	0.16	0.143	0.04
4-13	n/a	114	0.05	0.18	0.106	0.05
4-24	n/a	148	0.03	0.31	0.028	0.07
3-13	421	57	0.01	0.35	0.007	0.10
226.5	425	113	0.05	0.49	0.002	0.16
291	426	67	0.02	0.56	0.002	0.22
332	n/a	44	0.01	0.59	0.001	0.22
16PL-22	443	94	0.26	0.60	0.000	0.38
16PL-18	n/a	22	0.20	0.60	0.000	0.33
16PL-11	n/a	10	0.25	0.62	0.000	0.40

Table 2.4. Select lipid biomarker ratios and carbon and nitrogen stable isotope data for source biota and depositional environmental assessments

Sample	∑ Steranes (µg/gTOC)	∑ Hopanes (µg/gTOC)	Hop/Ster[1]	gammacerane/ C_{30}hop	2MeH/3MeH	2MeH Index (%)[2]	3MeH Index (%)[3]	% C_{29} steranes[4]	% C_{28} steranes[4]	% C_{27} steranes[4]	% C_{30}ipc steranes[4,5]	$C30_{ipc}/C30_{npc}$[6]	$\delta^{15}N_{total}$ (‰ vs air)	$\delta^{13}C_{TOC}$ (‰ VPDB)
UZ 1-9	21.03	71.78	3.4	0.03	5.2	8.1	1.7	64	14	21	n.d.7	0.0	5.0	-23.8
UZ 1-10	29.50	48.20	1.6	0.03	1.7	5.1	3.1	64	14	21	0.07	0.6	4.2	-25.9
UZ 1-14	5.23	20.50	3.9	0.03	1.3	7.0	5.5	65	14	21	0.08	0.4	4.7	-26.0
UZ 1-20	48.64	157.44	3.2	0.05	1.8	7.3	4.1	59	16	25	0.10	0.9	4.9	-23.0
UZ 1-21	17.74	135.90	7.7	0.02	3.8	5.7	1.6	62	16	22	n.d.	0.0	4.4	-23.6
UZ 1-22a	13.02	47.42	3.6	0.03	2.6	8.2	3.3	64	14	22	n.d.	0.0	4.7	-24.1
UZ 1-22b	38.11	286.56	7.5	0.02	4.0	8.5	2.3	63	14	22	n.d.	0.0	4.6	-23.1
UZ 1-26a	7.80	37.24	4.8	0.04	4.4	7.1	1.7	68	15	17	0.10	0.5	4.6	-25.4
UZ 1-26b	16.85	83.98	5.0	0.04	4.4	8.2	2.0	72	13	15	0.06	0.5	4.4	-24.2
UZ 1-27	12.24	61.71	5.0	0.04	3.3	5.9	1.9	67	14	18	n.d.	0.0	4.3	-25.2
UZ 1-28	19.74	78.26	4.0	0.04	3.1	9.9	3.4	70	14	16	0.15	0.7	4.1	-25.0
L-13-41	17.15	123.55	7.2	0.03	0.7	1.5	2.1	47	20	32	0.41	0.7	3.6	-30.0
L-13-44	7.33	61.01	8.3	0.02	0.0	0.2	3.7	57	16	27	0.61	1.2	4.5	-32.9
L-13-47	14.64	29.98	2.0	0.03	0.1	0.3	3.9	58	16	25	0.32	1.9	4.5	-33.9
L-13-71	4.11	144.95	35.3	0.01	0.1	0.1	0.9	50	21	24	n.d.	0.0	3.9	-33.1
L-13-73	1.39	101.89	73.4	0.01	0.1	0.1	0.8	40	26	23	n.d.	0.0	3.6	-32.8
L-13-75	0.44	13.02	29.5	0.02	0.7	0.4	0.7	53	21	20	n.d.	0.0	4.2	-29.6
87-13	4.12	114.85	27.8	0.00	2.7	3.9	1.5	44	28	26	n.d.	0.0	6.5	-31.2
87- 25	0.10	2.19	22.2	0.01	6.4	4.2	0.7	47	18	35	n.d.	0.0	4.9	-25.2
4-15	5.93	135.47	22.8	0.02	15.8	9.9	0.7	52	24	24	n.d.	0.0	4.6	-27.5
4-13	0.12	13.74	25.9	0.00	13.0	7.3	0.6	56	20	24	n.d.	0.0	4.9	-27.0
4-24	0.43	11.25	22.5	0.00	9.1	7.2	0.8	45	21	34	0.18	0.3	4.7	-27.6
3-13	0.69	15.43	119.2	0.01	1.5	0.4	0.2	73	9	15	n.d.	0.0	3.5	-31.6
226.5	12.89	207.44	16.1	0.01	2.1	5.1	2.4	65	14	21	n.d.	0.0	5.5	n/a
291	4.47	165.39	36.9	0.01	0.3	0.7	2.7	63	17	19	0.36	0.9	-2.8	-30.9
332	0.91	79.77	87.9	0.04	1.3	0.3	0.2	66	13	21	0.19	0.3	n/a	-33.1
16PL-22	1.14	9.17	8.1	0.13	2.2	5.4	2.6	48	22	30	n.d.	0.0	6.0	-26.8
16PL-18	0.76	8.44	11.1	0.09	2.3	5.6	2.5	51	21	27	n.d.	0.0	6.0	-27.0
16PL-11	0.55	6.35	11.5	0.10	2.3	5.9	2.7	65	15	20	n.d.	0.0	6.2	-24.0

[a]Hop/Ster is the ratio of major (C27–C35 hopane isomers)/(C_{27}–C_{30} diasteranes and regular steranes)
[b]C_{31} 2-methylhopane index (2-MeH index) calculated as [(C_{31} 2α-methylhopane+C_{31} 2β-methylhopane)/(C_{31} 2α-methylhopane+C_{31} 2β-methylhopane+C_{30} αβ hopane)*100]
[c]C_{31} 3-methylhopane index (3-MeH index) calculated as [(C_{31} 3β-methylhopane)/(C_{31} 3β-methylhopane+C_{30} αβ hopane)*100]
[d]Relative percent of Cn steranes to total C_{27}–C_{30} steranes
[e]24-isopropylcholestane abbreviated as C_{30} ipc
[f]24-n-propylcholestane abbreviated as C_{30} npc
[g]Not detected (n.d.) indicates that the peaks were below MRM–GC–MS detection limits due to negligible abundance

REFERENCES

Ader, M., Sansjofre, P., Halverson, G.P., Busigny, V., Trindade, R.I.F., Kunzmann, M., and Nogueira, A.C.R., 2014. Ocean redox structure across the Late Neoproterozoic Oxygenation Event: A nitrogen isotope perspective: *Earth and Planetary Science Letters* 396, 1–13, doi: 10.1016/j.epsl.2014.03.042.

Aksenov, E.M., Volkova, S.A., 1969. Volcanogenic-Sedimentary Horizons of Redkino Suite of Valday Series: D*oklady Akademii Nauk SSSR*, 188:3, 635-639.

Bauersachs, T., Schouten, S., Compaoré, J., Wollenzien, U., Stal, L.J., Damsteé, J.S.S., 2009. Nitrogen isotopic fractionation associated with growth on dinitrogen gas and nitrate by cyanobacteria. *Limnology and Oceanography* 54, 1403–1411.

Bazhenova, O.K., and Arefiev, O.A., 1996. Geochemical peculiarities of Pre-Cambrian source rocks in the East European Platform: *Organic Geochemistry* 25:5-7, 341–351, doi: 10.1016/S0146-6380(96)00138-6.

Bessonova, V.Ya., Velikanov, V.A., Keller, B.M., Kirsanov, V.V., 1980. Valday Epoch. In: Keller, B.M., Rozanov, A.Yu. (Eds.), Palaeogeography and lithology of Vendian and Cambrian of the western part of the East-European platform. Nauka, Moscow, USSR 15-24, *in Russian*

Biddanda, B., Ogdahl, M., and Cotner, J., 2001. Dominance of bacterial metabolism in oligotrophic relative to eutrophic waters: *Limnology & Oceanography* 46:3, 730-739, doi: 10.4319/lo.2001.46.3.0730

Bowyer, F., Wood, R.A., and Poulton, S.W., 2017. Controls on the evolution of Ediacaran metazoan ecosystems: A redox perspective: *Geobiology* 16:10, 339, doi: 10.1111/gbi.12232.

Brocks, J.J., Jarrett, A.J.M., Sirantoine, E., Hallmann, C., Hoshino, Y., Liyanage, T., 2017. The rise of algae in Cryogenian oceans and the emergence of animals. *Nature* 548, 578–581, doi: 10.1038/nature23457

Burzin, M.B., 1996. Late Vendian (Neoproterozoic III) microbial and algal communities of the Russian Platform: models of facies-dependent distribution, evolution and reflection of basin development. *Rivista Italiana di Paleontologia e Stratigrafia*, v. 102:3, 307-315.

Cao, C., Love, G.D., Hays, L.E., Wang, W., Shen, S., Summons, R.E., 2009. Biogeochemical evidence for euxinic oceans and ecological disturbance presaging the end-Permian mass extinction event. *Earth and Planetary Science Letters* 281, 188–201, doi:10.1016/j.epsl.2009.02.012

Carini, P., Van Mooy, B.A.S., Thrash, J.C., White, A., Zhao, Y., Campbell, E.O., Fredricks, H.F., and Giovannoni, S.J., 2015. SAR11 lipid renovation in response to phosphate starvation: *Proceedings of the National Academy of Sciences*, 112:25, 7767–7772, doi: 10.1073/pnas.1505034112.

Casey, J.R., Mardinoglu, A., Nielsen, J., Karl, D.M., 2016. Adaptive Evolution of Phosphorus Metabolism in Prochlorococcus. *mSystems* 1, e00065-16, doi: 10.1128/msystems.00065-16

Coplen, T.B., Brand, W.A., Gehre, M., Gröning, M., Meijer, H.A.J., Toman, B., Verkouteren, R.M., 2006. New Guidelines for δ 13 C Measurements. *Analytical Chemistry* 78, 2439–2441, doi: 10.1021/ac052027c

de Goeij, J.M., Oevelen, D. van, Vermeij, M.J.A., Osinga, R., Middelburg, J.J., Goeij, A.F.P.M. de, Admiraal, W., 2013. Surviving in a marine desert: the sponge loop retains resources within coral reefs. *Science*, 342, 108–10.

Droser, M.L., and Gehling, J.G., 2015. The advent of animals: The view from the Ediacaran: *Proceedings of the National Academy of Sciences*, 112, 4865–4870, doi: 10.1073/pnas.1403669112.

Droser, M.L., Tarhan, L.G., Gehling, J.G., 2017. The Rise of Animals in a Changing Environment: Global Ecological Innovation in the Late Ediacaran. *Annual Review of Earth and Planetary Sciences* 45, 593–617, doi: 10.1146/annurev-earth-063016-015645

Duda, J.-P., Thiel, V., Reitner, J., Grazhdankin, D., 2016. Opening up a window into ecosystems with Ediacara-type organisms: preservation of molecular fossils in the Khatyspyt Lagerstätte (Arctic Siberia). *PalZ* 90, 659–671, doi: 10.1007/s12542-016-0317-5

Dutta, S., Bhattacharya, S., and Raju, S.V., 2013. Biomarker signatures from Neoproterozoic-Early Cambrian oil, western India: *Organic Geochemistry*, 56, 68–80, doi: 10.1016/j.orggeochem.2012.12.007.

Fedorova, N.M., Levashova, N.M., Bazhenov, M.L., Meert, J.G., Sergeeva, N.D., Golovanova, I.V., Danukalov, K.N., Kuznetsov, N.B., Kadyrov, A.F., and Khidiyatov, M.M., 2013. The East European Platform in the late Ediacaran: new paleomagnetic and geochronological data: *Russian Geology and Geophysics*, 54, 1392–1401, doi: 10.1016/j.rgg.2013.10.003.

Fedonkin, M.A., Waggoner, B.M., 1997. The Late Precambrian fossil Kimberella is a mollusc-like bilaterian organism. *Nature* 388, 868–871, doi: 10.1038/42242

Fike, D.A., Grotzinger, J.P., Pratt, L.M., and Summons, R.E., 2006. Oxidation of the Ediacaran Ocean: *Nature*, v. 444, no. 7120, p. 744–747, doi: 10.1038/nature05345.

Gehling, J.G., Rigby, J.K., 1996. Long expected sponges from the Neoproterozoic Ediacara fauna of South Australia. *Journal of Paleontology* 70, 185–195, doi:10.1017/s0022336000023283

Gehling, J.G., Runnegar, B.N., Droser, M.L., 2014. Scratch Traces of Large Ediacara Bilaterian Animals. *Journal of Paleontology* 88, 284–298. doi: 10.1666/13-054

Giovannoni, S.J., 2017. SAR11 Bacteria: The Most Abundant Plankton in the Oceans: *Annual Review of Marine Science*, 9, 231–255, doi: 10.1146/annurev-marine-010814-015934.

Grazhdankin, D.V., 2014. Patterns of Evolution of the Ediacaran Soft-Bodied Biota: *Journal of Paleontology*, 88, 269–283, doi: 10.1666/13-072.

Grazhdankin, D.V., Maslov, A.V., 2015. The room for the Vendian in the International Chronostratigraphic Chart: *Russian Geology and Geophysics*, 56, 549-559, doi: 10.1016/j.rgg.2015.03.007

Grosjean, E., Love, G.D., Stalvies, C., Fike, D.A., and Summons, R.E., 2009. Origin of petroleum in the Neoproterozoic–Cambrian South Oman Salt Basin: *Organic Geochemistry*, 40, 87–110, doi: 10.1016/j.orggeochem.2008.09.011.

Gruber, N., and Sarmiento, J.L., 1997. Global patterns of marine nitrogen fixation and denitrification: *Global Biogeochemical Cycles*, 11, 235–266, doi: 10.1029/97GB00077.

Haddad, E.E., Tuite, M.L., Martinez, A.M., Williford, K., Boyer, D.L., Droser, M.L., Love, G.D., 2016. Lipid biomarker stratigraphic records through the Late Devonian Frasnian/Famennian boundary: Comparison of high- and low-latitude epicontinental marine settings. *Organic Geochemistry* 98, 38–53, doi: 10.1016/j.orggeochem.2016.05.007

Hayes, J.M., 1993. Factors controlling ^{13}C contents of sedimentary organic compounds: Principles and evidence. *Marine Geology* 113, 111–125, doi: 10.1016/0025-3227(93)90153-m

Ivantsov, A.Yu., Gritsenko, V.P., Paliy, V.M., Velikanov, V.A., Menasova, A.Sh., Fedonkin, M.A., Zakrevskaya, M.A., Serezhnikova, E.A. 2015. Upper Vendian macrofossils of Eastern Europe. 1–146

Johnston, D.J., Poulton, S.W., Goldberg, T., Sergeev, V.N., Podkovyrov, Vorob'eva N.G., Bekker A., and Knoll, A.H., 2012a. Late Ediacaran redox stability and metazoan evolution: *Earth and Planetary Science Letters*, 335-336, 25-35, doi: 10.1016/j.epsl.2012.05.010

Johnston, D.T., Macdonald, F.A., Gill, B.C., Hoffman, P.F., Schrag, D.P., 2012b. Uncovering the Neoproterozoic carbon cycle. *Nature* 483, 320–3, doi: 10.1038/nature10854

Kelly, A.E., Love, G.D., Zumberge, J.E., and Summons, R.E., 2011. Hydrocarbon biomarkers of Neoproterozoic to Lower Cambrian oils from eastern Siberia: *Organic Geochemistry*, 42, 640–654, doi: 10.1016/j.orggeochem.2011.03.028.

Kilner, B., Niocaill, C., and Brasier, M., 2005. Low-latitude glaciation in the Neoproterozoic of Oman: *Geology*, 33, 413, doi: 10.1130/G21227.1.

Klein, R., Salminen, J., and Mertanen, S., 2015. Baltica during the Ediacaran and Cambrian: A paleomagnetic study of Hailuoto sediments in Finland: *Precambrian Research*, 267, 94–105, doi: 10.1016/j.precamres.2015.06.005.

Knoll, A.H., Summons, R.E., Waldbauer, and J., Zumberge, J., 2007. The geological succession of primary producers in the oceans. In: Falkowski, P., Knoll, A.H. (Eds.), The Evolution of Primary Producers in the Sea. Elsevier, Burlington, 133–163.

Kodner, R.B., Pearson, A., Summons, R.E., and Knoll, A.H., 2008. Sterols in red and green algae: quantification, phylogeny, and relevance for the interpretation of geologic steranes: *Geobiology*, 6, 411–420, doi: 10.1111/j.1472-4669.2008.00167.x.

Kolesnikov, A.V., Marusin, V.V., Nagovitsin, K.E., Maslov, A.V., and Grazhdankin, D.V., 2015. Ediacaran biota in the aftermath of the Kotlinian Crisis: Asha Group of the South Urals: *Precambrian Research*, 263, 59–78, doi: 10.1016/j.precamres.2015.03.011.

Laflamme, M., Darroch, S.A.F., Tweedt, S.M., Peterson, K.J., Erwin, D.H., 2013. The end of the Ediacara biota: Extinction, biotic replacement, or Cheshire Cat? *Gondwana Research* 23, 558–573, doi: 10.1016/j.gr.2012.11.004

Lee, C., Fike, D.A., Love, G.D., Sessions, A.L., Grotzinger, J.P., Summons, R.E., and Fischer, W.W., 2013. Carbon isotopes and lipid biomarkers from organic-rich facies of the Shuram Formation, Sultanate of Oman: *Geobiology*, 11, 406–419, doi: 10.1111/gbi.12045.

Lenton, T.M., Boyle, R.A., Poulton, S.W., Shields-Zhou, G.A., and Butterfield, N.J., 2014. Co-evolution of eukaryotes and ocean oxygenation in the Neoproterozoic era: *Nature Geoscience*, 7, 257–265, doi: 10.1038/ngeo2108.

Li, C., Planavsky, N.J., Shi, W., Zhang, Z., Zhou, C., Cheng, M., Tarhan, L.G., Luo, G., and Xie, S., 2015. Ediacaran Marine Redox Heterogeneity and Early Animal Ecosystems: *Scientific Reports*, 5, 17097, doi: 10.1038/srep17097.

Liu, A.G., Kenchington, C.G., Mitchell, E.G., 2015. Remarkable insights into the paleoecology of the Avalonian Ediacaran macrobiota. *Gondwana Research* 27, 1355–1380. doi: 10.1016/j.gr.2014.11.002

Love, G.D., Snape, C.E., Carr, A.D., Houghton, R.C., 1995. Release of covalently-bound alkane biomarkers in high yields from kerogen via catalytic hydropyrolysis. *Organic Geochemistry* 23, 981–986, doi: 10.1016/0146-6380(95)00075-5

Love, G.D., Grosjean, E., Stalvies, C., Fike, D.A., Grotzinger, J.P., Bradley, A.S., Kelly, A.E., Bhatia, M., Meredith, W., Snape, C.E., Bowring, S.A., Condon, D.J., and Summons, R.E., 2009. Fossil steroids record the appearance of Demospongiae during the Cryogenian period: *Nature*, 457, 7230, p. 718–721, doi: 10.1038/nature07673.

Love, G.D., Summons, R.E., Smith, A., 2015. The molecular record of Cryogenian sponges - a response to Antcliffe (2013). *Palaeontology* 58, 1131–1136, doi: 10.1111/pala.12196

Marañón, E., Holligan, P., Barciela, R., González, N., Mouriño, B., Pazó, M., Varela, M., 2001. Patterns of phytoplankton size structure and productivity in contrasting open-ocean environments. *Marine Ecology Progress* Series 216, 43–56, doi: 10.3354/meps216043.

Martin, M.W., Grazhdankin, D.V., Bowring, S.A., Evans, D.A.D., Fedonkin, M.A., Kirschvink, J.L., 2000. Age of Neoproterozoic Bilatarian Body and Trace Fossils, White Sea, Russia: Implications for Metazoan Evolution. *Science* 288, 841–845, doi: 10.1126/science.288.5467.841

Marusin, V.V., Grazhdankin, D.V., and Maslov, A.V., 2011. Redkino stage in evolution of Vendian macrophytes: *Doklady Earth Sciences*, 436, 197–202, doi: 10.1134/S1028334X11020176.

McKenzie, N. R., Hughes, N. C., Gill, B. C., and Myrow, P. M., 2014. Plate tectonic influences on Neoproterozoic-early Paleozoic climate and animal evolution: *Geology*, 42, 127–130,

McKirdy, D.M., Webster, L.J., Arouri, K.R., Grey, K.G., and Gostin V.A., 2006. Contrasting sterane signatures in Neoproterozoic marine rocks of Australia before and after the Acraman asteroid impact: *Organic Geochemistry*, 37, 189-207, doi: 10.1016/j.orggeochem.2005.09.005

Mills, M.M., Moore, C.M., Langlois, R., Milne, A., Achterberg, E., Nachtigall, K., Lochte, K., Geider, R.J., La, R.J., 2008. Nitrogen and phosphorus co-limitation of bacterial productivity and growth in the oligotrophic subtropical North Atlantic. *Limnology and Oceanography* 53, 824–834, doi: 10.4319/lo.2008.53.2.0824

Narbonne, G.M., 2005. The Ediacara Biota: Neoproterozoic Origin of Animals and Their Ecosystems: *Annual Review of Earth and Planetary Sciences*, 33, 421–442, doi: 10.1146/annurev.earth.33.092203.122519.

Nehring-Lefeld M., Modliński, Z., and Swadowska,E., 1997. Thermal evolution of the Ordovician in the western margin of the East-European Platform: CAl and Ro data: *Geological Quarterly*, 41, 129-138.

Olson, S.L., Reinhard, C.T., and Lyons, T.W., 2016. Cyanobacterial Diazotrophy and Earth's Delayed Oxygenation: *Frontiers in Microbiology*, 7, 1903, doi: 10.3389/fmicb.2016.01526.

Ozaki, K., Tajika, E., 2013. Biogeochemical effects of atmospheric oxygen concentration, phosphorus weathering, and sea-level stand on oceanic redox chemistry: Implications for greenhouse climates. *Earth and Planetary Science Letters* 373, 129–139, doi:10.1016/j.epsl.2013.04.029

Pawlowska, M.M., Butterfield, N.J., and Brocks, J.J., 2013. Lipid taphonomy in the Proterozoic and the effect of microbial mats on biomarker preservation: *Geology,* 41, 103-106.

Pease, V., Daly, J.S., Elming, S.Å., Kumpulainen, R., Moczydlowska, M., Puchkov, V., Roberts, D., Saintot, A., and Stephenson, R., 2008. Baltica in the Cryogenian, 850–630 Ma: *Precambrian Research*, 160, 46–65, doi: 10.1016/j.precamres.2007.04.015.

Peters, K.E., Walters, C.C., and Moldowan, J.M., 2005. The Biomarker Guide: Cambridge University Press, Cambridge, UK.

Peters, S.E., Gaines, R.R., 2012. Formation of the 'Great Unconformity' as a trigger for the Cambrian explosion: *Nature*, 484, 363-366, doi:10.1038/nature10969.

Pirrus, E. 1992. Freshening of the Late Vendian Basin on the East European Craton. *Proc. Est. Acad. Sci. Geol*. 41, 115–123.

Planavsky, N.J., Rouxel, O.J., Bekker, A., Lalonde, S.V., Konhauser, K.O., Reinhard, C.T., Lyons, T.W., 2010. The evolution of the marine phosphate reservoir. *Nature* 467, 1088–1090, doi:10.1038/nature09485

Planavsky, N.J., Reinhard, C.T., Wang, X., Thomson, D., McGoldrick, P., Rainbird, R.H., Johnson, T., Fischer, W.W., and Lyons, T.W., 2014. Low Mid-Proterozoic atmospheric oxygen levels and the delayed rise of animals: *Science*, 346, 635–638, doi: 10.1126/science.1258410.

Podkovyrov, V.N., Maslov, A.V., Kuznetsov, A.B., and Ershova, V.B., 2017. Lithostratigraphy and geochemistry of Upper Vendian–Lower Cambrian deposits in the northeastern Baltic monocline: *Stratigraphy and Geological Correlation*, 25, 1–20, doi: 10.1134/S086959381606006X.

Polissar, P.J., Fulton, J.M., Junium, C.K., Turich, C.C., Freeman, K.H., 2009. Measurement of 13 C and 15 N Isotopic Composition on Nanomolar Quantities of C and N. *Analytical Chemistry* 81, 755–763, doi 10.1021/ac801370c

Popp, B.N., Laws, E.A., Bidigare, R.R., Dore, J.E., Hanson, K.L., Wakeham, S.G., 1998. Effect of Phytoplankton Cell Geometry on Carbon Isotopic Fractionation. *Geochimica et Cosmochimica Acta* 62, 69–77, doi: 10.1016/s0016-7037(97)00333-5

Reinhard, C.T., Planavsky, N.J., Gill, B.C., Ozaki, K., Robbins, L.J., Lyons, T.W., Fischer, W.W., Wang, C., Cole, D.B., Konhauser, K.O., 2017. Evolution of the global phosphorus cycle. *Nature* 541, 386–389, doi:10.1038/nature20772

Rii, Y.M., Duhamel, S., Bidigare, R.R., Karl, D.M., Repeta, D.J., Church, M.J., 2016. Diversity and productivity of photosynthetic picoeukaryotes in biogeochemically distinct regions of the South East Pacific Ocean: Picophytoplankton Diversity and Productivity in the S. Pacific. *Limnology and Oceanography* 61, 806–824, doi: 10.1002/lno.10255

Robinson, R.S., Kienast, M., Albuquerque, A.L., Altabet, M., Contreras, S., Holz, R.D.P., Dubois, N., Francois, R., Galbraith, E., Hsu, T.-C., Ivanochko, T., Jaccard, S., Kao, S.-J., Kiefer, T., Kienast, S., Lehmann, M., Martinez, P., McCarthy, M., Möbius, J., Pedersen, T., Quan, T.M., Ryabenko, E., Schmittner, A., Schneider, R., Schneider-Mor, A., Shigemitsu, M., Sinclair, D., Somes, C., Studer, A., Thunell, R., Yang, J.-Y., 2012. A review of nitrogen isotopic alteration in marine sediments. *Paleoceanography* 27, 36, doi: 10.1029/2012pa002321

Rohrssen, M., Love, G.D., Fischer, W., Finnegan, S., Fike, D.A., 2013. Lipid biomarkers record fundamental changes in the microbial community structure of tropical seas during the Late Ordovician Hirnantian glaciation. *Geology* 41, 127–130, doi: 10.1130/g33671.1

Sahoo, S.K., Planavsky, N.J., Jiang, G., Kendall, B., Owens, J.D., Wang, X., Shi, X., Anbar, A.D., and Lyons, T.W., 2016. Oceanic oxygenation events in the anoxic Ediacaran ocean: *Geobiology*, 14, 457–468, doi: 10.1111/gbi.12182.

Scalan, E.S., and Smith, J.E., 1970. An improved measure of the odd-even predominance in the normal alkanes of sediment extracts and petroleum: *Geochimica et Cosmochimica Acta*, 34, 611–620, doi: 10.1016/0016-7037(70)90019-0

Seilacher, A. and Pflüger, F. 1994. Biostabilization of Sediments (eds Krumbein, W. E., Paterson, D. M. & Stal L. J.) Bibliotheks und Informationssystem der Carl von Ossietzky University of Oldenburg, Oldenburg, Germany. 97–105

Sigman, D.M., Karsh, K.L., Casciotti, K.L., 2009. Ocean process tracers: nitrogen isotopes in the ocean. *Encyclopedia of Ocean Sciences* (eds Steele, J. H., Turekian, K. K. & Thorpe, S. A.) 4138–4153

Sliaupa, S., Fokin, P., Lazauskiene, J., and Stephenson, R.A., 2006. The Vendian-Early Palaeozoic sedimentary basins of the East European Craton: *Geological Society, London, Memoirs*, 32, 449–462, doi: 10.1144/GSL.MEM.2006.032.01.28.

Smith, K.S., Jakubzick, C., Whittam, T.S., Ferry, J.G., 1999. Carbonic anhydrase is an ancient enzyme widespread in prokaryotes. *Proceedings of the National Academy of Sciences* 96, 15184–15189, doi:10.1073/pnas.96.26.15184

Sperling, E.A., Peterson, K.J., Laflamme, M., 2011. Rangeomorphs, Thectardis (Porifera?) and dissolved organic carbon in the Ediacaran oceans. *Geobiology* 9, 24–33, doi: 10.1111/j.1472-4669.2010.00259.x

Sperling, E.A., Frieder, C.A., Raman, A.V., Girguis, P.R., Levin, L.A., and Knoll, A.H., 2013. Oxygen, ecology, and the Cambrian radiation of animals: *Proceedings of the National Academy of* Sciences, 110, 13446–13451, doi: 10.1073/pnas.1312778110.

Sperling, E.A., Wolock, C.J., Morgan, A.S., Gill, B.C., Kunzmann, M., Halverson, G.P., Macdonald, F.A., Knoll, A.H., Johnston, D.T., 2015. Statistical analysis of iron geochemical data suggests limited late Proterozoic oxygenation. *Nature* 523, 451–4, doi: 10.1038/nature14589

Summons, R.E., Bradley, A.S., Jahnke, L.L., and Waldbauer, J.R., 2006. Steroids, triterpenoids and molecular oxygen: *Philosophical Transactions of the Royal Society B: Biological Sciences*, 361, 951–968, doi: 10.1098/rstb.2006.1837.

Talyzina, N.M., 1998. Fluorescence intensity in Early Cambrian acritarchs from Estonia: *Review of Palaeobotany and Palynology*, 100, 99–108, doi: 10.1016/S0034-6667(97)00059-6.

Temperton, B., Gilbert, J.A., Quinn, J.P., McGrath, J.W., 2011. Novel analysis of oceanic surface water metagenomes suggests importance of polyphosphate metabolism in oligotrophic environments. *PloS one* 6, e16499, doi: 10.1371/journal.pone.0016499

Tolosa, I., Miquel, J.-C., Gasser, B., Raimbault, P., Goyet, C., Claustre, H., 2008. Distribution of lipid biomarkers and carbon isotope fractionation in contrasting trophic environments of the South East Pacific. *Biogeosciences* 5, 949–968, doi: 10.5194/bg-5-949-2008

Turner, E.C., Bekker, A., 2016. Thick sulfate evaporite accumulations marking a mid-Neoproterozoic oxygenation event (Ten Stone Formation, Northwest Territories, Canada): *GSA Bulletin*, 128, 203-222, doi: 10.1130/B31268.1.

Tostevin, R., Wood, R.A., Shields, G.A., Poulton, S.W., Guilbaud, R., Bowyer, F., Penny, A.M., He, T., Curtis, A., Hoffmann, K.H., Clarkson, M.O., 2016. Low-oxygen waters limited habitable space for early animals. *Nature communications* 7, 12818, doi:10.1038/ncomms12818

Veis, A.F., Vorob'eva, N.G., and Golubkova, E.Y., 2006. The early Vendian microfossils first found in the Russian plate: Taxonomic composition and biostratigraphic significance: *Stratigraphy and Geological Correlation*, 14, 368–385, doi: 10.1134/S0869593806040022.

Velikanov, V.A., Aseeva, E.A., and Fedonkin, M.A., 1983. The Vendian of Ukraine. Excursion Guide. Kiev: Naukova Dumka, 1–162 [in Russian].

Vinogradov, V.I., Burzin, M.B., Bujakaite, M.I., Golovin, D.I., Gorozhanin, V.M., Veis, A.F., Murav'ev, V.I., 2005. Rb-Sr and K-Ar Characteristics of Upper Vendian Clayey Rocks in the Russian Platform. *Lithology and Mineral Resources* 40, 332–352, doi: 10.1007/s10987-005-0032-x.

Vorob'eva, N.G., Sergeev, V.N., and Knoll, A.H., 2009. Neoproterozoic microfossils from the margin of the East European Platform and the search for a biostratigraphic model of lower Ediacaran rocks: *Precambrian Research,* 173, 163–169, doi: 10.1016/j.precamres.2009.04.001.

Ward, B.A., Dutkiewicz, S., Follows, M.J., 2013. Modelling spatial and temporal patterns in size-structured marine plankton communities: top–down and bottom–up controls. *Journal of Plankton Research* 36, 31–47, doi: 10.1093/plankt/fbt097

Wood, R.A., Poulton, S.W., Prave, A.R., Hoffmann, K.H., Clarkson, M.O., Guilbaud, R., Lyne, J.W., Tostevin, R., Bowyer, F., Penny, A.M., Curtis, A., and Kasemann, S.A., 2015. Dynamic redox conditions control late Ediacaran metazoan ecosystems in the Nama Group, Namibia: *Precambrian Research*, 261, 252–271, doi: 10.1016/j.precamres.2015.02.004.

CHAPTER THREE

Compound-specific stable carbon isotopic ($\delta^{13}C$) measurements of individual Ediacaran biomarker hydrocarbons

ABSTRACT

Here we report compound specific carbon isotope compositions for a suite of immature Ediacaran biomarker hydrocarbons from extraction of sedimentary rocks from across Baltica. Using the newly developed picomolar-scale compound-specific isotope analysis (pico-CSIA) method, we were able to measure not only the dominant *n*-alkanes and hopanes, but also for C_{29} ($\alpha\alpha\alpha$R) sterane, pristane, and phytane. The Utkina Zavod samples are enriched in ^{13}C compared to other Ediacaran samples by sometimes up to ca. 10‰. This enrichment is also recorded by the short-mid chain *n*-alkanes, hopanes, phytane, and C_{29} $\alpha\alpha\alpha$R sterane. C_{26}/C_{25} tricyclic terpanes and iron redox proxies support a brackish, more oxic environment for Utkina Zavod which may have had higher pH and bicarbonate concentrations which could result in dissolved CO_2 limitation and may have promoted carbon-concentration mechanisms (CCM) or active bicarbonate uptake by the phototrophs. The Redkino Horizon samples from the Lugovoe samples generally display an inverse isotopic ordering between *n*-alkanes and pristane/phytane, while the others only show small isotopic offsets from the $\delta^{13}C_{TOC}$. Pristane and phytane are also ca. 4-5‰ more negative relative to the hopanes, which suggests significant contributions by non-RuBisCO Calvin-Benson-Bassham utilizing organism, such as Archaea. Pico-CSIA

systematics of Ediacaran biomarker hydrocarbons from Baltica present a picture of regional environmental heterogeneity during the Kotlin Horizon superimposed on a fundamental temporal shift in the microbial community structure between the Redkino and Kotlin Horizons.

1. INTRODUCTION

Bulk organic carbon isotope ($\delta^{13}C_{TOC}$) compositions of ancient sedimentary rocks reflect the overall balance of the organic matter inputs from many contributing source biota, the taphonomy of organic matter preservation during diagenesis (e.g., contribution of benthic mats versus planktonic inputs, or oxic versus anoxic redox conditions), and the carbon isotopic composition of the marine dissolved inorganic carbon (DIC) pool used in the local depositional setting (Hayes et al., 1990; Freeman, 2001). While broad changes in $\delta^{13}C_{TOC}$ over geological time can represent global perturbations to the carbon cycle, including changes to total organic carbon burial and pCO_2, regional ecological and environmental factors often have a greater influence (Pagani et al., 1999; Pancost et al., 2013; Holtvoeth et al., 2019). Compound-specific carbon isotopic analysis (CSIA) can help disentangle this complex web of sources and preservational effects on $\delta^{13}C_{TOC}$ by constraining varying source organic matter influences on $\delta^{13}C_{TOC}$ and informing us about the pathways of carbon acquisition for different biomarker compounds and their parent biota (Hayes, 2001; Pancost and Sinninghe Damsté, 2003).

The abundance and diversity of eukaryotic organisms showed a fundamental increase in the marine realm throughout the end of the Proterozoic Eon (2500-541 Ma). The oceans of the Mesoproterozoic were bacterially dominated, however, during the Tonian Period (1000-720 Ma) eukaryotes increased their abundance. The most commonly found early-mid Neoproterozoic eukaryotes were the red algae and unicellular heterotrophs as gauged from the dominance of cholestane amongst the total detectable C_{27}-C_{30} steranes (Brocks et al., 2017; Zumberge et al., 2019). Following the Sturtian glaciation, green algae replaced red algae as the dominant eukaryotic primary producers, and these eukaryotes rivaled bacteria in terms of biomass within the oceans (Love et al., 2009; Hoshino et al., 2017; Brocks et al., 2017). As discussed in Chapter 2 however, even by the end of the Neoproterozoic Era, the contrast in biomarker assemblage patterns from Baltica compared to other contemporaneous settings suggested that there was great heterogeneity in the relative bacterial and eukaryotic contributions at different locations (Pehr et al., 2018; Bobrovskiy et al., 2020).

One enigmatic geochemical signal found in rocks and oils deposited during the Proterozoic Eon that has been potentially linked to the rise of eukaryotes is a switch in the relative carbon isotopic ordering of *n*-alkanes and the isoprenoids, pristane and phytane, commonly derived from photosynthetic organisms. Many Neoproterozoic samples are characterized by an'inverse ordering' where $\delta^{13}C$ of pristane and phytane is more negative with respect to the more more positive $\delta^{13}C$ of *n*-alkanes and bulk organic matter (Logan et al., 1995, 1997; Close et al., 2011). Usually Phanerozoic samples, as

well as some of the younger Ediacaran samples, show the opposite trend where bulk sedimentary organic matter consisting largely of kerogen have more positive $\delta^{13}C$ values relative to those of *n*-alkanes (Hayes et al., 2001). Pristane and phytane typically have more negative $\delta^{13}C$ than bulk organic matter, but have more positive $\delta^{13}C$ then *n*-alkanes. This isotopic ordering in most Phanerozoic samples reflects the isotopic ordering of originating from isotope fractionations in biosynthesis with organisms commonly using the RuBisCO Calvin-Benson-Bassham (RuBisCO-CBB) metabolic pathway for autotrophic carbon acquisition (Hayes, 2001), which accounts for the majority of primary productivity in modern oceans (Pearson, 2010).

Pristane and phytane are derived predominantly from the phytol side chain of chlorophyll a produced by phototrophic organisms (Rontani & Volkman, 2005), but less commonly may also be derived from Archaea (Koga et al., 1993; Koga et al., 1998; Wakeham et al., 2003). Logan et al., (1997) proposed that the isotopically ^{13}C-enriched *n*-alkanes relative to pristane, phytane, and bulk organic matter in Proterozoic samples were the result of intense microbial heterotrophy of n-alkyl lipids in the water column sustained by high dissolved organic matter (DOM) concentrations. Heterotrophic organisms are often slightly enriched in ^{13}C relative to their food source because isotopically light CO_2 is lost during respiration (Denirio and Epstein, 1978; Pearson, 2010). The ecological rise of macroscopic multicellular eukaryotes and the packaging of organic matter in fecal pellets may have facilitated increased sinking rates of organic matter which could have ended this intense water column heterotrophy in the late Ediacaran or early Phanerozoic Eon.

However, modeling by Close et al., (2011) suggests that intense heterotrophy of slow-sinking organic matter would only result in the inverse isotopic ordering under a narrow range of conditions that are unlikely to have been persistent across all Proterozoic depositional environemnts. They suggested instead that the most reasonable explanation for such appreciably ^{13}C-enriched *n*-alkanes might be due to a large difference in isotope fractionation between bacterial and eukaryotic primary producers.

Here we report compound-specific carbon isotope systematics for immature Ediacaran biomarker hydrocarbons obtained from solvent extraction of sedimentary rocks from cores drilled across Baltica. Using the newly developed picomolar-scale compound-specific isotope analysis (pico-CSIA) method, we were able to measure not only the dominant *n*-alkanes and hopanes, but also other individual biomarker compounds including C_{29} steranes, pristane, and phytane.

2. MATERIALS AND METHODS

Baltica hosts the most thermally immature Ediacaran rocks reported from this time interval (Pehr et al., 2018; Goryl et al., 2018). A subset of 12 Late Ediacaran samples and a single Early Cambrian sample were selected from the suite of thermally immature samples used for detailed biomarker analysis described in Chapter 2. The sedimentary rock samples chosen were collected from the Utkina Zavod and Lugovoe drill cores located near St. Petersburg in the northeastern part of the Balitc monocline, the Gavrilov-

Yam-1 drill core from the Moscow basin, the 4592 drill core from the Volyn region of Ukraine, and the 3628 drill core of Podillya basin in southwestern Ukraine. Detailed locations and descriptions of these samples can be found in Table 2.1 in Chapter 2, which is as it appears in Pehr et al., 2018.

2.1. Lipid biomarker analysis.

Rock samples were cut, crushed, solvent extracted, and separated into three fractions: aliphatic hydrocarbons, aromatics, and polar fractions, as described in the methodology given in Chapter 2. The aliphatic hydrocarbon fractions were analyzed to generate total ion chromatograms (Fig. 2.2) in full-scan mode using a gas chromatography–mass spectrometry (GC–MS) with an Agilent 7890A GC system coupled to an Agilent 5975C inert MSD mass spectrometer. The GC temperature program for full-scan analysis (m/z 60 to 800) was 60°C (held for 2 min), heated to 150°C at 20°C/min, then to 325°C at 2°C/min, and held at 325°C for 20 min. The GC was equipped with a DB1-MS capillary column (60 m × 0.32 mm, 0.25-μm film thickness) and helium was used as a carrier gas.

2.2. Pico-compound specific carbon isotope analysis

Aliphatic hydrocarbon fractions were analyzed using the pico-CSIA method developed at Pennsylvania State University (Baczynski et al., 2018). The pico-CSIA method uses a Thermo Trace 1310 GC coupled to a Thermo MAT 253 IRMS via a GC Isolink (see Baczynski et al., 2018, for details). The GC was fitted with a PTV injector that was held at 300°C and operated in splitless mode. A fused silica capillary column (Agilent J&W

DB-5, 10m, 0.10mm I.D., 0.10μm film thickness) was used with helium as the carrier gas. The carrier gas had a programmed pressure method to ensure a consistent flow of ~0.48 mL/min throughout the run. The oven temperature program began at a temperature of 60°C (held for 1.5 min), ramped to 230°C at 100°C/min (no hold) then to a maximum temperature of 320°C at 40 °C/min with a final hold time of 5 min. The auxiliary gas pressure to the microfluidic splitter was held at 24 psi while solvent was vented and then reduced to 18 psi while the GC effluent was directed to the IRMS.

Isotopic abundances were determined relative to a reference gas calibrated with Mix A (*n*-C_{16} to *n*-C_{30}; Arndt Schimmelmann, Indiana University). The $\delta^{13}C$ values were normalized to the standard Vienna Pee Dee Belemnite scale and are reported in standard delta notation. Standard errors of the mean for individual samples range from 0.00‰ to 1.36‰. Average standard error for *n*-alkanes was 0.22‰, 0.19‰ for phytane, and 0.28‰ for hopanes and C_{29} sterane.

2.3. Iron Mineral Speciation

Iron mineral geochemical speciation was performed in order to gauge the environmental redox conditions by quantifying the iron minerals that are considered highly reactive (Fe_{HR}) to reduction under anoxic conditions. Iron carbonate (Fe_{CARB}; including siderite and ankerite), ferric iron-(oxyhydr)oxide minerals (Fe_{OX}; including hematite and goethite), and magnetite (Fe_{MAG}), were separated following the sequential extraction technique described in Poulton and Canfield, (2005). Pyrite (Fe_{py}) was determined

stoichiometrically by weight from a Ag_2S precipitate formed after a HCl and chromous chloride distillation (Canfield et al., 1986; Poulton and Canfield, 2005). These four iron phases combined make up the pool of Fe_{HR} (Raiswell and Canfield, 1998;). Fe_{HR} increases in concentration in comparison to total iron (Fe_T) under anoxic water column conditions where Fe_{HR} easily precipitates out and is preserved. When $Fe_{HR}/Fe_T<0.22$ the water column was most likely oxic while $Fe_{HR}/Fe_T>0.38$ indicated anoxic conditions (Raiswell and Canfield, 1998; Raiswell et al., 2001; Poulton and Canfield, 2011). Fe_{py} is used to constain the type of anoxic conditions. When $Fe_{py}/Fe_T<0.7$ ferruginous conditions likely prevailed and when $Fe_{py}/Fe_T>0.7$ euxinic conditions likely persisted in the anoxic depositioal environments (Poulton et al., 2004; Poulton and Canfield, 2011).

3. RESULTS

3.1. $\delta^{13}C_{TOC}$ and Compound Specific Carbon Isotopes

Bulk organic carbon isotopes ($\delta^{13}C_{TOC}$), reported in Section 3.3 of Chapter 2 (Pehr et al., 2018), range markedly between drill-core locations (Table 2.4). Within the Utkina Zavod drill core, $\delta^{13}C_{TOC}$ are more positive, ranging from -26.0 to -23.0‰, in comparison to the nearby Lugovoe drill core, where samples from the same Kotlin Horizon are more negative in terms of $\delta^{13}C$ by up to 10‰, ranging from -30.0 to -33.9‰.

Hopanes and *n*-alkanes account for the two dominant series of resolvable biomarker compounds in the aliphatic hydrocarbon fractions. Compound specific isotope analysis of individual *n*-alkanes and hopane compounds reveal that $\delta^{13}C$ of both groups track fairly

closely with changes to $\delta^{13}C_{TOC}$ (Fig. 3.1, 3.2, and 3.3) often within 1.5±1.3‰ of bulk carbon. Hopanes are derived from hopanoids, which are cell membrane lipids synthesized by a wide variety of bacterial groups (Rohmer et al., 1984; Pearson et al., 2007). *N*-alkanes are widely distributed amongst organisms, including bacteria and algae, however culture analysis suggest algae often contribute greater proportions of long chain *n*-alkanes (>nC_{22}) than bacteria (Love et al., 2005).

The difference between $\delta^{13}C$ of the two most abundant hopane compounds [17α,21β-C_{30}(H) and 17α,21β-C_{31}(H)] and $\delta^{13}C_{TOC}$ ranges from 0.1‰ to 2.5‰ for all samples measured, whereas the range in $\delta^{13}C$ of 17α,21β-C_{30}(H) and 17α,21β,22R-C_{31}(H) between all samples measured is a much greater 10.2‰ and 11.2‰ respectfully. The *n*-alkanes of the Lugovoe, 4592, and Gavrilov Yam samples all fall within 2‰ of $\delta^{13}C_{TOC}$ but range between 6.2‰ and 11.3‰ among all of the samples we measured. The Utkina Zavod *n*-alkanes display a wider isotopic spread, particularly among the *n*-C_{22} to *n*-C_{25} alkanes, which were as much as 6.6‰ more negative than $\delta^{13}C_{TOC}$.

The hopanes show a general trend of increasingly more negative $\delta^{13}C$ with increasing carbon chain length. The C_{27} hopanes have, on average, the most positive $\delta^{13}C$ of the hopanes, followed by the C_{29}, and then the C_{30} hopanes. The C_{31} and C_{32} hopanes have the most negative $\delta^{13}C$.

Hopane $\delta^{13}C$ values of the Utkina Zavod samples are not exclusively either more positive or negative relative to $\delta^{13}C_{TOC}$ but differ from sample to sample. 4592 hopane $\delta^{13}C$ values are slightly more positive with respect to $\delta^{13}C_{TOC}$, while Gavrilov Yam hopanes are all more negative with respect to $\delta^{13}C_{TOC}$. Hopane $\delta^{13}C$ values in samples from the Lugovoe core switch from more negative with respect to $\delta^{13}C_{TOC}$ to more postive with respect to $\delta^{13}C_{TOC}$ between the Redkino and Kotlin Horizons.

The short-mid chain *n*-alkanes (*n*-C_{17} – *n*-C_{21}) are more negative in terms of $\delta^{13}C$ by up to ca. 4‰ (relative to $\delta^{13}C_{TOC}$) for the Utkina Zavod samples, but are closer in value (within ca. 1‰) for the remaining samples. The long chain *n*-alkanes (*n*-C_{22} – *n*-C_{29}) have the largest offsets from the $\delta^{13}C_{TOC}$ of the compounds measured in this study. The Utkina Zavod *n*-C_{22} to *n*-C_{25} are strongly depleted in ^{13}C (as much as 6.6‰ more negative than $\delta^{13}C_{TOC}$), while the *n*-C_{28} and *n*-C_{29} are more positive by up to ca. 2‰. The Lugovoe *n*-C_{22} to *n*-C_{25} $\delta^{13}C$ values in samples from the Redkino Horizon are more positive than $\delta^{13}C_{TOC}$ by up to 2.2‰, unlike samples from the Kotlin Horizon.

Despite the extremely high hopane/sterane compositional ratios of these samples, we were able to measure the $\delta^{13}C$ of the $C_{29}\alpha\alpha\alpha R$ sterane peak in samples with hopane/sterane less than 10. The $\delta^{13}C$ of the C_{29} sterane for these Kotlin Horizon samples are within 1‰ of $\delta^{13}C_{TOC}$. C_{29} steranes, derived from sterol precursors, represent contributions by green algae (and plants in age appropriate samples) (Moldowan et al., 1990; Brocks et al., 1999; Kodner et al., 2008).

Isotopic compositions of the acyclic isoprenoids pristane (2,6,10,14-tetramethylpentadecane; $C_{19}H_{40}$; Pr) and phytane (2,6,10,14-tetramethylhexadecane; $C_{20}H_{42}$; Ph) were also determined. Phytane $\delta^{13}C$ ranges from -1.8‰ to +0.2‰ relative to the $\delta^{13}C_{TOC}$ in the Kotlin Horizon samples. However, phytane and pristane in the Lugovoe sample 13-71 (Redkino Horizon) are very depleted in ^{13}C with $\delta^{13}C$ values that are -4.5‰ and -5.5‰ more negative than $\delta^{13}C_{TOC}$.

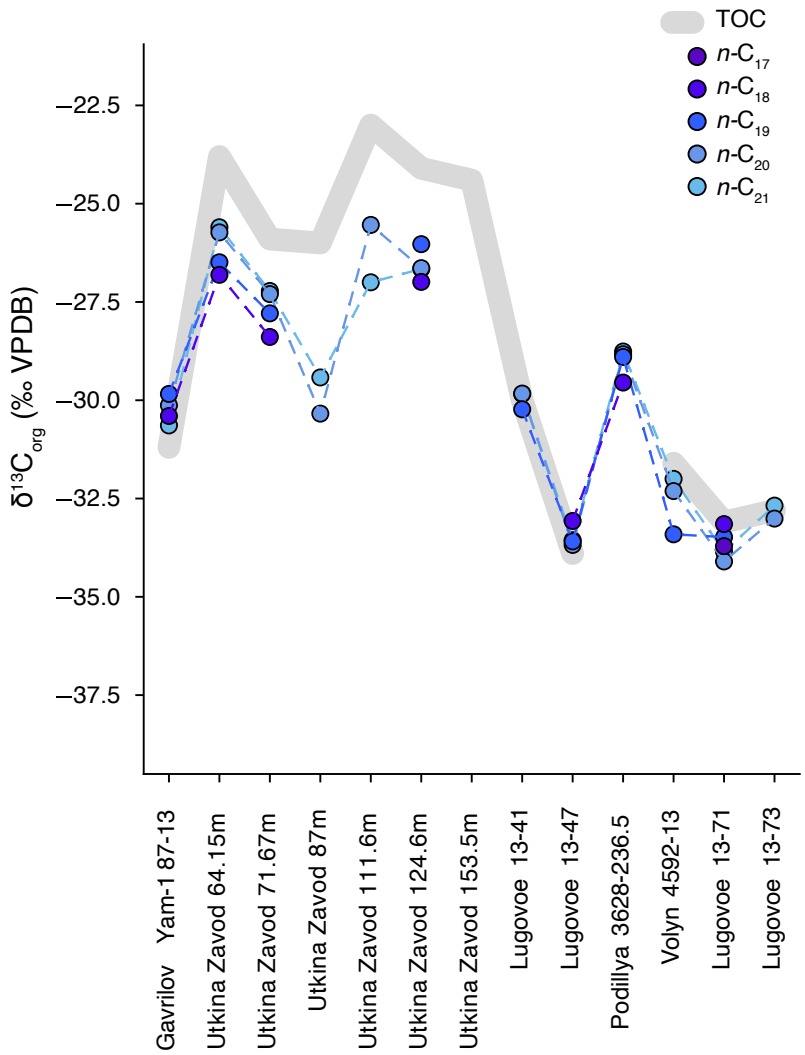

Figure 3.1. Compound specific carbon isotopes of short-mid chain *n*-alkanes and bulk organic matter (TOC) for Balitca samples of Late Ediacaran and Early Cambrian age. Note the close match of δ^{13}Corg for these these individual *n*-alkanes to the bulk TOC values for most samples. Offsets between csia and bulk TOC signatures are in the range of 0-6‰

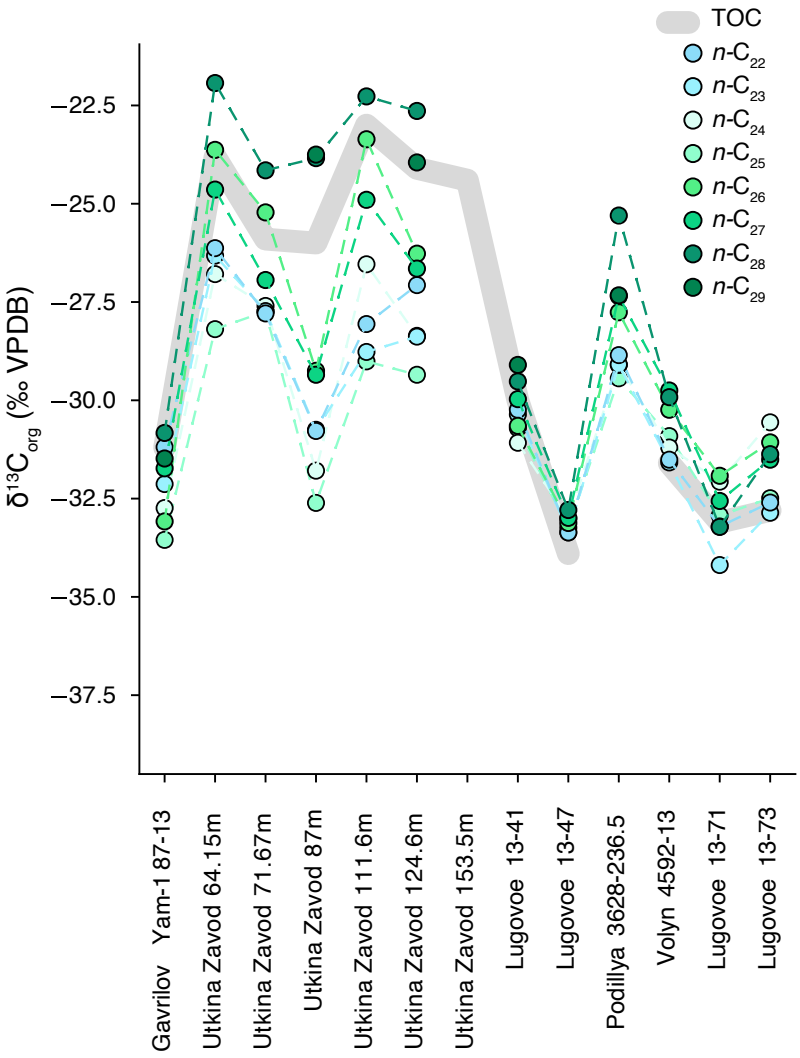

Figure 3.2. Compound specific carbon isotopes of long chain *n*-alkanes and bulk organic matter (TOC) for Balitca samples of Late Ediacaran and Early Cambrian age.

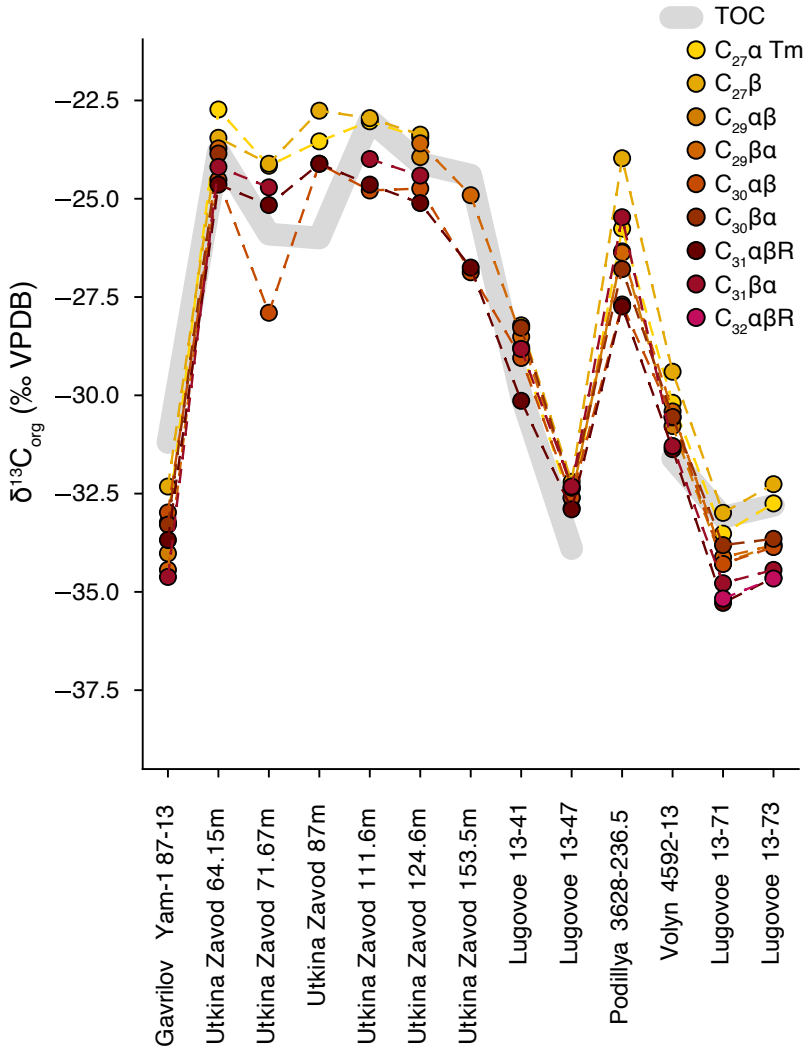

Figure 3.3. Compound specific carbon isotopes of hopanes and bulk organic matter (TOC) for Balitca samples of Late Ediacaran and Early Cambrian age. Note the close match of δ^{13}Corg for these these individual hopanes to the bulk TOC values for most samples. Offsets between csia and bulk TOC signatures are in the range of 0-3‰

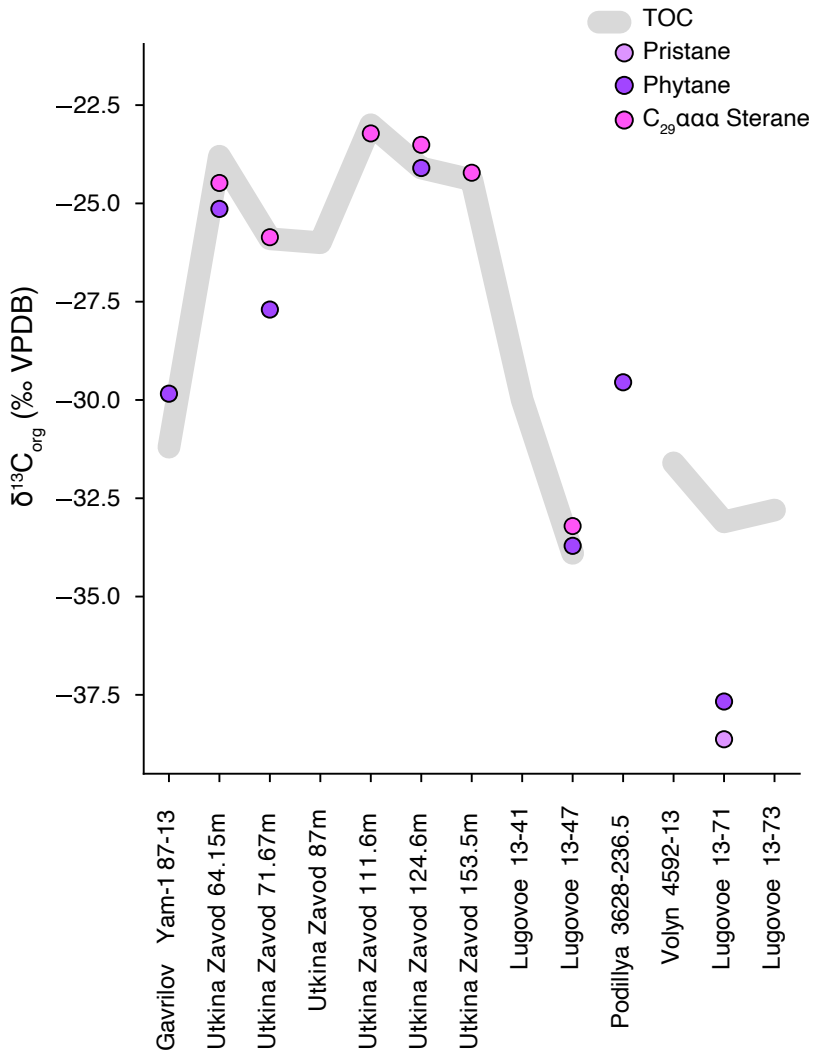

Figure 3.4. Compound specific carbon isotopes of pristane, phytane, C_{29} ααR sterane and bulk organic matter (TOC) for Balitca samples of Late Ediacaran and Early Cambrian age. The δ^{13}Corg of C_{29} ααR sterane which represent contributions by RuBisCO- utilizing green algae tracks closely with the bulk TOC values. Pristane and phytane show a large negative offset compared to the bulk TOC for Lugovoe 13-71, but closely match the bulk TOC in the other samples.

3.2. Lipid Biomarker

In addition to the *n*-alkane, hopane, and sterane biomarkers reported in Chapter 2 (Pehr et al., 2018), we also analyzed the relative abundances of tricyclic terpanes (TT) using MRM-GC-MS as a means to distinguish marine environments from fresh water/brackish settings. The abundance ratio for C_{26}/C_{25} TT gives elevated values, ranging from 1.6 to 2.8, for the Utkina Zavod samples and lower values 0.4 to 1.5 for the remaining samples (Fig. 3.5).

3.3. Iron Speciation

The Fe_{HR}/Fe_T ratios for Kotlin Horizon samples range in value from 0.15 to 0.92 (Table 3.4, Fig. 3.6). The majority of the Utkina Zavod and Volyn core samples of the Kotlin Horizon have lower Fe_{HR}/Fe_T ratios, with several samples below 0.22, indicative of deposition under oxic aquatic conditions. The Lugovoe samples from both Kotlin and Redkino Horizons are all above 0.38, indicative of deposition under anoxic conditions (Poulton and Canfield, 2005). The Fe_{py}/Fe_T is below 0.7 for all samples indicating that ferruginous, rather than euxinic, conditions persisted in the anoxic depositioal environments (Poulton et al., 2004; Poulton and Canfield, 2011). All samples analyzed for Fe speciation have total iron contents with $Fe_T > 0.5$ wt% of bulk rock.

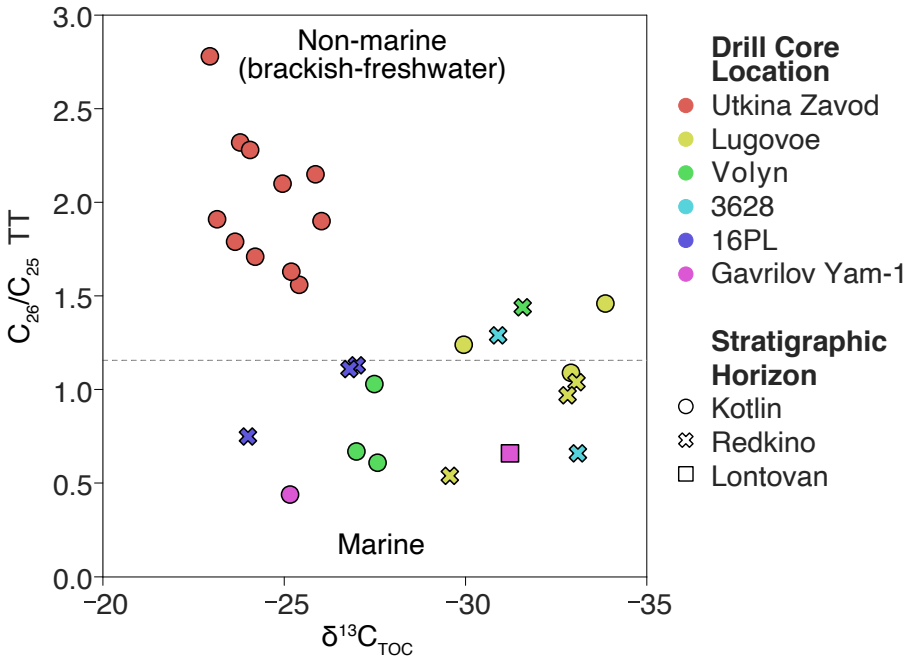

Figure 3.5. The ratio of C_{26}/C_{25} tricyclic terpanes (TT) is a parameter used to constrain water salinity, C_{26}/C_{25} TT < 1.2 is typically indicative of normal marine conditions, C_{26}/C_{25} TT > 1.2 suggests a non-marine including brackish or freshwater settings. The Utkina Zavod samples are all non-marine.

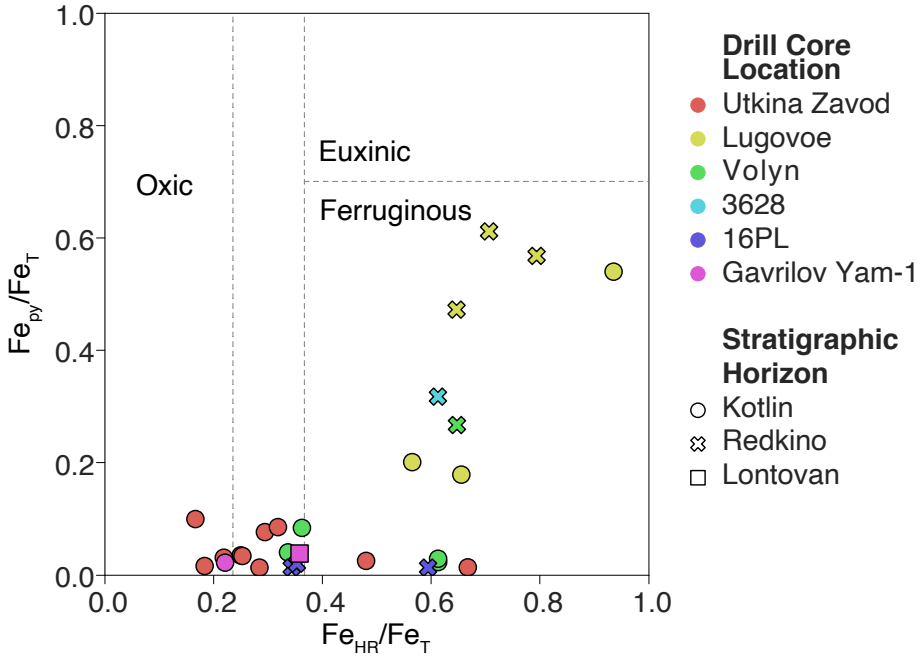

Figure 3.6. Crossplot of iron redox proxies Fe_{HR}/Fe_T and Fe_{py}/Fe_T. Baltica samples fall within either oxic or ferruginous fields.

4. DISCUSSION

4.1. Local environmental effects on $\delta^{13}C_{TOC}$

The Utkina Zavod core samples are distinctly more positive by ca. 10‰ in $\delta^{13}C$ for bulk TOC as well as for individual biomarker hydrocarbons compared to other Ediacaran marine organic matter; both from this study from Baltica, and those previously reported from other locations (Grosjean et al., 2009; Kelly et al., 2011; Lee et al., 2015; Pehr et al., 2018). Compound specific isotope analysis reveals that this ^{13}C-enrichment is represented within the hopanes, short-mid chain *n*-alkanes, phytane, and for the C_{29} ααα*R* sterane.

The more positive $\delta^{13}C$ values in compounds derived from RuBisCO-CBB utilizing photoautotrophs (C_{29} sterane, and phytane) could reflect changes in the $\delta^{13}C$ of the DIC pool (e.g. CO_2 versus bicarbonate prevalence) or changes in metabolic isotope fractionation related to growth rate or CO_2 concentrations (Popp et al., 1998; Fogel et al., 1992). Isotopic fractionation from RuBisCO can be as great as -29‰, although it differs between organisms (Pearson 2010, Scott et al., 2004; Guy et al., 1993; Roeske and O'Leary, 1984). Given the similarities between the hopane and sterane biomarker assemblages of Utkina Zavod and other Kotlin Horizon samples, it seems unlikely however that the more positive $\delta^{13}C$ values in the Utkina Zavod core are the result of large changes to the phytoplanktonic populations.

Two geochemical parameters that do differentiate between the Utkina Zavod and Lugovoe samples of the Kotlin Horizon are C_{26}/C_{25} tricyclic terpanes and Fe_{HR}/Fe_T which

track depositional environmental changes. The ratio of C_{26}/C_{25} tricyclic terpanes (TT) is an empirical parameter which correlates with changes in the salinity of the depositional environment (Zumberge, 1987). C_{26}/C_{25} TT values at or below ca. 1.2 are associated with marine conditions, whereas values greater than ca. 1.2 are typically associated with brackish or freshwater conditions (Zumberge, 1987; Grande et al., 1993). The Utkina Zavod core samples all fall within the range of brackish-freshwater conditions in contrast to the Lugovoe core samples which range from 0.5 to 1.5 placing them predominantly within typical marine conditions. Fe_{HR}/Fe_T values from iron mineral speciation indicate that the aquatic redox conditions during the deposition of the Utkina Zavod samples was more oxic, while Lugovoe was anoxic and ferruginous. These environmental differences suggest that the Utkina Zavod aquatic setting was potentially an estuarine type setting.

One potential scenario which would explain the more positive $\delta^{13}C$ values in the Utkina Zavod core is the presence of a more positive $\delta^{13}C$ DIC pool. The $\delta^{13}C$ of DIC pools in modern estuaries are typically more-negative than marine values, due to the remineralization of high terrestrial inputs of organic carbon, however terrestrial inputs of organic carbon should be low in the Ediacaran (Boschker et al., 2005; Fogel et al., 1992). $\delta^{13}C$ of the Ediacaran DIC pool was instead likely controlled by pCO_2, pH, and temperature. Of these three parameters, pH is the most reasonable to vary over short distances. If Utkina Zavod waters were more alkaline, this would increase the proportion of bicarbonate within the DIC pool, and drive $\delta^{13}C$ of the DIC pool more positive. It could also result in dissolved CO_2 limitation and may have promoted carbon-

concentration mechanisms (CCM) or active bicarbonate uptake by the phototrophs. Both CCM and bicarbonate uptake produce biomass that is less depleted in ^{13}C (Hayes et al., 1993; Smith et al., 1999) and are the most likely cause of the unusually ^{13}C-enriched signatures for bulk organic matter and individual hydrocarbon compounds for the Utkina Zavod strata from the Kotlin Horizon.

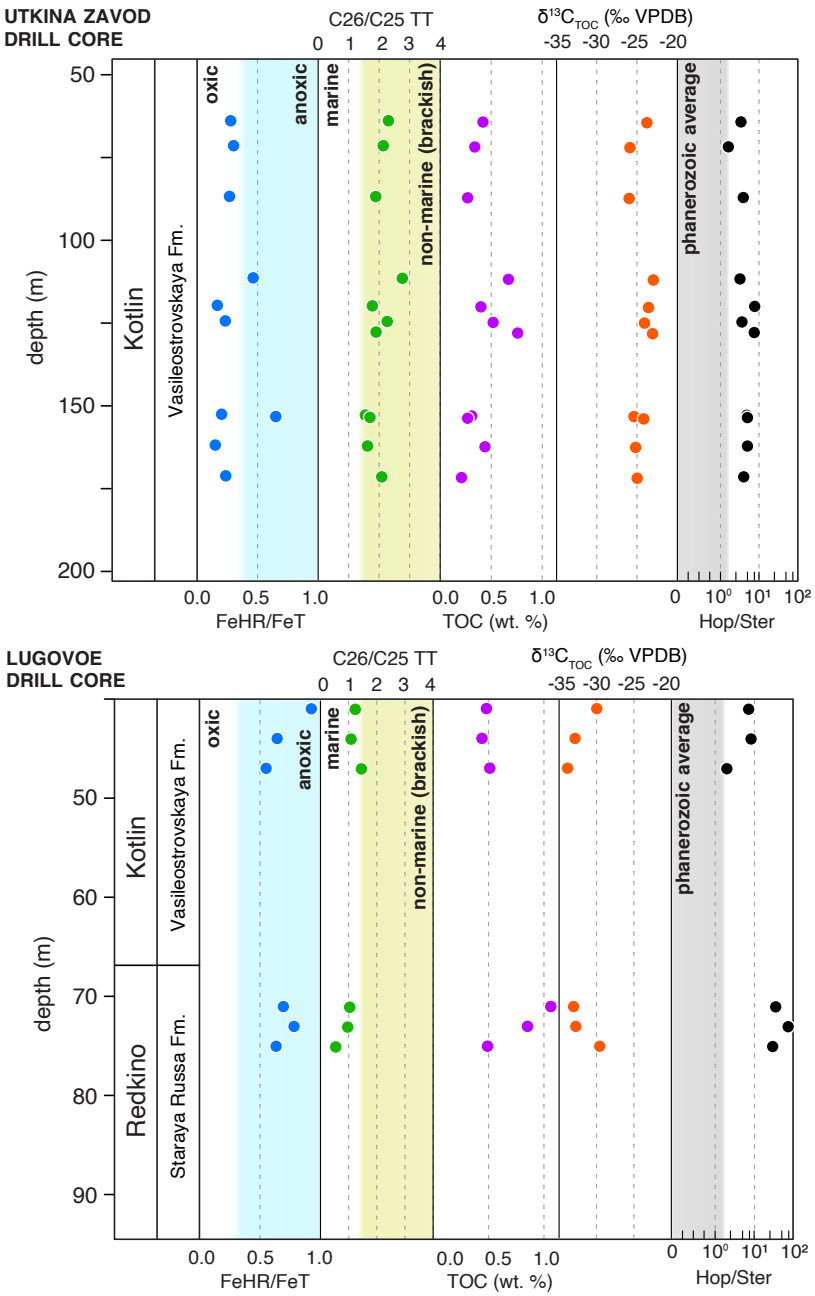

Figure 3.7. Stratigraphic trends for inorganic and organic geochemical parameters measured for sedimentary rocks from the Utkina Zavod and Lugovoe drill cores. C_{26}/C_{25} TT (tricyclic terpanes) and Fe_{HR}/Fe_T values are given in Table 3.1. TOC, $\delta^{13}C_{TOC}$, and Hop/Ster (hopane/sterane) values are given in Table 2.1 and 2.4. The threshold value for C_{26}/C_{25} TT is ca. 1.2 to distinguish low salinity waters (>1.2) from marine waters (≤1.2).

4.2. Inverse isotopic ordering

Samples from the Redkino Horizon of the Lugovoe core display an inverse carbon isotopic ordering between *n*-alkanes, pristane and phytane, and bulk TOC, which has been previously reported in Neoproterozoic samples (Logan et al., 1995, 1997;). The long-chain *n*-alkanes have a slight positive $\delta^{13}C$ offset relative to TOC however the most distinctive feature is the large negative $\delta^{13}C$ offset of pristane and phytane in sample L-13-71. $\delta^{13}C$ of the hopanes in the 'inverse' samples are slightly more negative relative to the *n*-alkanes and very postive relative to pristane and phytane. The large $\delta^{13}C$ difference (ca. 4‰) between pristane and phytane and the hopanes cannot be explained by variations in isotopic fractionation from RuBisCO alone. Alternative possibilities include: i) multiple autotrophic sources for the hopanes and pristane/phytane, some of which use an alternative carbon fixation pathway, therby imparting different isotopic compositions of individual biomarkers; ii) a single autotrophic source for the hopanes and pristane/phytane following a non-RuBisCO-CBB pathway; or iii) heterotrophic reworking of the organic matter either in the water column or in a microbial mat that results in the replacement of the hopanes and *n*-alkanes, or pristane and phytane, or both.

CSIA of culture studies for different metabolic pathways are limited, however studies of a photoheterotrophic pathway in a purple sulfur bacteria as well as of rTCA in a green sulfur bacteria and a purple sulfur bacteria reported instances where phytol or phytane are significantly depleted relative to *n*-alkanes (van deer Meer et al., 1998; Tang et al., 2017). However, the $\delta^{13}C$ of the bulk organic matter produced by these cultures was

significantly more positive than the $\delta^{13}C_{TOC}$ values for the Redkino Horizon Lugovoe samples and therefore does not match the signal observed in these samples.

Heterotrophic reworking produces organic matter with more positive $\delta^{13}C$ relative to the initial organic matter contribution. Preferential preservation of contributions from heterotophic bacteria could thus be responsible for the offset between *n*-alkanes and hopanes versus pristane and phytane. However, in this scenario, the initial $\delta^{13}C$ signal produced by primary producers would need to be more negative than the bulk TOC. Very negative $\delta^{13}C$ values of -38‰ or lower could indicate source contributions from organisms involved in methane cycling (Freeman et al., 1990). In particular, methangenic archaea as well as archaea methane oxidizers have been proposed as a source for phytane (Koga et al., 1993; Koga et al., 1998; Wakeham et al., 2003).

5. CONCLUSION

Bulk carbon isotope ratios for individual alkane compounds and bulk sedimentary organic matter are strongly controlled by local environmental and ecological conditions. During the late Ediacaran, Baltica consisted then of shallow, epicontinental seas, which likely contributed to varying local environments such as brackish and potentially CO_2 limited waters. Shallow, platform settings have previously been considered strongly susceptible to changes in circulation, redox, temperature or sea level which can all affect carbon isotopic acquisition relative to $\delta^{13}C_{TOC}$ and the magnitude of isotopic fractionations (Pancost et al., 2013).

The biomarker and stable carbon isotope ($\delta^{13}C_{org}$) characteristics of the Kotlin Horizon from the Utkina Zavod core suggest that this strata was deposited in a fresh-brackish water setting, such as in an estuary, rather than in a marine environment. $\delta^{13}C_{TOC}$ range from -26.0 to -23.0‰ for the Utkina Zavod core and generally have a close match of $\delta^{13}C_{org}$ for individual hydrocarbon compounds and the bulk organic carbon (TOC), with an offset typically within 2‰, further demonstrating that these were endogenous biomarker constituents in these rocks. This included a good match of $\delta^{13}C_{TOC}$ with pristane and phytane and C_{29} aaaR steranes, which are usually derived from photoautotrophs. Utkina Zavod may have had higher pH and bicarbonate concentrations which could result in dissolved CO_2 limitation and may have promoted carbon-concentration mechanisms (CCM) or active bicarbonate uptake by the phototrophs. In contrast to all of the Kotlin Horizon samples which contain a stong match of $\delta^{13}C_{TOC}$ with phytane, a large negative offset of ca. 4‰ in pristane and phytane from $\delta^{13}C_{TOC}$ in a Lugovoe sample from the Redkino Horizon with $\delta^{13}C_{TOC}$ of -33.7‰ was detected. Alternative sources of these acyclic isoprenoids such as contributions from archaea, perhaps involved in methane cycling may have been significant during the Redkino as well as increased bacterial heterotrophy. Pico-CSIA of Ediacaran biomarker hydrocarbons from Baltica is thus able to isolate inorganic environmentally induced changes such as esturine conditions from organic community induced changes such as methane cycling and reworking of organic matter.

Table 3.1. Mean carbon isotope compositions for individual extractable n-alkanes measured by pico-CSIA. Measurements were performed in triplicate. Average standard error for n-alkanes was 0.22‰.

	$\delta^{13}C_{n\text{-alkanes}}$ (‰)												
Sample	$\delta^{13}C_{nC17}$	$\delta^{13}C_{nC18}$	$\delta^{13}C_{nC20}$	$\delta^{13}C_{nC20}$	$\delta^{13}C_{nC21}$	$\delta^{13}C_{nC22}$	$\delta^{13}C_{nC23}$	$\delta^{13}C_{nC24}$	$\delta^{13}C_{nC25}$	$\delta^{13}C_{nC26}$	$\delta^{13}C_{nC27}$	$\delta^{13}C_{nC28}$	$\delta^{13}C_{nC29}$
UZ 1-9		-26.81	-26.49	-25.73	-25.6	-26.13	-26.32	-26.79	-28.19	-23.63	-24.64	-21.93	
UZ 1-10		-28.39	-27.79	-27.3	-27.22	-27.79	-27.73	-27.6	-27.74	-25.22	-26.94	-24.15	
UZ 1-14				-30.34	-29.42	-30.78	-30.75	-31.79	-32.61	-29.25	-29.35	-23.84	-23.75
UZ 1-20				-25.54	-27	-28.06	-28.77	-26.54	-29.01	-23.36	-24.9	-22.27	
UZ 1-22a		-26.99	-26.03	-26.64	-26.66	-27.07	-28.38	-28.36	-29.35	-26.27	-26.65	-22.64	-23.95
UZ 1-26b													
L-13-41			-30.23	-29.83	-29.84	-30.24	-30.36	-31.08	-30.71	-30.65	-29.97	-29.52	-29.1
L-13-47		-33.07	-33.59	-33.68	-33.56	-33.36	-33.36	-33.01	-33.24	-33.12	-32.99	-32.79	
L-13-71	-33.71	-33.15	-33.48	-34.1	-33.85	-33.21	-34.19	-32.07	-32.93	-31.92	-32.56	-33.22	
L-13-73				-33.01	-32.68	-32.6	-32.86	-30.56	-32.49	-31.07	-31.51	-31.37	
87-13		-30.4	-29.84	-30.13	-30.64	-31.19	-32.13	-32.74	-33.55	-33.08	-31.73	-30.83	-31.48
226.5		-29.55	-28.9	-28.83	-28.76	-28.85	-29.09	-29.1	-29.44	-27.76	-27.35	-25.3	-27.33
3-13			-33.41	-32.31	-32	-31.51	-31.58	-31.2	-30.91	-30.24	-29.75	-29.92	

Table 3.2. Mean carbon isotope compositions for individual extractable hopanes and hopenes measured by pico-CSIA. He = hopene. Measurements were performed in triplicate. Average standard error was 0.28‰ for hopanes.

	$\delta^{13}C_{hopanes}$ (‰)												
Sample	$\delta^{13}C$ $C_{27}H\alpha Tm$	$\delta^{13}C$ $C_{27}H\beta$	$\delta^{13}C$ $C_{29}He$	$\delta^{13}C$ $C_{29}H\alpha\beta$	$\delta^{13}C$ $C_{29}H\beta\alpha$	$\delta^{13}C$ $C_{30}H\alpha\beta$	$\delta^{13}C$ $C_{30}He$	$\delta^{13}C$ $C_{30}H\beta\alpha$	$\delta^{13}C$ $C_{31}H\alpha\beta S$	$\delta^{13}C$ $C_{31}H\alpha\beta R$	$\delta^{13}C$ $C_{31}H\beta\alpha$	$\delta^{13}C$ $C_{31}H\beta\beta$	$\delta^{13}C$ $C_{32}H\alpha\beta R$
UZ 1-9	-22.73	-23.45			-23.72	-24.52	-23.50	-23.85		-24.64	-24.19	-23.47	
UZ 1-10	-24.16	-24.11	-25.38			-27.90	-28.25			-25.16	-24.71	-23.77	
UZ 1-14	-23.54	-22.76	-25.60			-24.11				-24.11			
UZ 1-20	-23.03	-22.95				-24.79				-24.64	-23.99		
UZ 1-22a	-23.44	-23.37	-24.59	-23.94	-23.59	-24.74				-25.11	-24.41	-24.52	
UZ 1-26b					-24.91	-26.87				-26.75			
L-13-41	-28.78	-28.22			-28.51	-29.05		-28.28		-30.14	-28.82		
L-13-47	-32.87	-32.20	-33.94	-32.61	-32.38	-32.60		-32.35		-32.90	-32.32		
L-13-71	-33.52	-32.99		-34.28	-34.12	-34.29		-33.81	-35.34	-35.28	-34.78		-35.17
L-13-73	-32.75	-32.26		-33.8	-33.81	-33.86		-33.65	-34.87	-34.64	-34.44		-34.66
87-13	-33.23	-32.32	-31.57	-34.02	-34.44	-32.98		-33.29		-33.68	-34.62		
226.5	-25.76	-23.97	-27.88	-26.34	-26.37	-27.69		-26.79	-28.32	-27.74	-25.47		
3-13	-30.19	-29.4		-30.78	-30.41	-30.56		-30.55	-32.29	-31.37	-31.29		

Table 3.3. Mean carbon isotope compositions for extracted pristane (Pr), phytane (Ph), and C_{29} ααα*R* sterane, measured by pico-CSIA. Measurements were performed in triplicate. Average standard error was 0.19‰ for phytane and 0.44‰ for C_{29} ααα*R* sterane.

Sample	$\delta^{13}C_{Pr}$ (‰)	$\delta^{13}C_{Ph}$ (‰)	$\delta^{13}C$ C_{29} Ster ααα*R* (‰)
UZ 1-9		-25.14	-24.48
UZ 1-10		-27.70	-25.86
UZ 1-14			
UZ 1-20			-23.22
UZ 1-22a		-24.10	-23.51
UZ 1-26b			-24.22
L-13-41			
L-13-47		-33.71	-33.29
L-13-71	-38.63	-37.67	
L-13-73			
87-13		-29.84	
226.5		-29.55	
3-13			

Table 3.4. Selected iron mineral speciation redox proxies and tricyclic terpane (TT) abundance ratios that provide depositional environmental constraints

Sample	Drill Core	Location	Stage	Horizon	Depth (m)	26/25 TT	FeHR/ FeT	Fepy/ FeHR
UZ 1-9	Utkina Zavod	Baltic Monocline	Late Ediacaran	Kotlin	64.15	2.32	0.28	0.06
UZ 1-10	Utkina Zavod	Baltic Monocline	Late Ediacaran	Kotlin	71.67	2.15	0.30	0.07
UZ 1-14	Utkina Zavod	Baltic Monocline	Late Ediacaran	Kotlin	87	1.9	0.27	0.00
UZ 1-20	Utkina Zavod	Baltic Monocline	Late Ediacaran	Kotlin	111.6	2.78	0.47	0.01
UZ 1-21	Utkina Zavod	Baltic Monocline	Late Ediacaran	Kotlin	119.9	1.79	0.17	0.00
UZ 1-22a	Utkina Zavod	Baltic Monocline	Late Ediacaran	Kotlin	124.6	2.28	0.24	0.02
UZ 1-22b	Utkina Zavod	Baltic Monocline	Late Ediacaran	Kotlin	127.8	1.91		
UZ 1-26a	Utkina Zavod	Baltic Monocline	Late Ediacaran	Kotlin	152.8	1.56	0.20	0.02
UZ 1-26b	Utkina Zavod	Baltic Monocline	Late Ediacaran	Kotlin	153.5	1.71	0.65	0.00
UZ 1-27	Utkina Zavod	Baltic Monocline	Late Ediacaran	Kotlin	162.1	1.63	0.15	0.09
UZ 1-28	Utkina Zavod	Baltic Monocline	Late Ediacaran	Kotlin	171.4	2.1	0.24	0.02
L-13-41	Lugovoe #13	Baltic Monocline	Late Ediacaran	Kotlin	41	1.24	0.92	0.53
L-13-44	Lugovoe #13	Baltic Monocline	Late Ediacaran	Kotlin	44	1.09	0.64	0.17
L-13-47	Lugovoe #13	Baltic Monocline	Late Ediacaran	Kotlin	47	1.46	0.55	0.19
L-13-71	Lugovoe #13	Baltic Monocline	Late Ediacaran	Redkino	71	1.04	0.69	0.60
L-13-73	Lugovoe #13	Baltic Monocline	Late Ediacaran	Redkino	73	0.97	0.78	0.55
L-13-75	Lugovoe #13	Baltic Monocline	Late Ediacaran	Redkino	75	0.54	0.63	0.46
87-13	Gavrilov Yam -1	Moscow Syneclise	Early Cambrian	Lontovan	1860	0.66	0.34	0.03
87- 25	Gavrilov Yam -1	Moscow Syneclise	Late Ediacaran	Kotlin	2018	0.44	0.21	0.01
4-15	4529	Volyn Basin	Late Ediacaran	Kotlin	~195	1.03	0.60	0.01
4-13	4529	Volyn Basin	Late Ediacaran	Kotlin	~207	0.67	0.35	0.07
4-24	4504	Volyn Basin	Late Ediacaran	Kotlin	~200	0.61	0.32	0.03
3-13	4592	Volyn Basin	Late Ediacaran	Redkino	~166	1.44	0.63	0.25
226.5	3628	Podillya Basin	Late Ediacaran	Redkino	226.5	1.03		
291	3628	Podillya Basin	Late Ediacaran	Redkino	291	1.29		
332	3628	Podillya Basin	Late Ediacaran	Redkino	332	0.66	0.60	0.30
16PL-22	16PL	Podillya Basin	Late Ediacaran	Redkino	outcrop #22	1.11	0.34	0.01
16PL-18	16PL	Podillya Basin	Late Ediacaran	Redkino	outcrop #18	1.13	0.33	0.00
16PL-11	16PL	Podillya Basin	Late Ediacaran	Redkino	outcrop #11	0.75	0.58	0.00

REFERENCES

Baczynski, A.A., Polissar, P.J., Juchelka, D., Schwieters, J., Hilkert, A., Summons, R.E., Freeman, K.H., 2018. Picomolar-scale compound-specific isotope analyses. *Rapid communications in mass spectrometry : RCM* 32, 730–738.

Bobrovskiy, I., Hope, J.M., Golubkova, E., Brocks, J.J., 2020. Food sources for the Ediacara biota communities. *Nature Communications* 11, 1261.

Boschker, H.T.S., Kromkamp, J.C., Middelburg, J.J., 2005. Biomarker and carbon isotopic constraints on bacterial and algal community structure and functioning in a turbid, tidal estuary. *Limnology and Oceanography* 50, 70–80.

Brocks, J.J., Jarrett, A.J.M., Sirantoine, E., Hallmann, C., Hoshino, Y., Liyanage, T., 2017. The rise of algae in Cryogenian oceans and the emergence of animals. *Nature* 548, 578–581.

Brocks, J.J., Logan, G.A., Buick, R., Summons, R.E., 1999. Archean Molecular Fossils and the Early Rise of Eukaryotes. *Science* 285, 1033–1036.

Canfield, D.E., Raiswell, R., Westrich, J.T., Reaves, C.M., Berner, R.A., 1986. The use of chromium reduction in the analysis of reduced inorganic sulfur in sediments and shales. *Chemical Geology* 54, 149–155.

Close, H.G., Bovee, R., Pearson, A., 2011. Inverse carbon isotope patterns of lipids and kerogen record heterogeneous primary biomass. *Geobiology* 9, 250–65.

DeNiro, M.J., Epstein, S., 1978. Influence of diet on the distribution of carbon isotopes in animals. *Geochimica et Cosmochimica Acta* 42, 495–506.

Fischer, W.W., Pearson, A., 2007. Hypotheses for the origin and early evolution of triterpenoid cyclases. *Geobiology* 5, 19-34, doi:10.1111/j.1472-4669.2007.00096.x

Fogel, M.L., Cifuentes, L.A., Velinsky, D.J., Sharp, J.H., 1992. Relationship of carbon availability in estuarine phytoplankton to isotopic composition. *JSTOR* 82, 291–300.

Freeman, K.H., 2001. Isotopic Biogeochemistry of Marine Organic Carbon. *Reviews in Mineralogy and Geochemistry* 43, 579–605.

Freeman, K.H., Hayes, J.M., Trendel, J.-M., Albrecht, P., 1990. Evidence from carbon isotope measurements for diverse origins of sedimentary hydrocarbons. *Nature* 343, 254–256.

Goryl, M., Marynowski, L., Brocks, J.J., Bobrovskiy, I., Derkowski, A., 2018. Exceptional preservation of hopanoid and steroid biomarkers in Ediacaran sedimentary rocks of the East European Craton. *Precambrian Research* 316, 38–47.

Grande, S.M.B.D., Neto, F.R.A., Mello, M.R., 1993. Extended tricyclic terpanes in sediments and petroleums. *Organic Geochemistry* 20, 1039–1047.

Grosjean, E., Love, G.D., Stalvies, C., Fike, D.A., Summons, R.E., 2009. Origin of petroleum in the Neoproterozoic–Cambrian South Oman Salt Basin. *Organic Geochemistry* 40, 87–110.

Guy, R.D., Fogel, M.F., Berry, J.A., Hoering, T.C., 1987. *Progress in Photosynthesis Research* 597–600.

Hayes, J.M., 2001. Fractionation of Carbon and Hydrogen Isotopes in Biosynthetic Processes. *Reviews in Mineralogy and Geochemistry* 43, 225–277.

Hayes, J.M., 1993. Factors controlling 13C contents of sedimentary organic compounds: Principles and evidence. *Marine Geology* 113, 111–125.

Hayes, J.M., Freeman, K.H., Popp, B.N., Hoham, C.H., 1990. Compound-specific isotopic analyses: A novel tool for reconstruction of ancient biogeochemical processes. *Organic Geochemistry* 16, 1115–1128.

Holtvoeth, J., Whiteside, J.H., Engels, S., Freitas, F.S., Grice, K., Greenwood, P., Johnson, S., Kendall, I., Lengger, S.K., Lücke, A., Mayr, C., Naafs, B.D.A., Rohrssen, M., Sepúlveda, J., 2019. The paleolimnologist's guide to compound-specific stable isotope analysis – An introduction to principles and applications of CSIA for Quaternary lake sediments. *Quaternary Science Reviews* 207, 101–133.

Hoshino, Y., Poshibaeva, A., Meredith, W., Snape, C., Poshibaev, V., Versteegh, G.J.M., Kuznetsov, N., Leider, A., Maldegem, L. van, Neumann, M., Naeher, S., Moczydłowska, M., Brocks, J.J., Jarrett, A.J.M., Tang, Q., Xiao, S., McKirdy, D., Das, S.K., Alvaro, J.J., Sansjofre, P., Hallmann, C., 2017. Cryogenian evolution of stigmasteroid biosynthesis. *Science Advances* 3, e1700887.

Jahnke, L.L., Marais, D.J.D., 2019. Carbon isotopic composition of lipid biomarkers from an endoevaporitic gypsum crust microbial mat reveals cycling of mineralized organic carbon. *Geobiology* 17, 643–659.

Kelly, A.E., Love, G.D., Zumberge, J.E., Summons, R.E., 2011. Hydrocarbon biomarkers of Neoproterozoic to Lower Cambrian oils from eastern Siberia. *Organic Geochemistry* 42, 640–654.

Koga, Y., Morii, H., Akagawa-Matsushita, M., Ohga, M., 1998. Correlation of Polar Lipid Composition with 16S rRNA Phylogeny in Methanogens. Further Analysis of Lipid Component Parts. *Bioscience, biotechnology, and biochemistry* 62, 230–6.

Koga, Y., Nishihara, M., Morii, H., Akagawa-Matsushita, M., 1993. Ether polar lipids of methanogenic bacteria: structures, comparative aspects, and biosyntheses. *Microbiological reviews* 57, 164–82.

Kodner, R.B., Pearson, A., Summons, R.E., Knoll, A.H., 2008. Sterols in red and green algae: quantification, phylogeny, and relevance for the interpretation of geologic steranes. *Geobiology* 6, 411–420.

Lee, C., Love, G.D., Fischer, W.W., Grotzinger, J.P., Halverson, G.P., 2015. Marine organic matter cycling during the Ediacaran Shuram excursion. *Geology* 43, G37236.1.

Logan, G.A., Hayes, J.M., Hieshima, G.B., Summons, R.E., 1995. Terminal Proterozoic reorganization of biogeochemical cycles. *Nature* 376, 53–56.

Logan, G.A., Summons, R.E., Hayes, J.M., 1997. An isotopic biogeochemical study of Neoproterozoic and Early Cambrian sediments from the Centralian Superbasin, Australia. *Geochimica et Cosmochimica Acta* 61, 5391–5409.

Love, G.D., Bowden, S.A., Jahnke, L.L., Snape, C.E., Campbell, C.N., Day, J.G., Summons, R.E., 2005. A catalytic hydropyrolysis method for the rapid screening of microbial cultures for lipid biomarkers. *Organic Geochemistry* 36, 63–82.

Love, G.D., Grosjean, E., Stalvies, C., Fike, D.A., Grotzinger, J.P., Bradley, A.S., Kelly, A.E., Bhatia, M., Meredith, W., Snape, C.E., Bowring, S.A., Condon, D.J., and Summons, R.E., 2009. Fossil steroids record the appearance of Demospongiae during the Cryogenian period: *Nature*, 457, 7230, p. 718–721, doi: 10.1038/nature07673.

Meer, M.T.J. van der, Schouten, S., Damsté, J.S.S., 1998. The effect of the reversed tricarboxylic acid cycle on the 13C contents of bacterial lipids. *Organic Geochemistry* 28, 527–533.

Moldowan, J.M., Fago, F.J., Lee, C.Y., Jacobson, S.R., Watt, D.S., Slougui, N.-E., Jeganathan, A., Young, D.C., 1990. Sedimentary 12-n-Propylcholestanes, Molecular Fossils Diagnostic of Marine Algae. *Science* 247, 309–312.

Pagani, M., Arthur, M.A., Freeman, K.H., 1999. Miocene evolution of atmospheric carbon dioxide. *Paleoceanography* 14, 273–292.

Pancost, R.D., Freeman, K.H., Herrmann, A.D., Patzkowsky, M.E., Ainsaar, L., Martma, T., 2013. Reconstructing Late Ordovician carbon cycle variations. *Geochimica et Cosmochimica Acta* 105, 433–454.

Pancost, R.D., Damsté, J.S.S., 2003. Carbon isotopic compositions of prokaryotic lipids as tracers of carbon cycling in diverse settings. *Chemical Geology* 195, 29–58.

Pearson, A., Page, S.R.F., Jorgenson, T.L., Fischer, W.W., Higgins, M.B., 2007. Novel hopanoid cyclases from the environment. *Environmental Microbiology* 9, 2175–2188.

Pearson, A., 2010. *Handbook of Hydrocarbon and Lipid Microbiology* 143–156.

Pehr, K., Love, G.D., Kuznetsov, A., Podkovyrov, V., Junium, C.K., Shumlyanskyy, L., Sokur, T., Bekker, A., 2018. Ediacara biota flourished in oligotrophic and bacterially dominated marine environments across Baltica. *Nature Communications* 9, 1807.

Popp, B.N., Laws, E.A., Bidigare, R.R., Dore, J.E., Hanson, K.L., Wakeham, S.G., 1998. Effect of Phytoplankton Cell Geometry on Carbon Isotopic Fractionation. *Geochimica et Cosmochimica Acta* 62, 69–77, doi: 10.1016/s0016-7037(97)00333-5

Poulton, S.W., Fralick, P.W., Canfield, D.E., 2004. The transition to a sulphidic ocean ~ 1.84 billion years ago. *Nature* 431, 173–177.

Poulton, S.W., Canfield, D.E., 2011. Ferruginous Conditions: A Dominant Feature of the Ocean through Earth's History. *Elements* 7, 107–112.

Poulton, S.W., Canfield, D.E., 2005. Development of a sequential extraction procedure for iron: implications for iron partitioning in continentally derived particulates. *Chemical Geology* 214, 209–221.

Raiswell, R., Canfield, D.E., 1998. Sources of iron for pyrite formation in marine sediments. *American Journal of Science* 298, 219–245.

Raiswell, R., Newton, R., Wignall, P.B., 2001. An Indicator of Water-Column Anoxia: Resolution of Biofacies Variations in the Kimmeridge Clay (Upper Jurassic, U.K.). *Journal of Sedimentary Research* 71, 286–294.

Roeske, C.A., O'Leary, M.H., 1984. Carbon isotope effects on enzyme-catalyzed carboxylation of ribulose bisphosphate. *Biochemistry* 23, 6275–6284.

Rohmer, M., Knani, M., Simonin, P., Sutter, B., Sahm, H., 1993. Isoprenoid biosynthesis in bacteria: a novel pathway for the early steps leading to isopentenyl diphosphate. *Biochemical Journal* 295, 517–524.

Rontani, J.-F., Volkman, J.K., 2005. Lipid characterization of coastal hypersaline cyanobacterial mats from the Camargue (France). *Organic Geochemistry* 36, 251–272.

Scott, K.M., Schwedock, J., Schrag, D.P., Cavanaugh, C.M., 2004. Influence of form IA RubisCO and environmental dissolved inorganic carbon on the delta13C of the clam-chemoautotroph symbiosis Solemya velum. *Environmental Microbiology* 6, 1210–1219.

Smith, K.S., Jakubzick, C., Whittam, T.S., Ferry, J.G., 1999. Carbonic anhydrase is an ancient enzyme widespread in prokaryotes. *Proceedings of the National Academy of Sciences* 96, 15184–15189.

Tang, T., Mohr, W., Sattin, S.R., Rogers, D.R., Girguis, P.R., Pearson, A., 2017. Geochemically distinct carbon isotope distributions in Allochromatium vinosum DSM 180 T grown photoautotrophically and photoheterotrophically. *Geobiology* 15, 324–339.

Wakeham, S.G., Lewis, C.M., Hopmans, E.C., Schouten, S., Damsté, J.S.S., 2003. Archaea mediate anaerobic oxidation of methane in deep euxinic waters of the Black Sea. *Geochimica et Cosmochimica Acta* 67, 1359–1374.

Zumberge, J.E., 1987. Prediction of source rock characteristics based on terpane biomarkers in crude oils: A multivariate statistical approach. *Geochimica et Cosmochimica Acta* 51, 1625–1637.

Zumberge, J.A., Rocher, D., Love, G.D., 2019. Free and kerogen-bound biomarkers from late Tonian sedimentary rocks record abundant eukaryotes in mid-Neoproterozoic marine communities. *Geobiology* 115, 246.

CHAPTER FOUR

What can the Last Remaining Organic Molecules Tell Us? Investigating the Preservation of Covalently Bound Polyaromatic Hydrocarbons in Ancient Biogenic Kerogens and Insoluble Organic Macromolecules (IOM)

ABSTRACT

The likelihood of finding pristine molecular biosignatures from the shallow sub-surface of Mars is low given the highly oxidizing conditions present. Recently a suite of simple aromatic and other stable organic compounds have been detected from Gale Crater however, these highly derived organic compounds are not necessarily biogenic in origin. We are attempting to better understand the distributions and systematics of preservation of organic compounds that may persist in the accessible Martian sedimentary record specifically, polycyclic hydrocarbons (PAH), as both free hydrocarbons and bound in insoluble macromolecules. Here we report the distribution of bound PAHs in biogenic kerogens and in a selection of insoluble organic matter (IOM) from carbonaceous residues. The degree of thermal maturity of the sedimentary organic matter exerts the primary control on the preservation and distributions of the major 5-ring and 6-ring PAH compounds generated by catalytic hydropyrolysis (HyPy) from ancient biogenic kerogens. This holds for both Precambrian and Phanerozoic rocks, thus the primary biogenic organic matter inputs are of secondary importance since these large PAHs constitute highly derived and stable organic compounds. All ancient biogenic kerogens

analyzed to date contain detectable amounts of perylene, even for the most thermally transformed samples. Perylene persists to extremely high levels of thermal stress as a bound PAH constituent, including for overmature Archean kerogens and for ancient biogenic kerogens heated to elevated temperatures by volcanic intrusions. While perylene has also been found in low abundances in Murchison meteorite IOM, presence of perylene in HyPy products could prove to be an important and novel molecular signature for identifying macromolecular organic matter formed during protracted low temperature synthesis conditions. Bound perylene could be used to identify samples containing sedimentary organic matter that have undergone extended intervals of early diagenesis under low temperature conditions (<50°C). In contrast, perylene was not detected as a bound 5-ring PAH product from 2.1 Ga pyrobitumens and from an insoluble coke deposit, despite the generation of other stable PAH compounds. Such insoluble carbonaceous residues, generated here predominantly from hydrocarbon cracking reactions at high temperatures (>150°C), preserve a distinguishable bound PAH profile to that from ancient biogenic kerogens.

1. INTRODUCTION

Our close neighbor Mars may have once maintained early surface planetary conditions conducive to fostering microbial life. Searches for definitive evidence of fossil or extant extraterrestrial biosignatures on Mars or elsewhere in the solar system have, however, thus far returned inconclusive. One approach is to search for molecular organic fossils, known as biomarkers, in sedimentary rocks. The long-term preservation of lipids and

other biomolecules in the shallow sub-surface of Mars in recognizable form is of low probability. Due to Mars's thin atmosphere, lack of a robust ozone shielding layer, and loss of its magnetic field, any organic material remaining near the surface or buried in the shallow sub-surface, down to a few meters depth, may be heavily altered over time by solar ultraviolet and galactic cosmic irradiation (Parnell et al., 2007). Furthermore, the absence of plate tectonics on Mars has left surface sediments exposed for potentially billions of years (Carr and Bell, 2014). On Earth, we use lipid biomarkers that are structurally distinctive and minimally altered, and which are clearly the remains of biomolecules produced by organisms using enzymatic synthesis (Peters et al., 2005). We should not rely on the serendipity of finding well preserved lipid and other biomolecules as our only scoping strategy in the extraterrestrial search for organic biosignatures. Under such unsuitable conditions for preservation, organic molecules are more likely to be found cross-linked into insoluble and aromatic-rich carbonaceous residues in any case, rather than as discrete lipid biomarker compounds amenable to solvent extraction or volatilization (Killops and Killops, 2005).

Unlike polycyclic terpenoid biomarkers, such as hopanoids and steroids, stable aromatic compounds may have a variety of poorly defined biological and/or abiogenic sources, since they usually possess highly derived chemical structures (Peters et al., 2005). Detection of ^{13}C-depleted bulk $\delta^{13}C$ signatures of organic compounds or carbonaceous residues, on their own, does not automatically imply either that these constituents were produced by biosynthesis. Abiotic synthesis from chemical reactions may yield

significantly ^{13}C-depleted organic molecules, such as Fischer-Tropsch synthesis from CO/CO_2 sources at elevated temperatures and pressures in Earth's subsurface or under hydrothermal conditions, have been demonstrated experimentally (McCollom and Seewald, 2006). Indeed, none of the aromatic compounds detected so far on Mars (Freissinet et al., 2015; Eigenbrode et al., 2018; Szopa et al., 2019) and in Martian meteorites (McKay et al., 1996) are currently considered as conclusive evidence of past biological activity. If we ever hope to use these recalcitrant aromatic compounds as molecular biosignatures of past life on Mars, we need a better understanding of: i) their transformations and systematics of preservation in the rock record within ancient biogenic kerogens, in order to recognize ii) diagnostic compound distributions and abundance patterns that are highly suggestive of a possible biogenic or low temperature synthetic origin.

The organic matter found in sediments, soils or meteorite samples generally comprises complex mixtures of hydrocarbons and non-hydrocarbons which are preserved in one of two operationally defined phases that co-exist together: the soluble and insoluble organic phases. Organic matter that is soluble in common organic solvents (such as chloroform, or in solvent mixtures) is commonly called 'bitumen' or 'free organic matter' since many of the detectable organic compounds exist as discrete molecules. In contrast, insoluble organic matter consists of molecules which are bound together to form a complex macromolecular organic structure known as 'kerogen' or 'insoluble organic matter (IOM)'. Kerogen accounts for the vast majority of biogenic organic carbon retained in

sedimentary rocks on Earth (Killops and Killops, 2005), while insoluble organic matter is also the dominant form in meteorites (Sephton, 2005; Sephton et al., 1998). On Earth, lipids and other biochemicals can become covalently linked during early diagenesis to form kerogen via their reactive functional groups, commencing in the water column and continuing within years to decades of sedimentary burial and beyond (Farrimond et al., 2003; Lee et al., 2019). Organic molecular constituents bound within kerogen usually undergo less structural and stereochemical alteration than bitumen in the same sample due to steric protection offered by the host macromolecular kerogen matrix (Peters et al., 2005; Love et al., 1995). Molecular constituents of kerogen are also less susceptible to contamination than the extractable organics since contaminant molecules can migrate into the mobile bitumen phase more readily than the insoluble and immobile kerogen (Murray et al., 1998). For this study, the term *IOM* will be used when referring to insoluble organic matter from extraterrestrial samples (both meteorites and Martian regolith) and pyrobitumens (insoluble residues which were likely formed from thermal cracking of hydrocarbon and oil feedstocks). The term *kerogen* will be used for all other terrestrial samples, implying a mainly biogenic source contribution. Targeting insoluble organic matter becomes particularly important when attempting to recover molecular biosignatures from organic-lean and chemically altered rocks and soils since covalent binding cam help preserve organic compounds even after they have been completely degraded as readily extractable compounds from the bitumen phase.

Encouragingly, the Sample Analysis at Mars (SAM) instrument suite on the Mars Science Laboratory Curiosity Rover has already detected numerous aromatic and other volatile organic compounds in ancient Martian mudstones from Gale Crater (Szopa et al., 2019; Eigenbrode et al., 2018; Freissinet et al., 2015). The SAM instrument includes continuous-flow pyrolysis (Py) with low pressure helium as the carrier gas, evolved gas analysis (EGA), and gas chromatography–mass spectrometry (GC-MS). Samples taken from the Sheepbed mudstone were found to host 150 to 300 parts per billion of chlorobenzene (Freissinet et al., 2015). Aromatic sulfur compounds including thiophene (C_4H_4S), methanethiol (CH_4S), 2- and 3- methylthiophenes (C_5H_6S), and dimethylsulfide (C_2H_6S) were later reported from samples from Mojave and Confidence Hills sites and identified using GC-MS (Eigenbrode et al., 2018). EGA analysis of the same samples also detected signal peaks at temperatures suggestive of benzene, toluene, alkylbenzenes, and C_1 to C_5 aliphatic fragments, but these analytes were too low in abundance to be unequivocally confirmed by GC-MS. Total organic carbon (TOC) abundances in host sediments were calculated to be 10-100 nmol of organic carbon (Eigenbrode et al., 2018). More recently, Szopa et al., (2019) detected dichlorobenzene (DCBZ) isomers and trichloromethylpropane (TCMP) in a Cumberland mudstone. However, the source of this organic carbon remains unknown and an abiogenic origin could not be ruled out. Pyrolysis experiments in the presence of calcium perchlorate suggest that meteoritic organics, as well as individual polycyclic aromatic hydrocarbons, amino acids, or carboxylic acids could serve as plausible organic precursors for the chlorinated aromatic molecules detected by SAM (Szopa et al., 2019). Perchlorates and other strongly

oxidizing oxyanion salts significantly inhibit the detection of organic compounds from soils and sediments using conventional Py-GC-MS in a helium stream, unless a prior aqueous leaching or chemical reduction step is performed (Montgomery et al., 2019).

1.1. Polycyclic aromatic hydrocarbons (PAHs)

Polycyclic aromatic hydrocarbons (PAHs) are organic compounds comprised usually of two or more benzene (six-carbon rings with delocalized π bonds) or other aromatic rings bonded together. Fig. 4.1 displays the chemical structures for a range of parent PAHs discussed further in this paper. Polycyclic aromatic hydrocarbons most commonly encountered in the environment contain two (naphthalene, two-ring) to seven (coronene, seven-ring) fused benzene rings. They are ubiquitous in our natural environment and can constitute a significant portion of ancient and recent sedimentary organic matter. Owing to their high chemical stability, PAHs generally become more enriched with increasing thermal maturity of the host sediment. Polycyclic terpane biomarkers and other source-diagnostic lipids are typically lost through thermal transformations from the bitumen phase of rocks at high thermal maturity, such that these are undetectable at elevated vitrinite reflectance values of ~1.4 to ~1.8% R_o (Mißbach et al., 2016). Additionally, the kerogen structure becomes increasingly aromatic in its chemical composition with increasing thermal maturity and the dominant bound PAH moieties change in their distributions within the kerogen matrix (Marshall et al., 2007). Covalently linked PAHs are hence amongst the most recalcitrant and oldest surviving organic constituents of ancient biogenic organic matter found on Earth, which is composed predominantly of

highly aromatized kerogen. More generally, PAHs are the expected dominant molecular building blocks of any relic organic material remaining after being subjected to sustained heavy alteration and degradation by thermal, chemical or radiolytic processing.

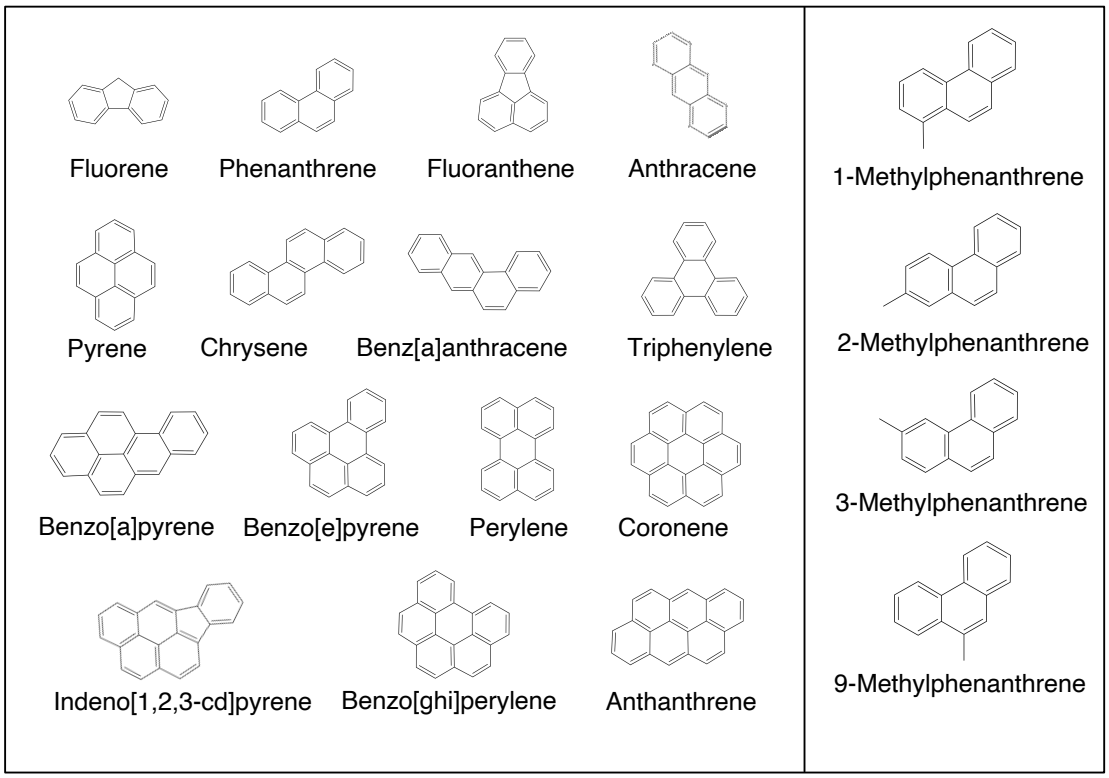

Figure 4.1: Chemical structures of selected polycyclic aromatic hydrocarbons (PAHs) discussed in the text.

PAHs are not known to be biosynthesized in appreciable amounts by living organisms and indeed such compounds may be highly toxic to living cells (Killops and Killops, 2005). Instead, two common sources of PAHs in sediments are (1) from the diagenetic and catagenetic alteration of biologically derived organic molecules during protracted burial (Wakeham et al., 1980; Grice et al., 2009), or (2) thermal cracking caused by the rapid and incomplete combustion or high temperature conversion of biomass, fossil fuels

and other carbonaceous feedstocks (Simoneit, 1998; Britt et al., 2001). Other possible anthropogenic sources of PAH's into the natural environment emanate from industrial processes and vehicle emissions from fossil fuel sources (Wickstrom and Tolonen, 1987). Thus, PAHs can be produced from both low and high temperature processing of precursor organics and on short (rapid combustion and pyrolysis) to long (geologic) timescales.

The ubiquity of PAHs found within thermally immature sediments most likely represent early diagenetic aromatization of biochemical precursors, along with more sporadic contributions from anthropogenic or natural sources arising from aerosols and soots produced from high temperature processing of fossil fuels or biomass. The exact mechanistic pathways have yet to be elucidated however the formation process is likely slow with many of the surviving ancient PAH patterns set by the protracted diagenesis of biochemicals during low temperature burial and microbial processing. Certain simple sedimentary PAH compounds, including perylene and retene, have been put forward as potential products formed from the diagenetic alteration of specific biogenic compounds (van Aarssen et al., 2000; Grice et al., 2009). PAH formation from incomplete combustion or fast pyrolysis (>400°C) is thought to occur in two steps: pyrolysis and subsequent pyrosynthesis as benzene and other aromatic ring building blocks fuse together to form larger PAH compounds and sheets (Simoneit, 1998; McGrath et al., 2003). As temperatures cool away from the hottest zone, the free radicals recombine to form small ring PAHs which can further pyrosynthesize into larger and larger PAHs.

PAHs formed through this 'zigzag' addition process (Sullivan et al 1989; Fetzer 2010) generally consist predominantly of the most thermodynamically stable isomers (Stein, 1986). Unlike polycyclic lipid biomarkers, PAHs have already been detected in a variety of extraterrestrial samples including carbonaceous chondrites (Sephton et al., 2004, 2005, 2013, Yabuta et al., 2007; Sephton et al., 2015), interstellar dust (Tielens, 2008), and from the ancient Martian surface (Eigenbrode et al., 2018). Proposed abiotic sources of cosmic PAHs include stellar ejecta, shattering of carbonaceous grains from interstellar shocks, as well as gas-PAH reactions in the cold interstellar medium (Tielens, 2008).

1.2. Release of kerogen-bound PAH using catalytic hydropyrolysis (HyPy)

Due to the low volatility and highly cross-linked nature of organic macromolecules such as kerogen, these can be difficult to structurally characterize at a molecular level. One powerful technique which converts bound organics into analyzable fragments is a "mild" pyrolysis technique termed catalytic hydropyrolysis (or HyPy). HyPy involves heating samples up to temperatures of 520°C in a continuous flow of high hydrogen gas pressures (15 MPa) with a molybdenum sulfide catalyst to cleave covalent bonds (Love et al., 1995, 1997, 2009). HyPy can generate high yields of soluble products while preserving the structural and stereochemical features of biomarker hydrocarbons to a high degree. HyPy is an established and effective continuous-flow pyrolysis technique and has been shown previously to generate higher pyrolysate yields and a wider range of gas chromatography-amenable aromatic hydrocarbons from the IOM in Murchison meteorite compared with other pyrolysis techniques (Sephton et al., 2004).

Previous HyPy studies of kerogen-bound PAH from ancient biogenic organic matter have revealed a complex mixture of fragment products are often produced, with strong thermal maturity controls on the overall product distributions. A comparison of total ion current (TIC) chromatograms overmature Archean kerogen from 3.4 Ga Strelley Pool Chert to that of an unmetamorphosed 1.4 Ga sample from the Urapunga 4 drill core of the Velkerris Formation, revealed that some prominent features of their PAH profiles were very similar (Marshall et al., 2006, 2007). The major aromatic compounds detected for both samples were pyrene (a four-ring PAH) and phenanthrene (a three-ring PAH) and the aromatic hydrocarbon products amenable to gas chromatography spanned a large range of molecular masses containing from one to seven aromatic rings. In addition to these compounds, both samples showed major peaks for naphthalene, methylphenanthrene, fluoranthene, methylpyrene, chrysene, methylchrysene, benzo(ghi)perylene, and benzo(e)pyrene. As anticipated though, the less thermally mature Velkerri Formation kerogen, possessing a higher atomic H/C ratio, generated a more complex distribution of PAH due to more extensive alkylation of aromatic rings surviving the milder burial regime (Marshall et al., 2007). This study hints though that certain patterns of kerogen-bound PAH distributions, based around the abundance profiles of the major parent PAH constituents, offers some promise as molecular biosignatures if shown to be regularly occurring pattern found in the fragmentation products of ancient biogenic kerogens.

These previous organic geochemical studies highlight the need to better constrain the role that protracted thermal alteration has on controlling the distribution patterns of PAH found in kerogen and IOM. It is already apparent that the systematics controlling the preservation of the free hydrocarbons present in the bitumen phase may be different to those influencing the corresponding bound distributions, including for PAHs (Marshall et al., 2007). PAH abundance patterns are determined by at least two major factors: the organic source material from which the PAHs were formed as well as the severity of the thermal transformation reactions that they have experienced (e.g. low temperature diagenesis or from high temperature cracking). It is necessary to disentangle these various influences on kerogen-bound PAH preservation and compound distributions.

The purpose of this investigation then was to assess the distribution of covalently linked PAH compounds preserved by binding within ancient biogenic kerogens and in IOM carbonaceous residues. In particular, we hoped to gain a better understanding of: i) how bound PAH distributions vary in ancient biogenic kerogens, particularly as a function of thermal maturity across a wide maturity range, and ii) how distinctive these ancient biogenic PAH profiles are in comparison with the bound PAH distributions released from fragmentation of thermally and/or chemically generated carbonaceous residues (such as the IOM in meteorites, coke deposits on catalysts and ancient pyrobitumens). We can use this information to better assess whether the molecular analysis of highly aromatic carbonaceous residues could be useful in the astrobiological search of past life. We are seeking to ascertain whether certain bound PAH abundance patterns might qualify as

possible “last resort” molecular biosignatures for highly altered organic matter on other planetary bodies, for samples that do contain obvious source-diagnostic biomarkers.

2. SAMPLES AND METHODS

2.1. Sample information

2.1.1. Ancient sedimentary rock description and collection for biogenic kerogens

We selected a suite of ancient rocks for kerogen analysis covering a wide range of thermal maturities, from thermally immature (pre-oil window stage prior to catagenesis) samples through to overmature rocks, and of different geological ages (Table 1 and 2). We ensured that this included a suite of rock samples containing overmature biogenic kerogen to compare their molecular fragment profiles generated by pyrolytic cleavage with those from pyrobitumens and coke samples. The level of thermal maturity of sedimentary organic matter is primarily controlled by both the peak and duration of temperature experienced through the burial history of the host strata (Killops and Killops, 2005).

We have separated the ancient rock samples in this study by their relative thermal maturity ordering with respect to the *oil window* (Peters et al., 2005*)*, see Fig. 4.2. Immature samples are those that have only undergone low temperature diagenesis and which have usually not experienced maximum burial temperatures in excess of 50°C. More mature samples lie within the oil window and the sedimentary organic matter in this case has undergone some degree of covalent bond cleavage during the catagenesis

stage, resulting in structural modification of organic compounds and macromolecules and generation of fragments. The oil window typically corresponds to burial temperatures of 50°C to 150°C; however, these boundaries are gradual and are not strictly fixed at these exact values (Killops and Killops, 2005). Overmature rocks have been heated to much higher sedimentary temperatures (typically >150°) over protracted geologic time such that the main residual organic component is aromatic-rich kerogen and a significant proportion of the original sedimentary organic matter has been lost as hydrocarbon fragments (as oil and then gas) generated by thermal cracking. The thermal maturity stage of the samples was determined using a variety of published information available involving a combination of Rock-Eval pyrolysis, vitrinite reflectance (% R_o) and organic matter reflectivity, lipid biomarker maturity parameters, presence/absence of polycyclic alkane biomarkers, and analysis of the mineral assemblage. Descriptions of sedimentary rocks used for kerogen HyPy are listed in order of increasing thermal maturity as gauged from the available maturity constraints.

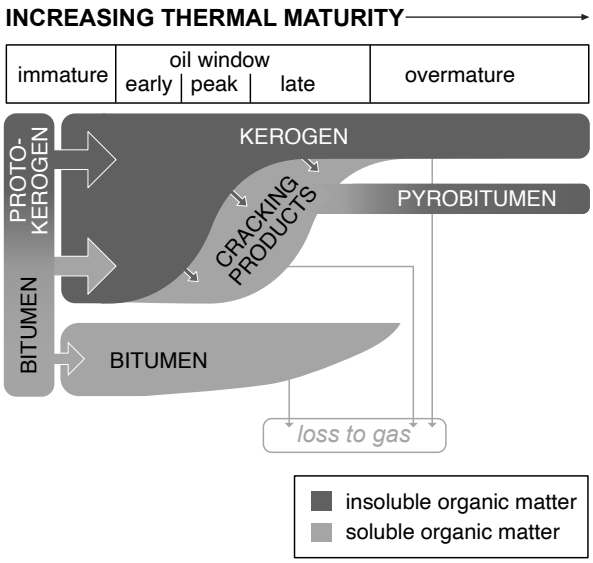

Figure 4.2: Simplified conceptual model of transformations of sedimentary organic matter phases with increasing thermal maturities showing preferential preservation of insoluble organic matter at higher maturities

The Demerara Rise samples are from Unit IV of the Ocean Drilling Program (ODP) site 1258, well holes 1258A, 1258B, and 1258C. They are finely laminated and organic-rich marine sedimentary deposits which span the OAE2 event at the Cenomanian-Turonian boundary during the Cretaceous Period. Trace metal and lipid biomarker data from the specific samples used in this study were previously reported in Owens, et al. (2016). Lipid biomarker maturity parameters indicate these samples are extremely thermally immature such that these have not yet passed into the oil window stage (Owens, et al., 2016). These were the least mature ancient sedimentary rock samples used in this investigation.

Ten upper Cretaceous marls from the Gulf Coast Basin represent the Boquillas Formation. Vitrinite reflectance measurements and lipid biomarkers place the five samples from the Duke Well within the early oil window and the five samples from the Queen Well within the late oil window stage.

The Jet Rock Formation sample is a Lower Jurassic (Toarcian) marine black shale collected from outcrop at Hawsker Bottoms in the Cleveland Basin of North Yorkshire. Lipid biomarker maturity parameters suggest that corresponds to an early-middle stage of oil window maturity (Bowden et al., 2006). This agrees with previously measured vitrinite reflectance values of % R_o = 0.55–0.69 (Ibrahim, 1995) and Rock-Eval pyrolysis parameters (Bowden et al., 2006; French et al., 2014) for the Jet Rock Formation.

A Paleoproterozoic dolomitic mudstone from the 1.64 Ga Barney Creek Formation was sampled from the GR-10 drill core of the Glyde Region of the McArthur Basin in northern Australia. The Barney Creek Formation contains some of the lowest thermal grade rocks of this age; preserving abundant and diverse lipid biomarker assemblages, including hopanes as well as a range of C_{40} carotenoid markers likely derived from anoxygenic phototrophic bacteria (Brocks et al,. 2005). Biomarker maturity and Rock-Eval pyrolysis constraints place the thermal maturity within an early stage of the oil window.

A Neoproterozoic sedimentary rock sample from the Visingsö Group in southcentral Sweden was collected from the Broken Nodule outcrop location on the southeastern shore of Lake Vättern and described in detail by Zumberge et al. (2019). This is a marine carbonaceous shale which was deposited during the Tonian Period (ca. 750 Ma). Thermal maturity parameters, including from temperature-programmed pyrolysis and lipid biomarker ratio parameters, indicate that the sample is in the transitional stage of early-middle oil window maturity.

Rocks from the Chuar Group are also Tonian in age (ca. 729 Ma) and these were sampled from the Walcott Member of the Kwagunt Formation. Two marine carbonaceous mudstones were collected from the Nankoweap Butte outcrop location and another two samples from Sixtymile Canyon outcrop site as previously described by Zumberge et al. (2019). Lipid biomarker and temperature-programmed pyrolysis parameters from this

prior study place the Sixtymile Canyon outcrop samples around peak oil window maturity whereas the Nankoweap Butte samples are of higher rank and correspond to late oil window thermal maturity.

Samples from the Alberta Basin (Canada) consist of lower Triassic marine phosphatic shales and were collected from the Heron Well, Skylark Well, and the Phoenix Well. The Skylark and Heron wells each have a sample from the Doig Formation and a sample from the Montney Formation. Two lower Triassic samples were collected from the Phoenix Well in the Alberta Basin but the lithology and stratigraphic position for this well is unassigned. Vitrinite reflectance values range from 1.2 to 1.5%, placing all these samples within a late stage of the oil window beyond peak oil generation.

Ediacaran (635-551 Ma) rocks are from the Doushantuo Formation within the Nanhua Basin in South China. Samples are interpreted as inner marine shelf facies Jiulongwan outcrop section and these are described in Li et al. (2010). Hydrogen indices are generally extremely low in value (≤22 mg/g TOC) for these rocks and thus are indicative of overmature sedimentary organic matter. Carbonaceous material (CM) Raman geothermometry and smectite illitization constraints of similar Doushantuo samples from the Nanhua Basin suggests that the host rocks may reach high high peak temperatures of 300°C (Wang et al., 2017; Derkowski et at., 2013) and these are thus generally classified as overmature, although maturity heterogeneities in Doushantuo strata can occur from sample location to location. This is further supported by the absence of any demonstrably

indigenous polycyclic alkane biomarkers within either the bitumen or kerogen phases. There is also evidence that the cap dolostone experienced hydrothermal alteration (Derkowski et at., 2013; Lin et al., 2011). Two rock samples from the oldest and deepest stratigraphic interval (DST I) of Doushantuo Fm., sampled near the Nantuo cap dolostone, are CapB and HJ01. These have negligible HI values (≤6 mg/g TOC) are therefore labeled as 'overmature (altered)' for the purposes of this study.

Samples from Pilbara Craton, Australia, come from the AIDP-2 drill core obtained by the 2012 Agouron Institute Australian Drilling Program in the Ripon Hills region (21°16'51"S, 120°50'2"E). Selected samples used are 2.63–2.67 Ga Archean carbonates from the Carawine Formation. Oil-based lubricants were avoided during drilling and yielded the three cleanest Archean rock cores ever returned for detailed organic geochemical work (French et al., 2015). The $\delta^{13}C_{org}$ signatures of individual PAH released by HyPy from extracted rocks were first described in French et al. (2015). Studies of the mineral assemblage and organic matter reflectivity place these samples within the prehnite−pumpellyite metamorphic facies and anthracite coal rank, implying maximum burial temperatures of 200–300°C which is consistent with overmature organic matter (Buick et al., 1995; Smith et al., 1982).

Six Carboniferous calcareous shales from the Stainmore Formation (formerly known as the Millstone Grit Group) were collected from the Boulmer Outcrop in the Northumberland Basin. The strata experienced two volcanic heating episodes: from

formation of a sill above the samples and from an intrusive feeder dyke into the sill. The samples were taken with relation to distance from the dyke to produce a thermal maturity gradient. In this study, samples closer to the dyke, 7.94m to 10.3m, are referred to as "proximal" while samples further from the dyke, 29.8m to 48.8m, are referred to as "distal". These samples all lack detectable polycyclic alkane biomarkers bound within their kerogen structure and have extremely low hydrogen index (HI) values (7-65 HI mg/g TOC), which suggests they are categorized as overmature (beyond the late oil window). High HI values correspond to a greater quantity of thermally labile kerogen remaining in source rocks and a greater potential to generate oil (Hunt, 1991). HI decreases with increasing maturity, although care must be taken as organic matter type and mineralogy may also influence HI values (Peters, 1986). At elevated thermal maturities of late oil window and beyond, the influence of organic matter source and mineralogy wanes and HI is primarily controlled by thermal maturity (Espitalié et al., 1984; Peters, 1986; Radke, 1988). While all these shales are at least 'overmature', the samples closest to the dyke likely experienced a rapid and intense heating event which may have resulted in extensive cracking of the organic matter. We have therefore categorized these samples separately as 'overmature (altered)'.

2.1.2. Pyrobitumens

In addition to the ancient biogenic kerogen samples, we also analyzed Paleoproterozoic pyrobitumens for comparison. Pyrobitumen is a solid, insoluble type of sedimentary organic matter and typically represents the small fraction of recalcitrant and high

molecular weight residue remaining after the thermal cracking of oils in rock (Peters et al., 2005), see Fig. 4.2. Pyrobitumen preserves a heavily thermally altered signal of organic material in a solid form, thought to be similar in bulk structural composition to highly mature kerogen, and is a good representative of cracked organic material. Since extensive cracking obliterates high molecular weight organic matter to small molecular weight radicals and volatile products, this process removes a high proportion of the original source-diagnostic features in stable organic compounds. For this reason, pyrobitumen has often been dismissed as an unreliable repository of ancient biogenic source inputs and very little research has been conducted on its molecular composition other than verifying a high proportion of aromatic carbon in the macromolecular structure (Bernard et al., 2012).

Pyrobitumens and shales were collected from the 2.1 Ga FC Formation, Francevillian Series in Gabon from two drill cores, LST1 and LST12. The FC formation contains black marine shales and dolostones with fractures filled with pyrobitumen and pyrite (Ossa Ossa et al 2018). Samples (LST1 60.6 P), (LST12 93 P), and (LST12 107.8 P) were hand-picked pieces which were selected to contain predominantly pyrobitumen, while the remaining Francevillian samples are a mixture of shale and pyrobitumen. The Francevillian Series samples are fairly rich in TOC content (Ossa Ossa et al., 2013). However, the organic matter present in the rocks has experienced high thermal alteration (Cortial et al., 1990). The pyrobitumen residues were likely generated, at least in part, from thermal cracking of hydrocarbon and non-hydrocarbon components of expelled

heavy bitumen or oil in the host rocks. While the hydrocarbon/bitumen feedstocks are biogenic in origin, the formation mechanism from a high temperature (>150°C) recombination of free organic radicals produced from thermal cracking reactions of hydrocarbons or expelled bitumen means that these can be regarded as model systems for gaining valuable insights into macromolecular structure of abiogenic IOM.

2.1.3. Coke residue from FCC (fluidized catalytic cracking) processing of hexadecane

An insoluble (coke) residue formed from high temperature laboratory simulation of fluid catalytic cracking (FCC) refinery process, using *n*-hexadecane as the organic feedstock, was used as a model system to investigate high temperature PAH formation in IOM. The coke residue sample was produced in a laboratory experiment conducted at University of Nottingham using a continuous-flow reactor oven with a catalyst bed. A commercial BASF FCC-75 refinery catalyst was placed in a microactivity test (MAT) unit as described in ASTM D-3970 and heated to 482°C at a rate of 20°C /min under a N_2 flow of 20 ml/min. Once the reaction temperature had been attained, the system was purged with N_2 for 30 min. A model compound precursor, *n*-hexadecane, was then introduced to the MAT reactor at a rate of 1.38 ml/min for 75 s. During this injection period, the N_2 flow was switched off. After injection, the reactor and product recovery system was purged with a N_2 flow of 20 ml/min for 15 min. The coke residue was then collected from the catalyst for subsequent HyPy treatment to fragment the macromolecular matrix to probe the distributions of bound PAH to be determined using gas chromatography-mass spectrometry (GC-MS).

2.2. Rock-Eval pyrolysis parameters

Rock-Eval pyrolysis analyses were conducted at GeoMark Research in Houston, TX. Approximately 100 milligrams of washed, ground (to 60 mesh) whole rock sample were analyzed with a Rock-Eval II instrument. Measurements include S1: free bitumen content (mg HC/g rock); S2: remaining generation potential (mg HC/g rock); T_{max}: temperature at maximum evolution of S2 hydrocarbons (°C); and S3: carbon dioxide yield from organic carbon (mg CO_2/g rock). The data was generated by heating according to the following parameters S1: 300°C for 3 minutes; S2: 300°C to 550°C ramping at 25°C/min, and then held at 550°C for 1 minute; S3: hold at temperature between 300 to 390°C. Instrument calibration was achieved using a rock standard with values determined based on a curve calibrated with pure hydrocarbons of varying concentrations. The standard was analyzed 3 times for every 10 samples as an unknown to check the instrument calibration. HI (in mg/g TOC) was calculated from: [(S2 × 100)/TOC], with TOC expressed in units of wt.% of bulk rock.

2.3. Rock extraction and bitumen fractionation

Solvent extraction of rock powders and subsequent separation of the rock bitumens was performed using established procedures (Haddad et al., 2016; Pehr et al., 2018; Zumberge et al., 2019). Rock samples were trimmed with a water-cooled rock saw to remove weathered and contaminated outer surfaces and to isolate the inner rock portion. The saw blade was extensively cleaned with a stepwise sequential solvent wash of hexane, dichloromethane (DCM), and methanol (MeOH) between samples. Trimmed rock pieces

from the inner portion were sonicated first in methanol and secondly in dichloromethane (DCM) to remove any vestiges of contaminants introduced during cutting. The cleaned rock fragments were powdered with a zirconia ceramic puck mill in a SPEX 8515 shatterbox. The ceramic puck mill was extensively cleaned with the above solvent rinse cycle and by powdering with pre-combusted quartz sand (850°C overnight) between samples to eliminate cross-contamination.

The powdered sample was extracted in a CEM Microwave Accelerated Reaction System (MARS) at 100°C in a 9:1 v:v DCM:MeOH solvent mixture for 15 min with constant stirring followed by a vacuum filtration at room temperature. After filtration, the extracted rock powder residue, containing kerogen as the principal sedimentary organic matter constituent, was collected and saved for subsequent continuous-flow hydrogen pyrolysis (HyPy) treatment. Full laboratory procedural blanks with combusted quartz sand (850°C) were run in parallel with each batch of samples as a control to ensure that any background signals were negligible in comparison with biomarker analyte abundances found. Elemental sulfur was removed from the bitumen extract using copper pellets activated with hydrochloric acid and rinsed with deionized water, methanol, and dichloromethane to remove the residual acid. The total bitumen extract was separated into aliphatic, aromatic, and polar fractions by pre-combusted silica gel (60 mesh, 450°C) column chromatography. The aliphatic fraction was eluted with hexane, followed by the aromatic fraction with 1:1 v:v hexane:DCM, and, finally, the polar fraction was eluted with 4:1 v:v DCM:MeOH.

2.4. Catalytic Hydropyrolysis (HyPy) of Extracted Rocks

The HyPy procedure for solvent-extracted rocks has been previously described in detail (French et al., 2015; Love et al., 1995, 2009; Lee et al., 2019; Zumberge et al., 2019). The residual organic matter in our solvent-extracted rock samples consists predominantly of kerogen. After the rock powders were exhaustively extracted with solvent, the powders (~0.5–1.5 g) were loaded with 5 wt% ammonium dioxydithiomolybdate catalyst, which reductively decomposes in situ under HyPy conditions above 250°C to form a catalytically active molybdenum sulfide (MoS_2) phase (Love et al., 1995, 2005). The catalyst-loaded sample powder was placed in a solvent-cleaned steel reactor tube and held in place with a steel wool ball, which was Soxhlet extracted (DCM, 48 hr) and then combusted (450°C, 2 hr) prior to use to ensure that no contaminants were introduced to the reactor tube. The samples were then heated from ambient temperature to 250°C at 100°C/min, immediately followed by 250–520°C at 8°C/min while maintaining constant hydrogen pressure of 120-150 bar with a flow rate of ~6 L/min. The hydrogen sweep gas flow ensured that volatile products were efficiently removed from the hot zone of the reactor to limit structural and stereochemical rearrangement of hydrocarbon products (Love et al., 2005). The pyrolysate for each sample was rapidly adsorbed onto pre-combusted silica gel (36–70 mesh) contained within a dry ice-cooled product trap. Blank HyPy runs, with the steel wool ball loaded in the reactor tube, were run to verify that the batch of steel wool was free of contamination and full procedural blanks, performed with pre-combusted sand, were performed to quantify the background signal. After each HyPy run, the silica gel containing the adsorbed pyrolysate product was fractionated into three

fractions (aliphatics, aromatic, and polars) and desulfurized using the same methods as described above for the rock bitumens (see Section **2.3**).

2.5. GC-MS Characterization of Pyrolysis Products

Aliphatic hydrocarbon fractions were analyzed by metastable reaction monitoring–gas chromatography–mass spectrometry (MRM–GC–MS) conducted at UC Riverside on a Waters Autospec Premier mass spectrometer equipped with an Agilent 7890A gas chromatograph and DB-1MS coated capillary column (60 m x 0.25 mm, 0.25 μm film) using He as a carrier gas. The GC temperature program started with an initial hold at 60°C for 2 min, heating to 150°C at 10°C/min followed by heating to 320°C at 3°C/min and a final hold for 22 min; analyses were performed via splitless injection in electron impact mode, with an ionization energy of 70 eV and an accelerating voltage of 8 kV.

The aliphatic and aromatic hydrocarbon fractions were analyzed at the University of California, Riverside by gas chromatography–mass spectrometry (GC–MS) on an Agilent 7890A GC system coupled to an Agilent 5975C inert Mass Selective Detector (MSD) mass spectrometer. The GC was equipped with a DB1-MS capillary column (60 m x 0.32 mm, 0.25 μm film thickness) using He as the carrier gas. Samples were injected in hexane solutions for saturates and 2:1 hexane:DCM solution for aromatics. The samples were run in full scan mode and injected into the GC in splitless mode with a programmable temperature vaporizing (PTV) inlet. The GC oven was held at 60°C for 2 min, heated at 20 °C/min to 150°C then 2°C/min to 325°C for 20 min. Total Ion

Chromatograms (TICs) for the aliphatic and aromatic fractions were generated by GC-MS in over a mass range of 50 to 800 Da. Compounds were identified on the GC-MS by the detection of their molecular ion and their retention time. The QTM PAH Mix standard was used to help verify the structures of the PAH compounds, using relative retention times and mass spectra.

2.6. Statistical Analysis of Compound Ratios for Bound PAH products

Principal component analysis (PCA) and Gaussian Mixture Model (GMM) clustering was applied to select bound PAH abundance ratios identified as potential source- and maturity-sensitive molecular parameters in order to check the efficacy of these parameters. See section 4.3 for a detailed explanation of the ratios selected. Both PCA and GMM clustering was performed using the Scikit-learn package in Python 3.7.3 (Pedregosa et al., 2011). Additional python packages used for analysis and data visualization include pandas (Mckinney 2010), matplotlib (Hunter 2007), and seaborn (Waskom et al. 2016).

3. RESULTS

A wide variety of resolvable PAH compounds were identified from the total ion chromatograms (TICs) from full scan GC-MS as major products in the aromatic hydrocarbons fractions generated from pyrolytic fragmentation (Fig. 4.3). These range in molecular weight from one- (benzene) to seven-ring (coronene) aromatic compounds, along with their alkylated derivatives. Common PAHs and other aromatic moieties

identified in the hydropyrolysates include phenanthrene (Phe), methylphenanthrenes (MP), carbazole (Car), pyrene (Py), methylpyrenes (MePy), chrysene (Chr), benzo[e]pyrene (BeP), benzo[a]pyrene (BaP), perylene (Per), benzo[ghi]perylene (B(ghi)Per), and coronene (Cor). The aromatic hydrocarbon profiles in total ion chromatograms range in complexity, as anticipated, with the less mature samples generally yielding more complex distributions and a wider variety of alkylated PAHs. C_1 and C_2-substituted aromatic compounds generally account for the majority of the alkylated PAH products in the more mature samples, of oil window-maturity or higher, and the PAHs mostly contain simple substituents (methyl-, ethyl, etc.) that do not show a high degree of branched alkylation. (See Figs. 4.3 and 4.4).

Phenanthrene and pyrene are commonly the dominant three to seven ring parent PAH compounds in the majority of ancient biogenic kerogen pyrolysates, accompanied by methylphenanthrenes and methylpyrenes and other alkylated compounds in lower abundance. The five ring PAHs (benzofluoranthene, benzo[e]pyrene, benzo[a]pyrene, and perylene) while not the most abundant PAHs, were also consistently detected in all biogenic kerogen samples regardless of age or thermal maturity. In contrast, the pyrobitumen samples contain little to no phenanthrene and are instead characterized by abundant benzo[ghi]perylene and coronene. So, there are certain discernible and common bound PAH profile features in TIC traces from ancient biogenic kerogens (Fig. 4.3) that hint that these compound distributions might potentially constitute a molecular biosignature, but we have to delve deeper into the detail and explore the modifying

effects of thermal maturity on these molecular patterns. The systematics of preservation of the major kerogen-bound PAH distributions, as revealed from detailed GC-MS analyses using selection ion chromatograms, are now discussed in detail.

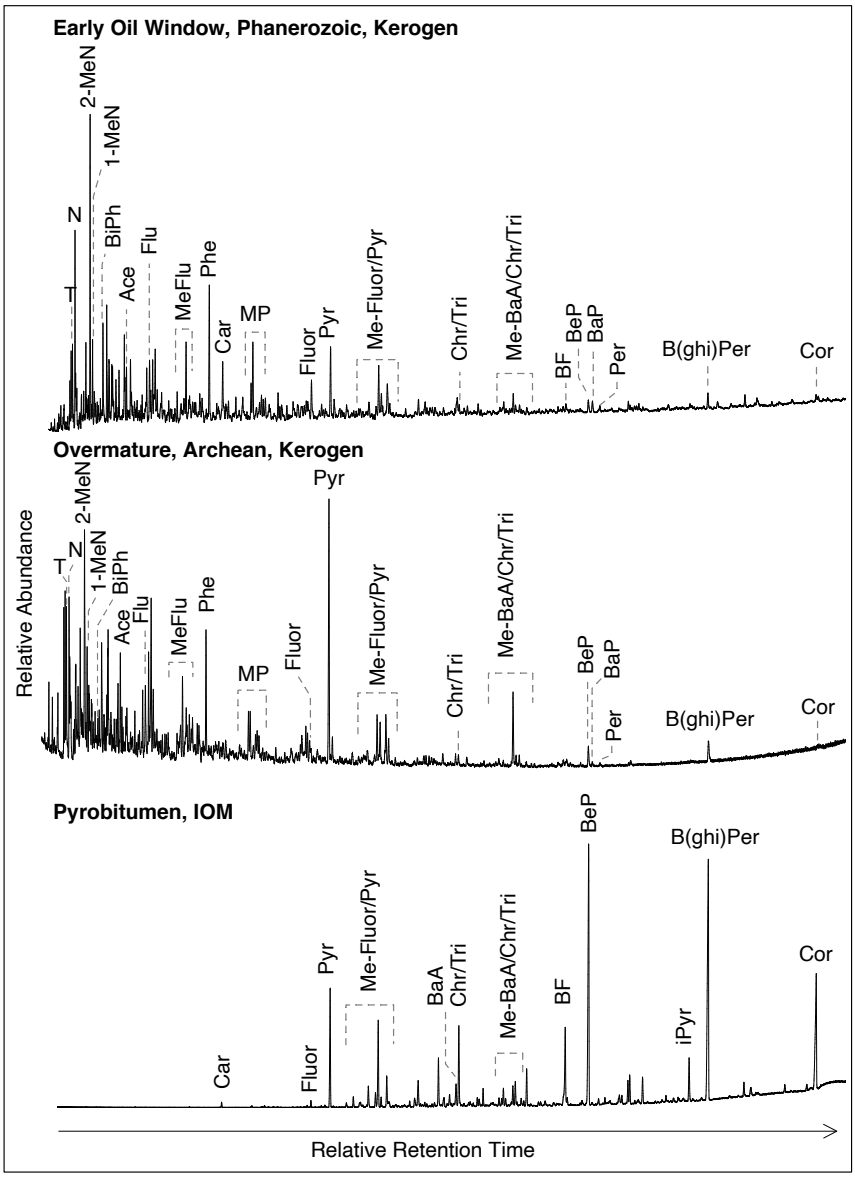

Figure 4.3: Total ion chromatograms (TIC) of the aromatic hydrocarbon distributions from HyPy of samples FPC 933687 (early oil window, Phanerozoic, kerogen), 2/1/004 (overmature, Archean, kerogen), and LST12 107.8 P (pyrobitumen, insoluble organic matter (IOM)); abbreviations are T: tetralin, N: naphthalene, 1-,2-MeN: 1-, 2-methylnaphthalene, BiPh: biphenyl, Ace: acenaphthene, Flu: fluorene, MeFlu: methylfluorenes, Phe: phenanthrene, Car: carbazole, MP: methylphenanthrenes, Fluor: fluoranthene, Pyr: pyrene, Me-Fluor/Pyr: methylfluoranthenes and methylpyrenes, BaA: benz[a]anthracene, Chr/Tri: chrysene and triphenylene, Me-BaA/Chr/Tri: methylbenz[a]anthracenes, methylchrysenes and methyltriphenylenes, BF: benzofluoranthene, BeP: benzo[e]pyrene, BaP: benzo[a]pyrene, Per: perylene, iPyr: indeno[1,2,3-cd]pyrene, B(ghi)Per: benzo[ghi]perylene, and Cor: coronene

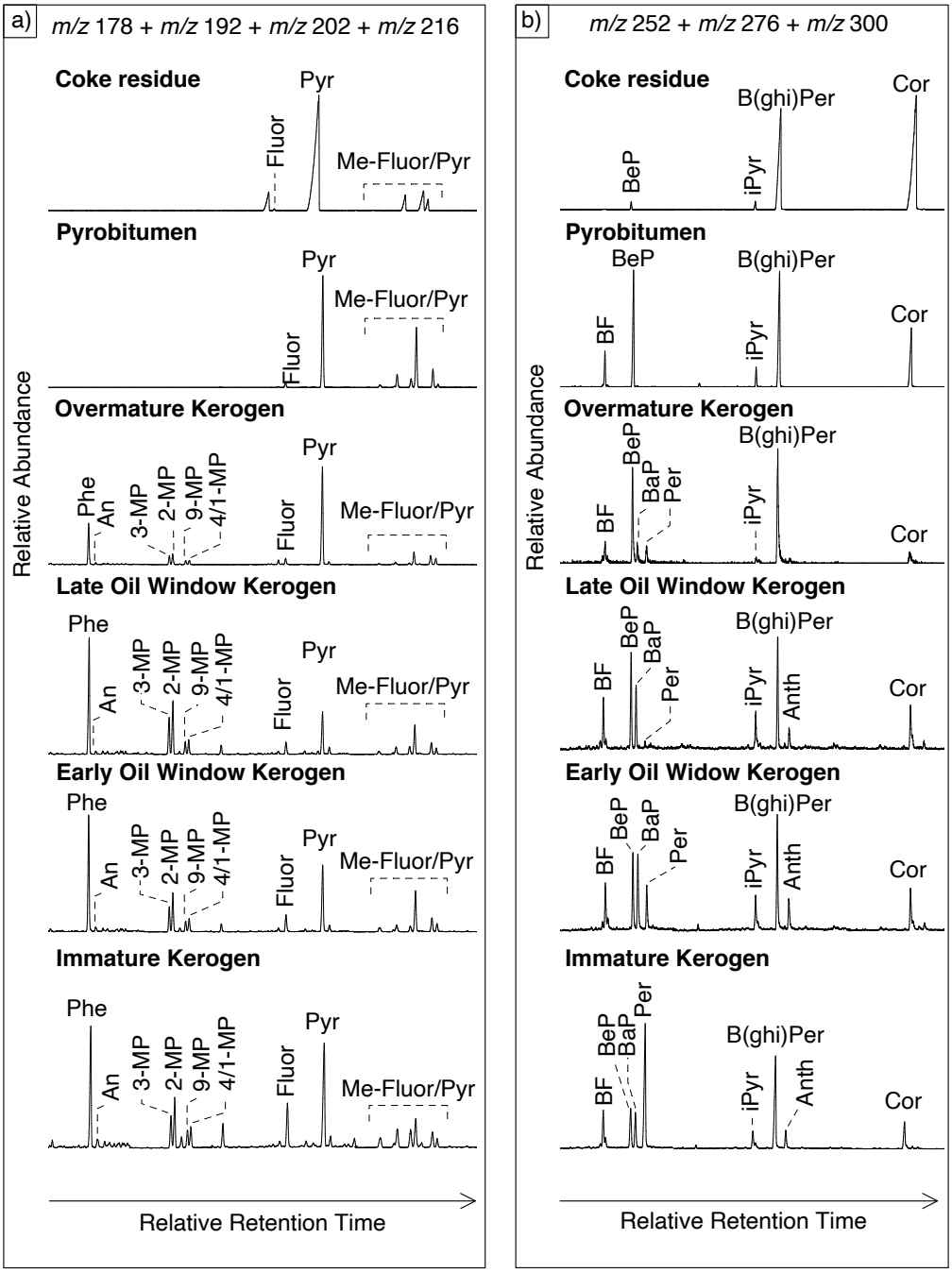

Figure 4.4: Sample names are from top to bottom: BASF, LST12 107.8 P, 2/1/004, FPC 905756, FPC 933687, and C-17R-2 12-13; (a) Partial summed mass chromatograms (m/z 178 + 192 + 202 + 216) for HyPy samples of varying thermal maturities; (b) Partial summed mass chromatograms (m/z 252 + 276 + 300) for HyPy samples of varying thermal maturities; abbreviations are 4/1-MP: 4- and 1-methylphenanthrene, 2-MP: 2-methylphenanthrene, 3-MP: 3-methylphenanthrene, 9-MP: 9-methylphenanthrene, additional abbreviations are given in Fig. 4.3.

4. DISCUSSION

4.1. Suitable Molecular Maturity Parameters for Ancient Biogenic Kerogen

4.1.1. Five-ring PAHs

We begin the discussion of bound PAHs, with the five-ring PAHs as these appear to have the most potential for providing useful astrobiological insights amongst the condensed PAH compounds. The relative abundances of the common five-ring parent PAHs (as revealed by *m/z* 252 ion chromatograms) are strongly correlated with varying thermal maturity, (see Table 3). The main parent 5-ring PAH compounds commonly detected are benzo[e]pyrene (BeP), benzo[a]pyrene (BaP), perylene (Per), and with benzofluoranthene (BF) isomers in lower abundance. Overall, we find that benzo[e]pyrene increases in abundance with increasing maturity in comparison to both benzo[a]pyrene and perylene, both of which decrease but at different rates with increasing maturity. Perylene contributions decrease at an earlier maturity stage and more rapidly than benzo[a]pyrene. By the late oil window stage, perlyene contributes less than 15% of the total kerogen bound five-ring PAHs in the m/z 252 ion chromatogram. These preservational systematics are generally consistent with the 5-ring PAH relationships and relative stabilities of free compounds in the bitumen phase. Specifically, benzo[a]pyrene and perylene are more susceptible to degradation with increasing temperatures than benzo[e]pyrene, which is the most thermally stable form (Marynowski et al., 2015). However, both perylene and benzo[a]pyrene persist at a higher thermal maturity as compounds bound by covalent linkages within kerogen as compared to the corresponding free form of these same compounds within the bitumen phase.

Kerogen-bound benzo[a]pyrene continuously decreases in abundance with increasing thermal maturity across the maturity range investigated in this study (see Table 3). The BaP/(BeP+BaP) ratios for samples described in this study range from 0.00 to 0.62 and so these differences are readily measurable and distinguishable from peak area integration. BaP/(BeP+BaP) remains above 0.15 for the majority of samples in this study, and only approaches zero for samples with the highest degree of alteration (ancient biogenic kerogens associated with intrusive dikes and in the pyrobitumen residues) (Fig. 4.5a). This wide range of values makes BaP/(BeP+BaP) an ideal parameter for distinguishing samples within and beyond the late oil window. Importantly, our data set clearly shows that this ratio, and the distribution of the major 5-ring PAHs more generally, is not simply correlated to geological age. Precambrian kerogens, spanning from Neoproterozoic to Archean age, specifically the 729 Ma Chuar Group, 750 Ma Visingsö Group, 1.64 Ga Barney Creek Formation and 2.6 Ga Carawine Formation samples all contain BaP/(BeP+BaP) ratios as high as 0.5. In contrast, the younger Stainmore Formation samples proximal to the intrusive dike all have BaP/(BeP+BaP) ratios as low as 0.05 and only date to the Carboniferous Period. The Precambrian and the Phanerozoic samples both follow a similar maturity trend (Fig. 4.7) in terms of their 5-ring PAH abundance patterns and thus these highly derived compounds are not controlled by fundamental differences in original biogenic organic source inputs. It is apparently the overall degree of thermal maturity (a function of time and temperature history) of the sedimentary

organic matter that primarily controls the relative abundances of the major 5-ring PAH compounds bound within kerogen.

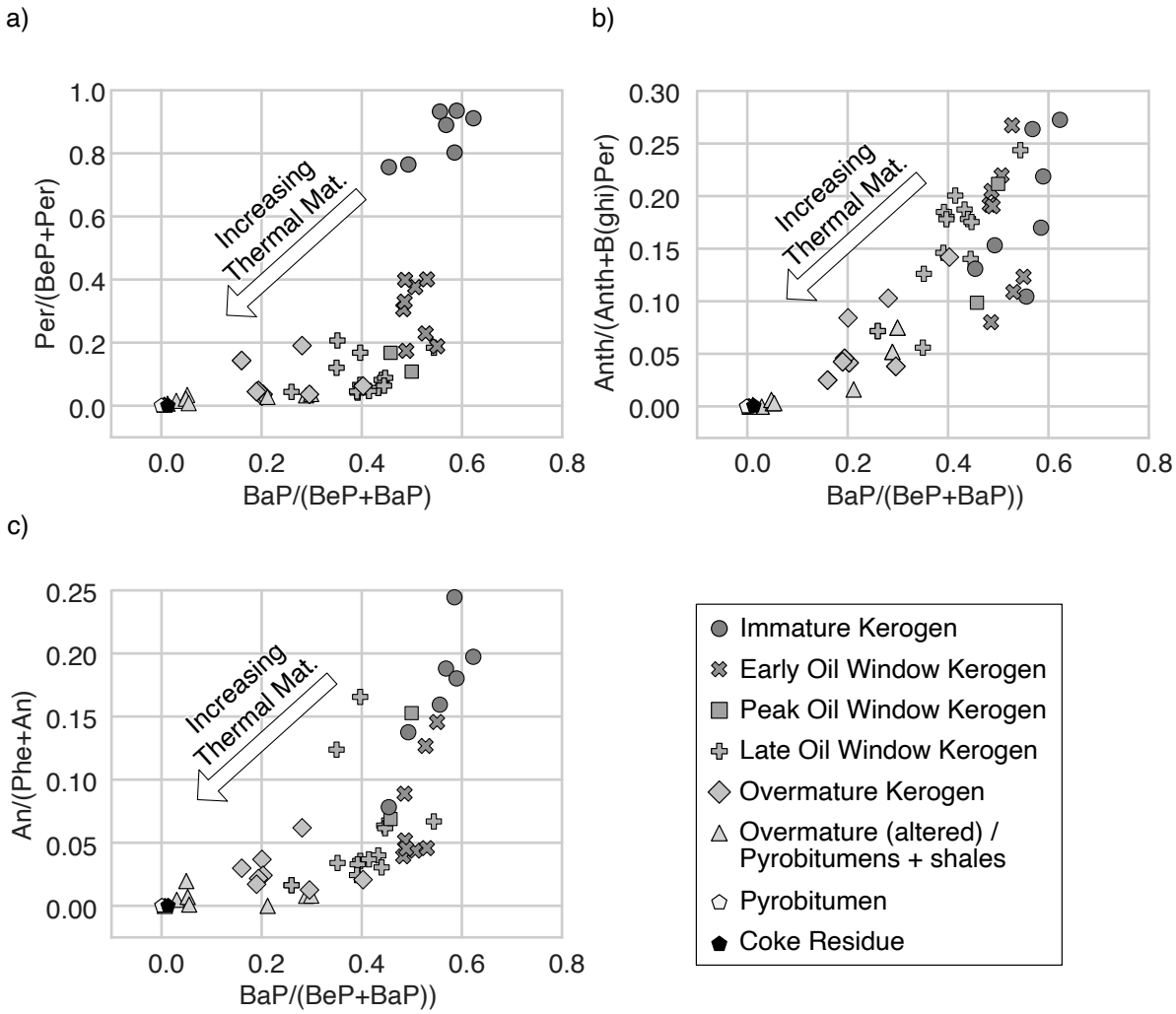

Figure 4.5: Systematics of five-ring bound PAH patterns generated from HyPy: (a) Cross-plot of BaP/(BeP + BaP) versus Per/(BeP + Per) for HyPy samples, Perylene (Per) rapidly drops in abundance between immature and peak oil window whereas benzo[a]pyrene (BaP) abundance decreases steadily from immature to overmature samples; (b) Cross-plot of BaP/(BeP + BaP) versus Anth/(Anth+B(ghi)Per) for HyPy samples, anthanthrene (Anth) decreases in abundance between peak oil window and overmature samples; (c) Cross-plot of BaP/(BeP + BaP) versus An/(Phe+An) for HyPy samples, anthracene (An) drops in abundance once samples reach overmature thermal maturity; for PAH abbreviations see Fig. 4.3.

There has been a great interest and speculation into the origins of perylene by organic geochemists due to its prominence in solvent extracts of numerous thermally immature rocks and sediments deposited in terrestrial, lacustrine and marine settings. A major source of perylene has been suggested to be from wood-degrading fungi and hence its first appearance has been linked to the expansion of vascular plants in the Devonian (Grice et al., 2009, Suzuki et al., 2010, Itoh et al., 2012, Marynowski et al., 2013). Complicating the efforts to pinpoint perylene's source(s) however, is its low thermal stability in the bitumen phase along with the scarcity of pre-Devonian samples for study which are sufficiently immature to permit the preservation of perylene. Perylene is not detectable as a free PAH compound in the bitumen phase for rocks that have reached the stage of early catagenesis and beyond of early oil window and higher maturity as it is lost by destruction due to catagenesis as vitrinite reflectance approaches ~0.7% (Marynowski et al., 2015). This is highlighted in Fig. 4.6 for a Jet Rock Formation sample (HB4), of early-middle oil window maturity, from our investigation that shows significant amounts of detectable bound perylene released by HyPy fragmentation of the kerogen but no detectable free perylene in the corresponding solvent extracts from the same sedimentary rock sample.

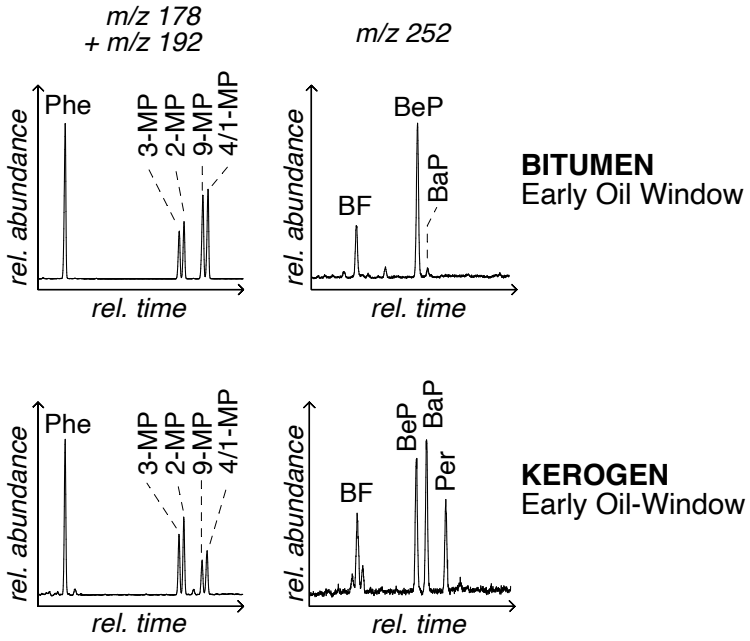

Figure 4.6: Comparison of the partial summed mass chromatograms of m/z 178 +192 and m/z 252 for the bitumen versus kerogen phase for a Jurassic Jet Rock Formation black shale (sample HB4). Note that kerogen incorporates and preserves compounds differently than bitumen. Perylene is still found as a bound constituent of kerogen but not as a free hydrocarbon the bitumen.

In contrast to the well-established occurrences of perylene in bitumens from only immature sedimentary rocks, we detected bound perylene in kerogens ranging in thermal maturities from immature, oil window-mature and even in trace amounts in highly overmature rocks. Perylene abundances, reported here as Per/(BeP+Per) drop rapidly in biogenic kerogens approaching the late oil window (%Ro >1.2), but remain above the detection limit for all samples (Fig. 4.5a). The long-term survival of bound perylene therefore represents the transformation of the bulk of organic matter into kerogen prior to reaching the oil-window, resulting in the sequestration of a portion of perylene in a sterically bulk macromolecular matrix and significantly enhancing its preservation potential. Thus, perylene persists in this kerogen-bound form to the highest stages of thermal maturity covered by our investigation.

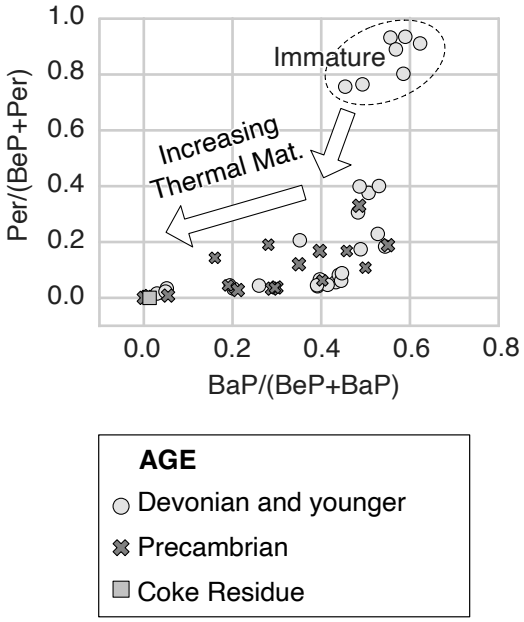

Figure 4.7. Perylene abundances for samples older and younger than the expansion of vascular plants. The Per/(BeP + Per) ratios of Precambrian pyrolysates reach as high as 0.33. The largest Per/(BeP + Per) values are exclusive to samples of immature thermal maturity and these are the pre-oil window rocks. Samples of oil-window maturity and greater do not show a correlation between geologic age and Per/(BeP + Per); for PAH abbreviations see Figures 4.3 and 4.4.

A comparison of perylene abundance in our Precambrian versus Phanerozoic samples shows no significant differences, for samples covering thermal maturities of early oil window and greater (Fig. 4.7). Perylene was detected even in the oldest samples included in this study, specifically the 2.6 Ga Archean dolomites from the Carawine Formation where Per/(BeP+Per) still reaches 0.19. There was no significant terrigenous or woody plant inputs as organic matter sources to the Precambrian samples. In all samples of early oil window and greater maturity, perylene remains less abundant than benzo[e]pyrene. Perylene only surpasses all other 5-ring PAHs in abundance in samples of immature thermal maturity, however we were unable to include immature samples of pre-Devonian age for comparison. Our results do not dismiss fungal wood degradation as a potential end-member source for perylene in immature Devonian and younger rocks. They do suggest though that additional ubiquitous sources must exist for the lower contributions of perylene detected in pre-Devonian samples from generic organic matter diagenesis and

alteration. Again, as for the benzopyrenes, the degree of thermal maturity of the sedimentary organic matter exerts the primary control on the relative abundance of perylene relative to other five-ring PAHs bound within kerogen.

The presence of perylene in HyPy products could prove to be an important and novel molecular signature for identifying macromolecular organic matter formed during protracted low temperature alteration regimes; especially from early diagenesis at low temperature burial conditions (<50°C). Murchison meteorite was shown to have low amounts of perylene in its HyPy products (Sephton et al., 2004) which could represent the formation of perylene at very low presolar temperatures (Sephton et al., 2015). So, while this cannot be considered as a molecular biosignature feature per se, the detection of perylene could be used to identify of organic matter that first underwent a protracted low temperature (<50ºC) history prior to any subsequent higher temperature alteration. In other words, it could help select for samples that could contain other molecular or isotopoc biosignatures and that warrant further investigation. Detectable amounts of kerogen-bound perylene can be readily detected in hydropyrolysates even for overmature ancient biogenic kerogens including 3.4-2.6 Ga Archean kerogens, long after free perylene has been completely degraded in the bitumen phase. While there is significant variability in Per/(BeP+Per) value for samples of equivalent thermal maturity in the low maturity range, it does appear to be a useful molecular parameter for pinpointing samples for which a low temperature synthesis of PAH has occurred for an extended duration of the overall burial/thermal history. All ancient biogenic keorgens analyzed to date from

HyPy contain detectable amounts of perylene; even for the most thermally transformed samples, including here for our overmature Archean kerogens and for ancient kerogens heated by volcanic intrusions (Table 3).

4.1.2. Six-ring PAHs

Three six-ring PAH compounds (benzo[ghi]perylene, indeno[1,2,3-cd]pyrene, and anthanthrene) are readily resolvable and commonly detected in the pyrolysates, as revealed by m/z 276 ion chromatograms. The six-ring PAH distributions are dominated by the peri-condensed and the most thermally stable isomer, benzo[ghi]perylene, over a wide thermal maturity range for ancient kerogens. Indeno[1,2,3-cd]pyrene is present in all samples but the relative abundance does not show any obvious positive or negative correlation with the level of maturity. The relative abundance of anthanthrene, expressed as Anth/(Anth+B[ghi]Per), generally decreases with increasing thermal maturity for most samples (Fig. 4.5b). Anth/(Anth+B[ghi]Per) drops below 0.10 for the majority of the overmature samples, after passing a maturity threshold corresponding to the late oil window stage. While it is a complementary molecular parameter to the five-ring PAH ratios, it spans a lower range of absolute values (0.27-0.00) and there are more outliers (e.g., the immature samples give a range of values of 0.27-0.13) than other PAH parameters. So, it is a less robust molecular parameter for distinguishing thermal maturity compared to the five-ring PAH ratios, although there is a strong thermal maturity influence on bound six-ring PAH distributions.

4.1.3. Four-ring PAHs

A number of individual four-ring PAHs are commonly detected; including pyrene, fluoranthene, benz(a)anthracene, chrysene and triphenylene. Pyrene and fluoranthene were identified by their mass ion of m/z 202 while benz(a)anthracene, chrysene and triphenylene have a mass ion of m/z 228. Pyrene is consistently the most abundant of the four-ring PAHs in all samples from the TIC analyte response, as expected from its high thermal stability. Fluoranthene was detected in all samples and is present at its highest concentrations in both the Demerara Rise and Stainmore Formation samples, despite their vastly different thermal maturities. Any direct biological source(s) of fluoranthene have not yet been determined but there is likely factors other than thermal maturity influencing the abundance of this signal and other four-ring PAH compounds. Methylpyrenes and methylfluoanthenes (m/z 216) were also detected in all samples. It is likely that chrysene decreases with thermal maturity, due to its lower stability however we were unable to separate it from the more thermally stable compound, triphenylene with which it co-elutes (see Fig. 4.3). None of the parent four-ring PAH compound ratios that we investigated here were individually either particularly sensitive or robust thermal maturity indicators for ancient biogenic kerogens.

4.1.4. Three-ring PAHs

A commonly utilized PAH-based thermal maturity ratio, conventionally applied to the free hydrocarbon components found in rock bitumens or oils, is the methylphenanthrene

index (MPI). Previous studies of kerogen-bound methylphenanthrenes have found that the free versus bound compound distributions systematics differ such that this relationship does not hold for kerogen (Marshall et al., 2007; Nabbefeld at al. 2010b; Wu et al., 2015). MPI is based around a systematic transition from higher abundances of free 9- and 1-MP to 2- and 3-MP with increasing maturity (Radke et al., 1986). however our data display a wide variability in kerogen bound (2-MP + 3-MP)/ (9-MP + 1-MP) and 2-MP/ 1-MP ratios of equivalent thermal maturity, which is in agreement with previous studies (Table 4.3, Fig. 4.8). Notably, all HyPy products investigated for this study were found to contain greater abundances of 2- and 3-MP in comparison to 9- and 1-MP independent of the methylphenanthrene distributions in the bitumen fraction (Fig. 4.4, Fig. 4.8). This suggests that methylphenanthrene abundances within kerogen may be a result of preferential incorporation or preservation of 2- and 3-MP over 9- and 1-MP or that the 2- and 3-MP structural isomers are preferentially generated from HyPy cleavage.

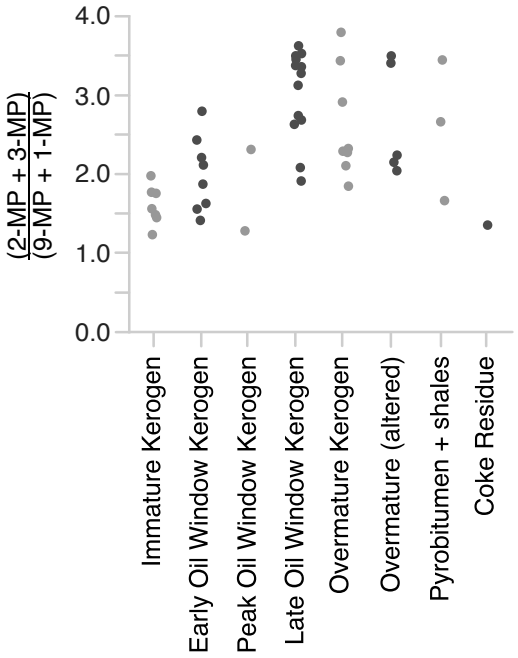

Figure 4.8: Relative abundance of 2- and 3- versus 9- and 1- methylphenanthenes of HyPy samples. Bound methylphenanthrenes, unlike free methylphenanthrenes, exhibit a large variability between samples of equivalent thermal maturities. Abbreviations are 2-MP: 2-methylphenanthrene, 3-MP: 3-methylphenanthrene, 9-MP: 9-methylphenanthrene, 1-MP: 4- and 1-methylphenanthrene.

Marshall et al., (2007) showed that a very good maturity correlation existed for a suite of overmature Archean kerogen concentrates collected from the 3.4 Ga Strelley Pool cherts between the bound methylphenanthrene/phenanthrene (MP/Phe) ratio and the predicted thermal maturity ordering of kerogens as predicted from atomic H/C ratios from elemental analysis and from structural parameters derived from Raman spectroscopy. The authors noted though that the methylphenanthrene distributions did not behave in a parallel fashion to the equivalent free compounds in the rock bitumens, thus all MP contributions were summed together. However, we find no clear trend here between MP/Phe and level of thermal maturity for the samples used in this study, likely exacerbated by volatile losses during our product trapping and work-up from offline pyrolysis. The MP/Phe ratio can be prone to artifacts arising from preferential evaporative losses of phenanthrene relative to methylphenanthrenes, thus volatile losses

have to be avoided as best as possible. Marshall et al. (2007) used Archean kerogen concentrates for their HyPy study, which possessed sufficiently high TOC contents to generate high masses of pyrolysates (many milligrams), and so the evaporative losses from both product trapping and work-up were minimized. This was supported and verified from the good preservation of light ends in aliphatic and aromatic hydrocarbon chromatograms from full scan GC-MS. This allowed for product analysis without the need for excessive solvent concentration to produce a strong GC-MS signal. Thus, the MP/Phe maturity trend reported in Marshall et al. (2007) is robust but this molecular ratio parameter may be compromised if only very low pyrolysate yields (sub-milligram) are generated, and this is particularly acute for high maturity samples. In addition, experiments conducted with combustion of coal (Rebiero et al., 2012) and oil (Wang et al., 1999) have indicated that phenanthrene and methylphenanthrene concentrations are significantly lost during cracking, which can skew MP/Phe. 2.1 Ga Pyrobitumen samples from the Francevillian, as well as the synthetic coke residue, all generated low concentrations of 3-ring PAHs in comparison to larger PAH compounds (Fig. 4.9). We, therefore, prefer the five-ring PAH ratios over the MP/Phe ratio for distinguishing the maturity ordering of samples of high thermal maturity due to the possibility of evaporative losses skewing the three-ring compound ratio from offline pyrolysis.

In addition to phenanthrene, the three-ring PAH compound anthracene was also detected in ancient biogenic kerogen pyrolysates. Anthracene (An) shows a strong correlation with thermal maturity in the ratio of An/(Phe+An) (Fig. 4.5c), with An dropping in abundance

relative to the more stable Phe for samples reaching the oil-window and beyond. Bound An disappears completely in the 2.1 Ga pyrobitumen concentrates and the synthetic coke residue samples which have experienced high alteration temperatures and which were produced mainly from thermal cracking reactions of hydrocarbons. This is to be expected as anthracene is a linear PAH compound, which are generally less stable than condensed PAH such as phenanthrene (Killops and Killops, 2005, and so would likely have been absent from the precursor hydrocarbons which underwent thermal cracking reactions. Unlike perylene, which is detectable in all our ancient biogenic kerogen samples, An is below detection limits in one of our most thermally altered kerogens from the Carboniferous Stainmore Formation. Thus, bound An is found in all of our ancient biogenic kerogen pyrolysates across the entire maturity range, except for one extremely cooked sample. The detection of low but finite amounts of perylene for this same sample though helps confirm that this mainly consist of overmature biogenic kerogen.

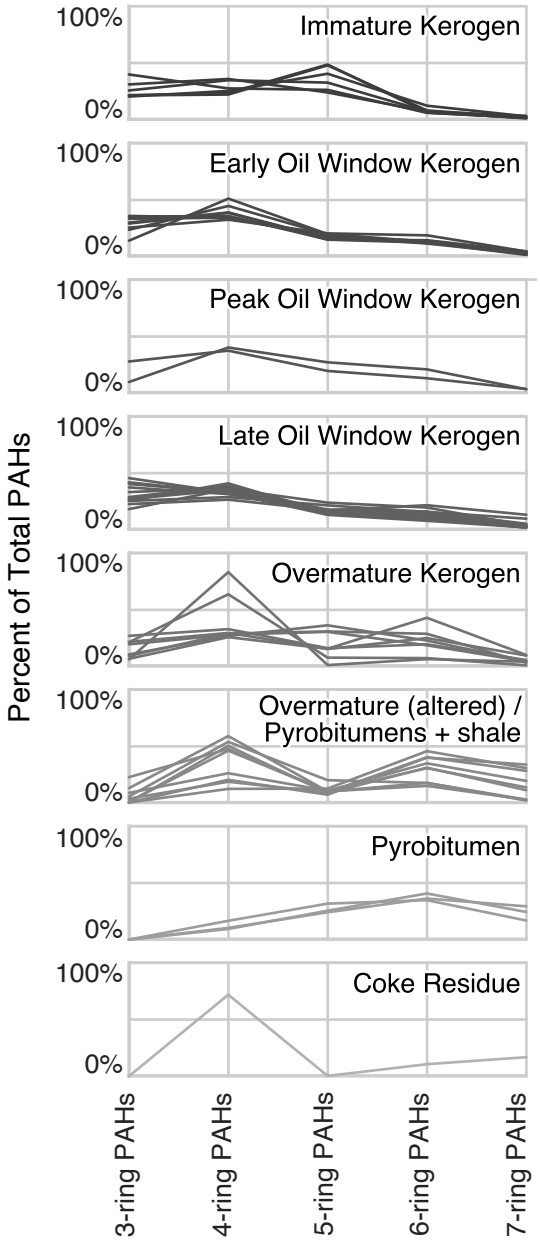

Figure 4.9: Relative abundance of the 3- to 7- ring parent PAHs for HyPy samples; 3- ring PAHs decline in abundance with increasing thermal maturity while 6- and 7- ring PAHs are more abundant in samples containing organic matter derived from hydrocarbon cracking; PAHs included are 3-ring: phenanthrene and anthracene, 4-ring: pyrene, fluoranthene, benz(a)anthracene, chrysene and triphenylene, 5-ring: benzofluoranthene, benzo(e)pyrene, benzo(a)pyrene, perylene, 6-ring: indeno(1,2,3-cd)pyrene, benzo(GHI)perylene, anthanthrene, 7-ring: coronene; alkylated PAHs were not included.

4.2. Identifying Bound Molecular Patterns in High Temperature Cracking Products

The synthetic coke residue generated from laboratory fluidized catalytic cracking (FCC) treatment represents a useful model system for studying the bound PAH characteristics from an insoluble macromolecular residue representative of generation by one possible high temperature abiogenic formation mechanism. In this case, the IOM was generated by a rapid and high temperature (482°C) cracking of a simple hydrocarbon (hexadecane) feedstock passed over a typical FCC industrial catalyst in a laboratory reactor. The HyPy fragmentation products are characterized by a striking lack of the less thermally stable PAHs including anthracene, perylene, and anthanthrene, and higher abundances of large (6-7 ring) PAHs and condensed PAH compounds (Fig. 4.3). This preference for condensed PAHs is indicative of a sequential one-ring build-up synthesis mechanism to sequentially grow larger clusters from smaller PAH precursors (Stein, 1986; Sullivan et al., 1989). This mechanism has been proposed to explain similar PAH distributions of thermally stable, large ring PAHs in hydrocracking products (Fetzer, 2010; Sullivan et al., 1989) and in hydrothermal vents (Simoneit and Fetzer, 1996). In addition, experiments of burning coal (Rebeiro et al., 2012) and oil (Wang et al., 1999) as well as artificial maturation of coal under an inert gas at high temperatures (400°C) (Vukovic et al., 2016) all result in increased yields of large-ring PAH at the expense of 2-3 ring PAH compounds.

The close similarity of the 2.1 Ga Francevillian pyrobitumen concentrates and the synthetic coke residue supports a IOM source coming predominantly from hydrocarbon

cracking products within these samples. The presence of detectable perylene, albeit in extremely low relative abundances in m/z 252 ion chromatograms, in the samples containing both pyrobitumen and shales from the Francevillian might seem at first to contradict an oil cracking mechanism for the pyrobitumen. Particularly, as perylene is known to degrade as a free stable hydrocarbon by the early oil-window (Fig. 4.6). We propose two sources of insoluble organic matter within these 2.1 Ga rock samples. The first source is the IOM organic matter formed from cracked hydrocarbon fluids which migrated into the rock sample and were heated, leaving behind a residue that solidified into pyrobitumen. This component likely contained no free or bound perylene. The second is a component of indigenous disseminated kerogen in the host source rock. We interpret the product distributions such that the bound perylene detected is preserved within the kerogen and not within the pyrobitumen component. This view is strongly supported by the lack of perylene in three hand-picked pyrobitumen concentrates, visually selected to contain only pyrobitumen fragments (LST1 60.6 P, LST12 93 P, and LST12 107.8 P) and which represent hydrocarbon cracking products. One Francevillian sample (LST12 32) shares more characteristics with samples of overmature kerogen, though the organic matter is still likely derived from a mixed pyrobitumen and ancient biogenic kerogen source.

The Neoproterozoic Doushantuo cap dolostone samples (CapB and HJ01), which may have experienced hydrothermal alteration and which were from the oldest Doushantuo (DST1) stratigraphic position, have slightly lower BaP/ (BeP+BaP) ratios than the

younger and less altered Doushantou Formation rocks. However, their overall PAH patterns are still characteristic of overmature biogenic kerogen, rather than from neoformed residues generated from thermal cracking reactions. All four Doushantuo Formation samples, as for all our ancient biogenic kerogens, contain detectable perylene in their aromatic hydrocarbon products (Table 3).

The highly altered Carboniferous Stainmore Formation samples (proximal to dyke and significantly altered by intrusive heating) have similar bound PAH profiles as the 'pyrobitumen and shale mixture' samples from the 2.1 Ga Francevillian. They have significantly lower BaP/ (BeP+BaP) ratios than all of the overmature kerogens samples, including in comparison with the other Stainmore Formation samples situated laterally further away from dyke heating alteration. They also still preserve very low, but detectable, perylene with Per/ (BeP+BaP) ratios of 0.02 to 0.03. These samples most likely represent a mixture of highly mature biogenic kerogen but with some significant organic contribution of products formed from thermal cracking reactions. Thus, this explains why these particular ancient kerogen samples show the PAH patterns closest to the pyrobitumen concentrates and coke residue.

4.3 Statistical Analysis

The abundance ratios for selected bound 3-, 5-, and 6-ring PAH compounds; namely An/(Phe+An), BaP/(BeP+BaP), Per/(BeP+Per), and Anth/(Anth+ B[ghi]Per), were utilized as the best candidates for resolving the characteristics of degree of thermal

maturity and IOM source (e.g., biogenic kerogen versus hydrocarbon cracking products). Principal component analysis (PCA) was conducted to determine how strongly these ratios controlled the variance in PAH abundances in the samples that generated these as detectable PAH products. The first principal component is strongly negatively correlated with thermal maturity as shown in Fig. 4.10a and accounts for 76.0% of the variance. This confirms that these four PAH compound ratios are primarily controlled by thermal maturity. The second principal component contains 15.60% of the variance but does not correlate with either thermal maturity or age. Together, the two components account for 91.70% of the total data variance among the set of samples.

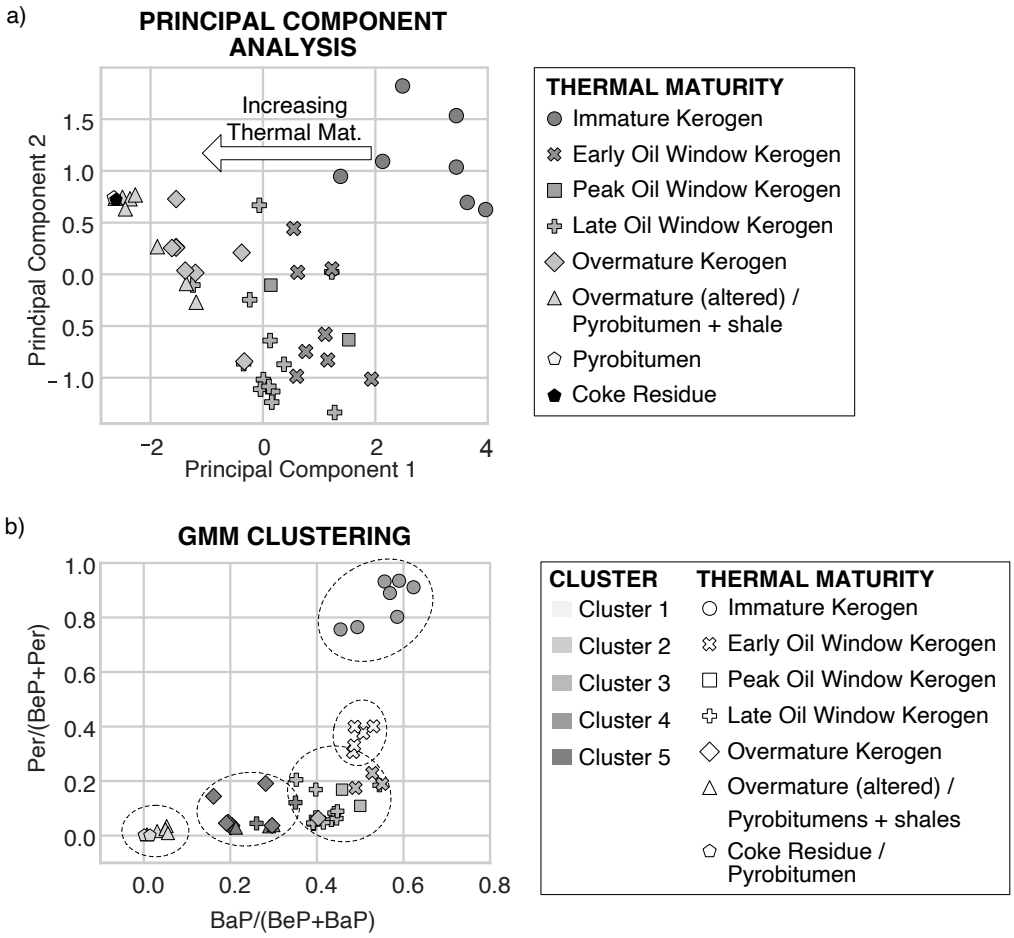

Figure 4.10: Statistical analysis of the selected PAH ratios An/(Phe+An), BaP/(BeP+BaP), Per/(BeP+Per), and Anth/(Anth+ B[ghi]Per) for our overall bound PAH compounds in our sample suite, from (a) principal component analysis; (b) cluster analysis conducted using Gaussian Mixture Model (GMM) clustering for n=5 clusters plotted onto a cross-plot of BaP/(BeP + BaP) versus Per/(BeP + Per). For PAH abbreviations see Fig. 4.3.

In order to test how well these four selected PAH abundance ratios can separate samples of different source and thermal maturities across the whole possible range from immature to overmature, we scrutinized these ratio values using Gaussian Mixture Model (GMM) clustering. Clustering provides a means to separate multidimensional data into groups whose identities are not known in advance. The groups formed by GMM clustering can

then be compared with known groups, e.g. groups of different thermal maturities previously identified independently of PAH abundance ratios. Since GMM clustering groups data into a preselected number of clusters, we iterated over a range of clusters from n=2 to n=8. When the number of clusters was restricted to three, the clusters separated between samples of approximately immature, mature, and overmature thermal maturities. However, when the number of clusters was increased to five, groups representing multiple stages within the oil window as well as a group corresponding to highly altered kerogen and IOM emerged (Fig. 4.10b, cluster 2). This group contained samples from overmature altered kerogen, pyrobitumens and shales, pyrobitumens, and the coke residue. Increasing the number of clusters further did not result in the separation of overmature altered kerogen (including the pyrobitumen and shale mixtures) from the pyrobitumen concentrates or the coke residue. This indicates that the ratios used were effective at separating kerogen of different thermal maturities. The pyrobitumen concentrates and coke residue were not separated from overmature kerogen due to the low values of these ratios in overmature kerogen which plot closely with zero. However the pyrobitumens can be isolated by their absence of perylene. GMM clustering highlights the ability of these four PAH abundance ratios to assess the relative maturity of ancient biogenic kerogens across the entire thermal maturity range.

4.4. Carbonaceous Chondrite Meteorite Comparisons

Source input from certain meteorites, particularly carbonaceous chondrites, may deliver a possible background organic signal that needs to be considered when searching for

organic biosignatures on planetary bodies such as Mars. Carbonaceous chondrites are fragments of primitive asteroids formed 4.56 billion years ago that have not been altered from melting or differentiation of the parent body (McSween, 1979) although they have undergone some aqueous alteration (Abreu, 2012; Jilly-Rehak et al, 2018). As such they are considered some of the most primitive objects within our solar system. Carbonaceous chondrites typically contain 2 to 5% (by mass) of organic carbon, with ca. 70% of the organic material consisting of a complex, high molecular weight macromolecular IOM (Sephton et al., 1998; Sephton, 2013; Sephton et al., 2015; Alexander et al., 2017). The majority of this macromolecular organic matter consists of bound, aromatic ring structures as determined by series of pyrolysis studies on previously thermally extracted, solvent-extracted, or acid demineralized samples of Allende (CV3) (Simmonds et al., 1969; Levy et al., 1970), Murchison (CM2) (Sephton et al., 2004; Remusat et al., 2005; Okumura & Mimura, 2011; Sephton et al., 2015), Erakot (CM2), Essebi (CM2), Kivesvaara (CM2), Mighei (CM2), Murray (CM2), Nogoya (CM2) (Sephton et al., 2010), Orgueil (CI1) (Remusat et al., 2005), and a number of Antarctic carbonaceous chondrites (Komiya et al, 1993; Kitajima et al., 2002; Sephton et al., 2010). Common free and IOM-bound aromatic compounds detected in carbonaceous chondrites include benzene, toluene, alkylbenzenes, naphthalene, alkylnaphthalenes, indenes, acenaphthene, fluorene, phenanthrene, biphenyl, and pyrene.

Previous HyPy analysis of the IOM from the Murchison meteorite revealed significant amounts of high molecular weight PAH and heterocyclic aromatics with 1-7 fused

aromatic rings and with varying degrees of alkylation (Sephton et al., 2004, Sephton et al., 2015). From this work, there appears to be at least two distinct phases of IOM in Murchison meteorite: a thermally labile fraction and a recalcitrant organic phase which possess fundamentally different structural and stable carbon isotopic characteristics and which may have different origins or synthesis mechanisms (Sephton et al., 2015). HyPy yielded a significantly larger mass range of PAH products from bound phases in meteorites than other pyrolysis methods, yielding aromatic compounds ranging from benzene up to coronene. This was due to the overall higher conversions of soluble and volatile products using the high pressure hydrogen and continuous-flow conditions of HyPy (Sephton et al., 2004), particularly for the more recalcitrant organic matter. The most abundant 1-4 ring compounds detected by HyPy of Murchison meteorite (Sephton et al., 2015; Sephton et al., 2004) include a complex variety of C_1-, C_2-, and C_3-aromatic and naphthenoaromatic compounds. Pyrene was the most abundant PAH detected from full scan GC-MS analysis. While the bulk of PAH products consisted of a wide variety of two- to four-ring aromatics and naphthenoaromatics, five- to seven-ring PAHs were also detected in lower abundance. Benzo[a]pyrene and low amounts of perylene were both detected, with the highly stable benzo[e]pyrene as the most abundant 5-ring PAH. The recalcitrant phase of Murchison meteorite IOM of 3+ ring PAHs thus shares the most common structural characteristics with the overmature biogenic kerogens presented in this study (see Fig. 4.11). Thus, constraints from these carbonaceous meteorite PAH patterns informs us that the finding of detectable bound perylene from insoluble

carbonaceous residues does not represent an entirely robust a marker for past biological activity when used on its own.

Despite some similarities in compound distributions, meteoritic IOM is easily distinguished from biologically derived ancient kerogen by utilizing the highly characteristic systematics of compound-specific carbon isotope ratios found previously for meteorite PAH. Compound specific carbon isotopes of bound aromatics in the Murchison meteorite span an unprecedented range (differences for individual compounds spanning ca. 23‰ for different PAH compounds) which suggests multiple different formation pathways and/or source environments between the labile (1-2 ring) aromatics versus the refractory (3+ ring) aromatics (Sephton et al., 2015). The $\delta^{13}C$ for the 1-2 ring aromatics range from -6.3‰ to -2.5‰ in contrast to the more depleted $\delta^{13}C$ of -25.5‰ to -20.5‰ for the 3-5 ring aromatic compounds. In comparison, the range of compound-specific $\delta^{13}C$ signatures for individual PAH generated from HyPy of highly mature 2.6-3.4 Ga Archean kerogens typically exhibit a much smaller range of signature values, varying only by ca. 1-6‰ across the PAH product range (French et al, 2015; Marshall et al., 2015). Two proposed potential source environments for the free and bound aromatic constituents of carbonaceous chondrites include presolar environments (Sephton and Gilmour, 2000; Busemann et al., 2006) and the protoplanetary disk (Remusat et al., 2009). Presolar material originated as condensates in the outflows and ejecta of evolved stars. They exhibit a wide range of anomalous isotopic compositions due to the nuclear processes occurring within the stars including enriched ^{13}C (Nittler, 2003; Liu et al,.

2016). In contrast, protoplanetary disk material formed in the material surrounding our sun as a protostar (Willacy et al 2015). Formation within protoplanetary disks thus occurs at significantly colder temperatures then presolar and is thought to follow different formation pathways. Thus, the kerogen-bound PAH abundance profiles and their individual $\delta^{13}C$ signatures should be able to readily distinguish any significant organic matter contributions from carbonaceous chondrite meteorites on other planetary bodies.

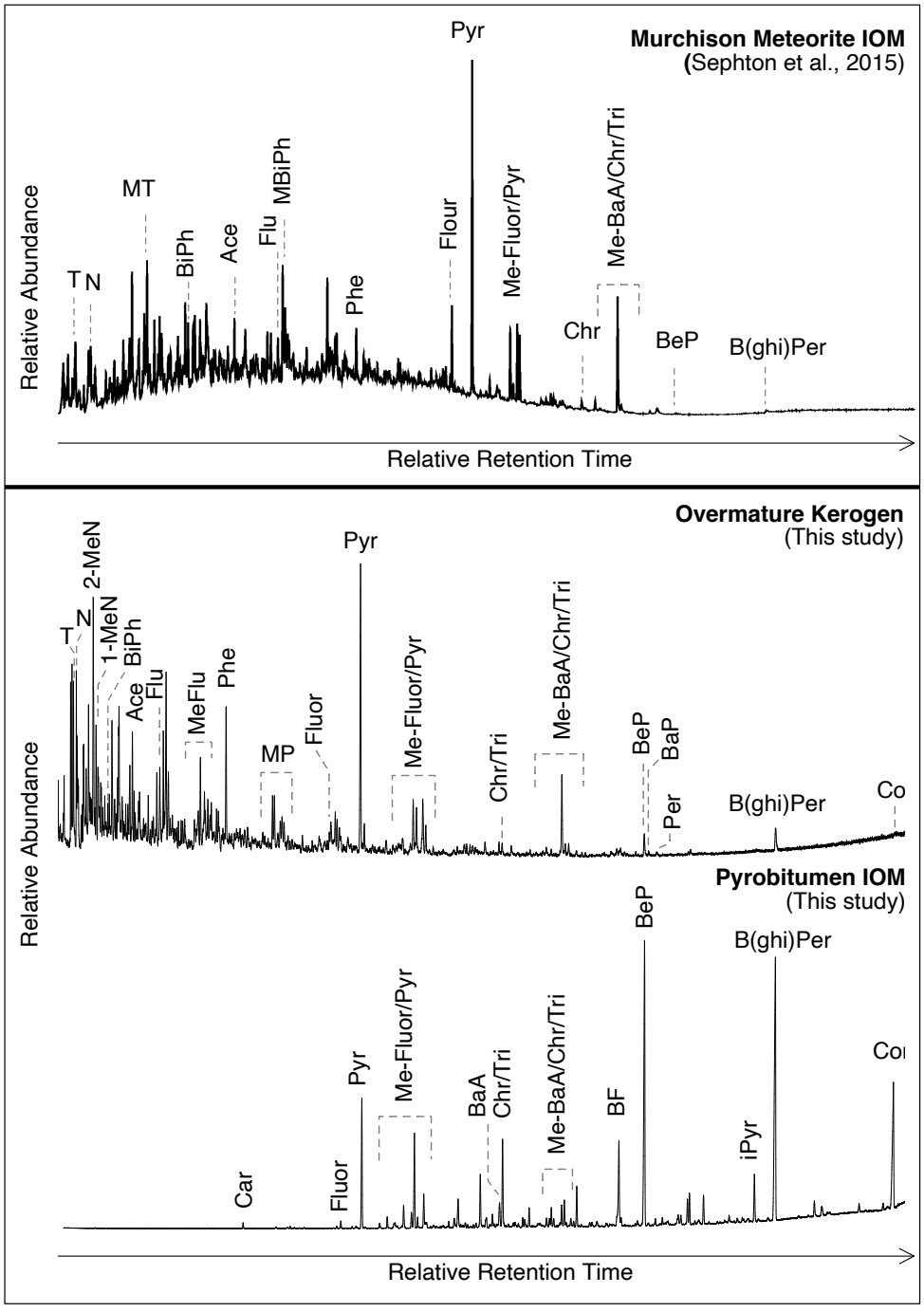

Figure 4.11: Total ion chromatograms (TIC) of the aromatic hydrocarbon fraction generated from HyPy treatment of the insoluble organic matter for samples 2/1/004 (2.6 Ga Archean dolomite), LST12 107.8 P (2.1 Ga pyrobitumen) and from Murchison meteorite from Sephton *et al.,* (2015). Murchison meteorite IOM shares many similarities with overmature kerogen within the 3- to 7- ring PAHs. Compound abbreviations are given in Fig. 4.3

5. CONCLUSIONS

We found that systematic patterns exist for the distributions of bound-PAH compounds generated by the HyPy technique from the fragmentation of kerogen and IOM. Strong controls on PAH distributions are found as a function of thermal alteration and the mode of generation (biogenic kerogens versus carbonaceous residues formed from high temperature hydrocarbon cracking). Understanding how compounds are altered by thermal maturity opens up future possibilities for uncovering potential biosignatures from bound PAHs, even for samples for which suites of diagnostic polycyclic alkane biomarkers have been lost by chemical or thermal degradation. Highly altered organic matter is often disregarded as a potential source of biosignatures when compared with the abundant store of well-preserved organics in the rock record. However, there are obvious cases of astrobiological interest where organic matter preservation is limited, including for rock samples of immense age (e.g. Archean) and for extraterrestrial samples subject to highly oxidizing surficial conditions, such as on Mars. It is clear from the systematics of free versus bound perylene, that molecular preservation is enhanced within the kerogen since the host matrix is capable of sterically protecting the compounds bound within the macromolecular structure even after the same compounds are completely degraded as free hydrocarbons in the bitumen phase. By expanding the molecular mass range of PAH fragments and exploring the preservation systematics of kerogen-bound PAH thermal maturity parameters, we have gained better insights into which PAH compounds and which abundance ratios can be detected and informative across the entire

thermal maturity range possible (from immature samples and through the oil window and beyond, encompassing highly altered overmature rocks).

We determined the influence of thermal maturity on bound PAHs in ancient biogenic kerogens ranging from immature (prior to oil window-maturity) and up to overmature (post oil window-maturity). At more elevated stages of thermal and chemical alteration, the complexity of PAH distributions and their degree of alkylation became more restricted and the compound patterns became more dominated by parent PAH. Kerogen-bound PAHs display some similar maturity pattern trends to free PAH controlled by the relative thermal stability of individual compounds, but the changes compared to their bitumen counterpart. The maturity trends for ancient biogenic kerogens were best tracked using the abundance ratios of parent PAH generated by HyPy fragmentation: An/(Phe+An), BaP/(BeP+BaP), Per/(BeP+Per), and Anth/(Anth+ B[ghi]Per). While no single PAH ratio is uniformly sensitive across the entire thermal maturity range, these maturity ratios are complementary and they can be synergistically used together. The five-ring PAHs benzo[a]pyrene and perylene decline in abundance with increasing maturity relative to benzo[e]pyrene. Perylene abundance relative to other five-ring PAH is most sensitive over a low maturity range up to the peak of the oil window, while reduction in benzo[a]pyrene signal tracks all the way to high maturity, including for overmature samples. In addition to the five ring PAHs, anthracene and anthanthrene also systematically decrease with increasing thermal maturity up to the highest rank possible. By combining the suite of bound PAH ratios, particularly when using multivariate

statistical analysis, we were able to better distinguish ancient kerogens and robustly assess the relative order of their thermal maturities. The bound PAH systematics were notably independent of their geologic age, since PAH are highly derived in structure from their biochemical precursors and, thus, both Precambrian an Phanerozoic biogenic kerogens show similar compound abundance ratio systematics governed primarily by thermal maturity.

Systematic abundance patterns using bound PAHs helped distinguish different end-member mechanisms of organic macromolecule formation. A suite of PAH abundance ratios were identified, especially when utilized with clustering statistics, which succeeded in separating biogenic kerogens (including highly overmature samples) versus abiogenic IOM formed from thermal cracking reactions. The absence of any traces of bound perylene further served as an indicator of organic matter sourced predominantly from hydrocarbon cracking, such as the pyrobitumen concentrates and the coke residue. Bound PAHs of thermal IOM residues were additionally characterized by a preponderance of large (6-7 ring) PAHs, especially for the more highly condensed and thermally stable PAH compounds.

Ancient biogenic kerogen samples get progressively enriched in aromatic carbon with increasing thermal maturity through progressive catagenesis, but their formation first involves a protracted stage of low-temperature diagenesis (<50^{o}C) during which a variety of PAH compounds can be formed, sequestered and protected for long-term burial

and preservation. The bound PAH patterns of abiogenic kerogens differ to those for insoluble carbonaceous material produced mainly as a residue from high-temperature cracking (>150ºC) of hydrocarbons and bitumen. We used 2.1 Ga pyrobitumen concentrates as well as a synthetic coke residue produced from laboratory fluidized catalytic cracking of hexadecane to look at abiotic PAH formation and preservation in IOM at high temperatures. These high temperature residues generated no detectable signals for perylene and/or anthanthrene in their pyrolysis products, in contrast to our maturity suite of ancient biogenic kerogens. While not a definitive biosignature, the ability to recognize aromatics formed from low-temperature processing of organic material will aid in the search for past and extant life on extraterrestrial bodies such as Mars, since aromatic-rich macromolecules may comprise the majority of organic matter. If PAHs indicative of low-temperature synthesis are found on Mars, (and the carbon isotopes systematics do not suggest a meteoritic origin) then this could be an important step towards finding preserved biogenic organic matter. Additional work is needed to expand the range of IOM samples produced by abiotic mechanisms in order to investigate the compound patterns preserved by covalent binding in the host matrix under such regimes. It is possible that abiogenic carbonaceous residues formed at a low temperature, from chemical or radiolytic processes, could show similar abundance and stable isotopic patterns to biogenic kerogens but this will be the focus of future work.

Table 4.1. Sample details and locations

Sample	Location/Source	Age	Depth (m)
B-45-R 3, 1-2	Demerara Rise, Site 1258B	Upper Cretaceous	420.19 [a]
B-45-R 3, 80.0-81.0	Demerara Rise, Site 1258B	Upper Cretaceous	420.98 [a]
A-42-6 47-49	Demerara Rise, Site 1258A	Upper Cretaceous	421.95 [a]
A-42-7 100-101	Demerara Rise, Site 1258A	Upper Cretaceous	423.89 [a]
C-17R-1 27-28	Demerara Rise, Site 1258C	Upper Cretaceous	425.06 [a]
C-17R-2 12-13	Demerara Rise, Site 1258C	Upper Cretaceous	426.3 [a]
FPC 933686	Boquillas Fm., Duke Well	Upper Cretaceous	911.4
FPC 933687	Boquillas Fm., Duke Well	Upper Cretaceous	917.46
FPC 933688	Boquillas Fm., Duke Well	Upper Cretaceous	956.61
FPC 933689	Boquillas Fm., Duke Well	Upper Cretaceous	964.52
FPC 933695	Boquillas Fm., Duke Well	Upper Cretaceous	969.92
HB4	Jet Rock Fm., Hawsker Bottoms	Lower Jurassic	-
V12	Visingso Gp., Broken Nodule	Tonian	-
BC6331	1.64 Ga Barney Creek Fm.	Paleoproterozoic	133.8
SWE2	Chuar Gp., Sixtymile Canyon	Tonian	-
SW4	Chuar Gp., Sixtymile Canyon	Tonian	-
FPC 933690	Boquillas Fm., Queen Well	Upper Cretaceous	2534.49
FPC 933691	Boquillas Fm., Queen Well	Upper Cretaceous	2557.96
FPC 933692	Boquillas Fm., Queen Well	Upper Cretaceous	2564.54
FPC 933693	Boquillas Fm., Queen Well	Upper Cretaceous	2578.61
FPC 933694	Boquillas Fm., Queen Well	Upper Cretaceous	2593.47
FPC 905757	Alberta Basin, Heron Well	Lower Triassic	2199.9
FPC 905758	Alberta Basin, Heron Well	Lower Triassic	2056
FPC 905755	Alberta Basin, Skylark Well	Lower Triassic	2754.5
FPC 905756	Alberta Basin, Skylark Well	Lower Triassic	2951.98
FPC 905753	Alberta Basin, Phoenix Well	Lower Triassic	3061.8
FPC 905754	Alberta Basin, Phoenix Well	Lower Triassic	3161.75
Chuar 36	Chuar Gp., Nankoweap Butte	Tonian	595
Chuar 50	Chuar Gp., Nankoweap Butte	Tonian	749
HN21	Nanhua, Doushantuo Fm.	Ediacaran	140.9 [b]
HN10	Nanhua, Doushantuo Fm.	Ediacaran	152 [b]
2/1/004	2.6 Ga Pilbara, Carwine Fm.	Archean	170.4 [c]
2/1/001	2.6 Ga Pilbara, Carwine Fm.	Archean	116.09 [c]
2/1/003	2.6 Ga Pilbara, Carwine Fm.	Archean	146.2 [c]
FPL 910060A	Stainmore Fm., Boulmer, Distal	Carboniferous	29.8*
FPL 910060B	Stainmore Fm., Boulmer, Distal	Carboniferous	29.8*
FPL 910062A	Stainmore Fm., Boulmer, Distal	Carboniferous	48.8*
CapB	Nanhua, Doushantuo Fm.	Ediacaran	-
HJ01	Nanhua, Doushantuo Fm.	Ediacaran	0.7 [b]
FPL 910058B	Stainmore Fm., Boulmer, Proximal	Carboniferous	7.94*
FPL 910058A	Stainmore Fm., Boulmer, Proximal	Carboniferous	7.94*
FPL 910059	Stainmore Fm., Boulmer, Proximal	Carboniferous	10.3*

Table 4.1. continued

LST1 42.3	2.1 Ga Francevillian, FC Fm.	Paleoproterozoic	42.3
LST12 55.9	2.1 Ga Francevillian, FC Fm.	Paleoproterozoic	55.9
LST12 26.05	2.1 Ga Francevillian, FC Fm.	Paleoproterozoic	26.05
LST12 32	2.1 Ga Francevillian, FC Fm.	Paleoproterozoic	32
LST1 60.6 P	2.1 Ga Francevillian, FC Fm.	Paleoproterozoic	60.6
LST12 93 P	2.1 Ga Francevillian, FC Fm.	Paleoproterozoic	93
LST12 107.8 P	2.1 Ga Francevillian, FC Fm.	Paleoproterozoic	107.8
BASF	Fluid Catalyst Cracking	-	-

Note: * = distance to intrusive feeder dyke; '-' = not determined; [a] Owens et al., 2016; [b] Zumberge et al., 2019; [c] Li et al., 2010; [d] French et al., 2015;

Table 4.2. Sample geochemical characteristics and thermal maturity

Sample	Ro (%)	HI (mg/g TOC)	TOC (%)	Thermal Maturity & Organic Matter Type
B-45-R 3, 1-2	-	-	14.73 [a]	Immature Kerogen
B-45-R 3, 80.0-81.0	-	-	11.34 [a]	Immature Kerogen
A-42-6 47-49	-	-	6.37 [a]	Immature Kerogen
A-42-7 100-101	-	-	17.27 [a]	Immature Kerogen
C-17R-1 27-28	-	-	21.97 [a]	Immature Kerogen
C-17R-2 12-13	-	-	7.11 [a]	Immature Kerogen
FPC 933686	0.75	513	2.3	Early Oil Window Kerogen
FPC 933687	0.75	471	5.2	Early Oil Window Kerogen
FPC 933688	0.75	437	5.4	Early Oil Window Kerogen
FPC 933689	0.75	478	5.4	Early Oil Window Kerogen
FPC 933695	0.75	513	1.5	Early Oil Window Kerogen
HB4	-	-	-	Early Oil Window Kerogen
V12	-	225 [b]	1.13 [b]	Early Oil Window Kerogen
BC6331	-	542	2.8	Early Oil Window Kerogen
SWE2	-	132 [b]	5.61 [b]	Peak Oil Window Kerogen
SW4	-	119 [b]	3.57 [b]	Peak Oil Window Kerogen
FPC 933690	1.19	83	1.8	Late Oil Window Kerogen
FPC 933691	1.19	88	1.7	Late Oil Window Kerogen
FPC 933692	1.19	79	2.8	Late Oil Window Kerogen
FPC 933693	1.19	-	1.7	Late Oil Window Kerogen
FPC 933694	1.19	57	4.4	Late Oil Window Kerogen
FPC 905757	1.2	-	5.4	Late Oil Window Kerogen
FPC 905758	1.2	-	2.8	Late Oil Window Kerogen
FPC 905755	1.3	17	3.8	Late Oil Window Kerogen
FPC 905756	1.3	-	-	Late Oil Window Kerogen
FPC 905753	1.4	27	-	Late Oil Window Kerogen
FPC 905754	1.5	24	-	Late Oil Window Kerogen
Chuar 36	-	88 [b]	4.70 [b]	Late Oil Window Kerogen
Chuar 50	-	64 [b]	3.54 [b]	Late Oil Window Kerogen
HN21	-	6	5.2 [c]	Overmature Kerogen
HN10	-	22	0.3 [c]	Overmature Kerogen
2/1/004	-	-	1.3 [d]	Overmature Kerogen
2/1/001	-	-	0.4 [d]	Overmature Kerogen
2/1/003	-	-	1.6 [d]	Overmature Kerogen
FPL 910060A	-	6	4.7	Overmature Kerogen
FPL 910060B	-	6	4.7	Overmature Kerogen
FPL 910062A	-	65	0.5	Overmature Kerogen
CapB	-	3	-	Overmature (altered)
HJ01	-	18	0.0 [c]	Overmature (altered)
FPL 910058B	-	7	5.2	Overmature (altered)
FPL 910058A	-	7	5.2	Overmature (altered)
FPL 910059	-	9	4.6	Overmature (altered)

Table 4.2. continued

LST1 42.3	-	-	-	Pyrobitumen & Shale
LST12 55.9	-	-	14.8	Pyrobitumen & Shale
LST12 26.05	-	-	1.8	Pyrobitumen & Shale
LST12 32	-	-	0.7	Pyrobitumen & Shale
LST1 60.6 P	-	-	-	Pyrobitumen
LST12 93 P	-	-	16.4	Pyrobitumen
LST12 107.8 P	-	-	60.6	Pyrobitumen
BASF	-	-	-	Coke Residue

Note: Ro% = vitrinite reflectance; HI = Hydrogen Index; TOC = total organic content; * = distance to intrusive feeder dyke; '-' = not determined; [a] Owens et al., 2016; [b] Zumberge et al., 2019; [c] Li et al., 2010; [d] French et al., 2015;

Table 4.3. Selected PAH ratios of abundances generated by catalytic hydropyrolysis (HyPy) of kerogens and IOM.

Sample	MP/ Phe	(2-MP + 3-MP)/ (9-MP + 1-MP)	2-MP/ 1-MP	An/ (Phe+An)	BaP/ (BeP+BaP)	Per/ (BeP+Per)	BeP/(BeP+ B[ghi]Per)	Anth/ (Anth+ B[ghi]Per)
B-45-R 3, 1-2	1.19	1.77	1.10	0.20	0.62	0.91	0.35	0.27
B-45-R 3, 80.0-81.0	1.51	1.56	0.98	0.18	0.59	0.94	0.36	0.22
A-42-6 47-49	1.64	1.45	1.17	0.19	0.57	0.89	0.34	0.26
A-42-7 100-101	2.08	1.23	1.27	0.24	0.59	0.80	0.50	0.17
C-17R-1 27-28	1.26	1.49	1.31	0.14	0.49	0.76	0.44	0.15
C-17R-2 12-13	1.06	1.98	1.53	0.08	0.45	0.76	0.29	0.13
FPC 933686	1.44	1.56	1.39	0.13	0.53	0.23	0.42	0.27
FPC 933687	0.81	2.43	1.57	0.04	0.51	0.38	0.38	0.22
FPC 933688	1.11	2.21	1.48	0.05	0.49	0.40	0.43	0.20
FPC 933689	0.91	2.80	1.54	0.04	0.48	0.31	0.37	0.19
FPC 933695	0.78	2.12	1.51	0.05	0.49	0.17	0.38	0.19
HB4	1.58	1.63	1.25	0.05	0.53	0.40	0.32	0.11
V12	2.42	1.87	1.30	0.09	0.49	0.33	0.41	0.08
BC6331	3.94	1.41	1.15	0.15	0.55	0.19	0.40	0.12
SWE2	1.94	1.28	0.20	0.15	0.50	0.11	0.48	0.21
SW4	3.13	2.31	1.56	0.07	0.46	0.17	0.42	0.10
FPC 933690	0.89	3.36	1.54	0.04	0.40	0.07	0.51	0.18
FPC 933691	1.06	3.53	1.55	0.03	0.39	0.04	0.55	0.18
FPC 933692	1.08	3.38	1.51	0.04	0.43	0.06	0.50	0.19
FPC 933693	0.95	3.46	1.56	0.04	0.41	0.05	0.53	0.20
FPC 933694	0.86	3.63	1.73	0.03	0.44	0.08	0.41	0.18
FPC 905757	2.47	2.63	1.27	0.06	0.45	0.09	0.43	0.18
FPC 905758	1.49	3.13	1.45	0.07	0.54	0.18	0.45	0.24
FPC 905755	1.92	2.69	1.31	0.06	0.44	0.06	0.39	0.14
FPC 905756	1.08	3.50	1.43	0.02	0.39	0.05	0.46	0.15
FPC 905753	1.51	3.28	1.50	0.03	0.35	0.21	0.47	0.13
FPC 905754	1.27	2.74	1.49	0.02	0.26	0.04	0.37	0.07
Chuar 36	3.51	1.91	1.31	0.17	0.40	0.17	0.45	0.18
Chuar 50	1.98	2.08	1.29	0.12	0.35	0.12	0.39	0.06
HN21	0.62	3.44	1.56	0.02	0.40	0.06	0.35	0.14
HN10	0.78	3.80	1.53	0.01	0.30	0.04	0.30	0.04
2/1/004	0.71	2.33	1.21	0.03	0.16	0.14	0.42	0.03
2/1/001	1.33	1.85	1.23	0.06	0.28	0.19	0.19	0.10
2/1/003	0.94	2.11	1.07	0.02	0.19	0.04	0.11	0.04
FPL 910060A	0.67	2.29	1.60	0.02	0.20	0.04	0.53	0.04
FPL 910060B	0.91	2.28	1.65	0.02	0.19	0.05	0.43	0.05
FPL 910062A	0.61	2.91	1.42	0.04	0.20	0.03	0.52	0.08
CapB	0.25	3.50	1.74	0.01	0.29	0.03	0.14	0.05
HJ01	0.37	3.41	1.56	0.01	0.30	0.04	0.18	0.07
FPL 910058B	0.45	2.04	1.68	0.00	0.03	0.02	0.31	0.00
FPL 910058A	0.23	2.24	1.64	0.01	0.05	0.03	0.28	0.00
FPL 910059	1.13	2.15	1.65	0.02	0.05	0.02	0.44	0.01

Table 4.3. continued

LST1 42.3	26.45	1.67	2.31	0.00	0.01	0.00	0.20	0.00
LST12 55.9	1.61	3.45	1.76	0.00	0.05	0.01	0.21	0.00
LST12 26.05	u.d.	u.d.	u.d.	u.d.	0.01	0.01	0.13	0.00
LST12 32	24.86	2.66	2.31	0.00	0.21	0.03	0.17	0.02
LST1 60.6 P	u.d.	u.d.	u.d.	u.d.	0.00	0.00	0.34	0.00
LST12 93 P	0.00	u.d.	u.d.	0.00	0.00	0.00	0.38	0.00
LST12 107.8 P	u.d.	u.d.	u.d.	u.d.	0.00	0.00	0.44	0.00
BASF	2.02	1.36	1.50	0.00	0.01	0.00	0.03	0.00

Note: methylphenanthrenes used to calculate ‘MP/Phe’ consist of 1-MP, 2-MP, 3-MP, and 9-MP; for PAH structures and abbreviations see Figures 4.1, 4.3 and 4.4; u.d. = undetermined due to all PAHs in the ratio remaining undetected

REFERENCES

Ader, M., Sansjofre, P., Halverson, G.P., Busigny, V., Trindade, R.I.F., Kunzmann, M., and Nogueira, A.C.R., 2014. Ocean redox structure across the Late Neoproterozoic Oxygenation Event: A nitrogen isotope perspective: *Earth and Planetary Science Letters* 396, 1–13, doi: 10.1016/j.epsl.2014.03.042.

Abreu, N.M. 2012. Low and High Temperature Aqueous Alteration of the Matrices of CR Chondrites: Nano-SEM, EPMA, and TEM Study. *Lunar and Planetary Science Conference*: 43.

Alexander, C.M.O., Cody, G.D., De Gregorio, B.T., Nittler, L.R., and Stroud, R.M. 2017. The nature, origin and modification of insoluble organic matter in chondrites, the major source of Earth's C and N. Chemie der Erde – *Geochemistry* 77, 227–256, doi: 10.1016/j.chemer.2017.01.007.

Bernard, S., Wirth, R., Schreiber, A., Schulz, H.-M., Horsfield, B., 2012. Formation of nanoporous pyrobitumen residues during maturation of the Barnett Shale Fort Worth Basin.. *International Journal of Coal Geology* 103, 3–11, doi: 10.1016/j.coal.2012.04.010

Bowden, S.A., Farrimond, P., Snape, C.E., Love, G.D., 2006. Compositional differences in biomarker constituents of the hydrocarbon, resin, asphaltene and kerogen fractions: An example from the Jet Rock Yorkshire, UK.. *Org. Geochem*. 37, 369–383, doi: 10.1016/j.orggeochem.2005.08.024

Britt, P.F., Buchanan, A.C., Kidder, M.M., Owens, C., Ammann, J.R., Skeen, J.T., Luo, L., 2001. Mechanistic investigation into the formation of polycyclic aromatic hydrocarbons from the pyrolysis of plant steroids. *Fuel* 80, 1727–1746, doi: 10.1016/S0016-236101.00058-8

Brocks J. J., Love G. D., Summons R. E., Knoll A. H., Logan G. A. and Bowden S. A. 2005. Biomarker evidence for green and purple sulphur bacteria in a stratified Paleoproterozoic sea. *Nature* 437, 866–870, doi: 10.1038/nature04068

Buick, R., Thornett, J.R., McNaughton, N.J., Smith, J.B., Barley, M.E., and Savage, M. 1995. Record of emergent continental crust ~3.5 billion years ago in the Pilbara craton of Australia. *Nature* 375, 574–577, doi: 10.1038/375574a0.

Busemann, H., Young, A.F., Alexander, C.M.O., Hoppe, P., Mukhopadhyay, S., and Nittler, L.R. 2006. Interstellar Chemistry Recorded in Organic Matter from Primitive Meteorites. *Science* 312, 727–730, doi: 10.1126/science.1123878.

Carr, M.H., and Bell, J.F. 2014. Mars: Surface and Interior, in Encyclopedia of the Solar System, Elsevier, 359–377.

Cortial, F., Gauthier-Lafaye, F., Lacrampe-Couloume, G., Oberlin, A., and Weber, F. 1990. Characterization of organic matter associated with uranium deposits in the Francevillian formation of Gabon lower proterozoic.. *Organic Geochemistry* 15, 73–85, doi: 10.1016/0146-638090.90185-3.

Derkowski, A., Bristow, T.F., Wampler, J.M., Środoń, J., Marynowski, L., Elliott, W.C., and Chamberlain, C.P. 2013. Hydrothermal alteration of the Ediacaran Doushantuo Formation in the Yangtze Gorges area South China.. *Geochimica et Cosmochima Acta* 107, 279–298, doi: 10.1016/j.gca.2013.01.015.

Eigenbrode, J.L., Summons, R.E., Steele, A., Freissinet, C., Millan, M., Navarro-González, R., Sutter, B., McAdam, A.C., Franz, H.B., Glavin, D.P., Archer, P.D., Jr., Mahaffy, P.R., Conrad, P.G., Hurowitz, J.A., et al. 2018. Organic matter preserved in 3-billion-year-old mudstones at Gale crater, Mars. *Science* 360, 1096–1101, doi: 10.1126/science.aas9185.

Espitalié, J., Marquis, F., and Barsony, I., 1984. Geochemical Logging. In Analytical Pyrolysis: Techniques and Applications 276-304

Farrimond, P., Love, G.D., Bishop, A.N., Innes, H.E., Watson, D.F., Snape, C.E., 2003. Evidence for the rapid incorporation of hopanoids into kerogen. *Geochimica et Cosmochimica Acta* 67, 1383–1394. doi.org: 10.1016/S0016-703702.01287-5.

Fetzer, J.C., 2010. The Chemistry and Analysis of Large PAHs. *Polycyclic Aromatic Compounds* 27, 143–162, doi: 10.1080/10406630701268255.

Freissinet, C., Glavin, D.P., Mahaffy, P.R., Miller, K.E., Eigenbrode, J.L., Summons, R.E., Brunner, A.E., Buch, A., Szopa, C., Archer, P.D., Jr., Franz, H.B., Atreya, S.K., Brinckerhoff, W.B., Cabane, M., et al. 2015. Organic molecules in the Sheepbed Mudstone, Gale Crater, Mars. J*ournal of Geophysical Research: Planets* 120, 495–514, doi: 10.1002/2014JE004737.

French, K.L., Hallmann, C., Hope, J.M., Schoon, P.L., Zumberge, J.A., Hoshino, Y., Peters, C.A., George, S.C., Love, G.D., Brocks, J.J., Buick, R., and Summons, R.E. 2015. Reappraisal of hydrocarbon biomarkers in Archean rocks. *Proceedings of the National Academy of Sciences* 112, 5915–5920, doi: 10.1073/pnas.1419563112.

French, K.L., Sepúlveda, J., Trabucho-Alexandre, J., Gröcke, D.R., Summons, R.E. 2014. Organic geochemistry of the early Toarcian oceanic anoxic event in Hawsker Bottoms, Yorkshire, England. *Earth and Planetary Science Letters* 390, 116-127, doi: 10.1016/j.epsl.2013.12.033

Grice, K., Lu, H., Atahan, P., Asif, M., Hallmann, C., Greenwood, P., Maslen, E., Tulipani, S., Williford, K., and Dodson, J. 2009. New insights into the origin of perylene in geological samples. *Geochimica et Cosmochima Acta* 73, 6531–6543, doi: 10.1016/j.gca.2009.07.029.

Haddad, E.E., Tuite, M.L., Martinez, A.M., Williford, K., Boyer, D.L., Droser, M.L., and Love, G.D. 2016.. Lipid biomarker stratigraphic records through the Late Devonian Frasnian/Famennian boundary: Comparison of high-and low-latitude epicontinental marine settings. *Organic Geochemistry*, 98, 38–53, doi: 10.1016/j.orggeochem.2016.05.007

Huang, W.-L. 1996. Experimental study of vitrinite maturation: effects of temperature, time, pressure, water, and hydrogen index. *Organic Geochemistry* 24, 233–241, doi: 10.1016/0146-638096.00032-0.

Hunt, J.M. 1991. Generation of gas and oil from coal and other terrestrial organic matter. *Organic Geochemistry* 17, 673–680, doi: 10.1016/0146-638091.90011-8.

Hunter, J. D. 2007..Matplotlib: A 2D graphics environment. *Computing In Science & Engineering* 9, 90–95, doi: 10.1109/MCSE.2007.55

Ibrahim, B.A., 1995. A geochemical study of the Jet Rock, the Kimmeridge Clay and the associated concretions. M. Phil. Thesis, University of Newcastle Upon Tyne.

Itoh, N., Sakagami, N., Torimura, M., Watanabe, M., 2012. Perylene in Lake Biwa sediments originating from Cenococcum geophilum in its catchment area. *Geochimica et Cosmochima Acta* 95, 241–251, doi: 10.1016/j.gca.2012.07.037

Jilly-Rehak, C.E., Huss, G.R., and Nagashima, K. 2017. 53Mn–53Cr radiometric dating of secondary carbonates in CR chondrites: Timescales for parent body aqueous alteration. *Geochimica et Cosmochima Acta* 201, 224–244, doi: 10.1016/j.gca.2016.08.033.

Killops, S and Killops, V. 2005.. Long-Term Fate of Organic Matter in the Geosphere. In Introduction to Organic Geochemistry, Blackwell Publishing, Malden, MA, pp. 117-165, doi:10.1002/9781118697214.ch4

Komiya, M., Shimoyama, A., and Harada, K. 1993. Examination of organic compounds from insoluble organic matter isolated from some Antarctic carbonaceous chondrites by heating experiments. *Geochimica et Cosmochima Acta* 57, 907–914, doi: 10.1016/0016-703793.90177-X.

Lee, C., Love, G.D., Jahnke, L.L., Kubo, M.D., and Marais, Des, D.J. 2019. Early diagenetic sequestration of microbial mat lipid biomarkers through covalent binding into insoluble macromolecular organic matter (IMOM) as revealed by sequential chemolysis and catalytic hydropyrolysis. *Organic Geochemistry* 132, 11–22, doi: 10.1016/j.orggeochem.2019.04.002.

Levy, R.L., Grayson, M.A., and Wolf, C.J. 1973. The organic analysis of the murchison meteorite. *Geochimica et Cosmochima Acta* 37, 467–483, doi: 10.1016/0016-703773.90212-3.

Li, C., Love, G.D., Lyons, T.W., Fike, D.A., Sessions, A.L., and Chu, X. 2010. A Stratified Redox Model for the Ediacaran Ocean. *Science* 328, 80–83, doi: 10.1126/science.1182369.

Liao, J., Lu, H., Sheng, G., Peng, P., and Hsu, C.S. 2015. Monoaromatic, Diaromatic, Triaromatic, and Tetraaromatic Hopanes in Kukersite Shale and Their Stable Carbon Isotopic Composition. *Energy & Fuels* 29, 3573–3583, doi: 10.1021/acs.energyfuels.5b00106.

Lin, Z., Wang, Q., Feng, D., Liu, Q., and Chen, D. 2011. Post-depositional origin of highly 13C-depleted carbonate in the Doushantuo cap dolostone in South China: Insights from petrography and stable carbon isotopes. *Sedimentary Geology* 242, 71–79, doi: 10.1016/j.sedgeo.2011.10.009.

Liu, N., Nittler, L.R., Alexander, C.M.O, Wang, J., Pignatari, M., Jośe, J., Nguyen, A. 2016. Stellar origins of extremely 13C-and 15N-enriched presolar SiC grains: Novae or supernovae? *Astrophysical Journal* 820, 1-14 doi: 10.3847/0004-637X/820/2/140.

Love, G.D., Grosjean, E., Stalvies, C., Fike, D.A., Grotzinger, J.P., Bradley, A.S., Kelly, A.E., Bhatia, M., Meredith, W., Snape, C.E., Bowring, S.A., Condon, D.J., and Summons, R.E. 2009. Fossil steroids record the appearance of Demospongiae during the Cryogenian period. *Nature* 457, 718–721, doi: 10.1038/nature07673.

Love, G.D., Bowden, S.A., Jahnke, L.L., Snape, C.E., Campbell, C.N., Day, J.G., Summons, R.E. 2005. A catalytic hydropyrolysis method for the rapid screening of microbial cultures for lipid biomarkers. *Organic Geochemistry* 36, 63–82. doi: 10.1016/j.orggeochem.2004.07.010

Love, G.D., McAulay, A., Snape, C.E., and Bishop, A.N. 1997. Effect of Process Variables in Catalytic Hydropyrolysis on the Release of Covalently Bound Aliphatic Hydrocarbons from Sedimentary Organic Matter. *Energy & Fuels* 11, 522–531, doi: 10.1021/ef960194x.

Love, G.D., Snape, C.E., Carr, A.D., and Houghton, R.C. 1995. Release of covalently-bound alkane biomarkers in high yields from kerogen via catalytic hydropyrolysis: *Organic Geochemistry* 23, 981–986, doi: 10.1016/0146-638095.00075-5.

Marshall, C.P., Allwood, A.C., Love, G.D., Walter, M.R., and Summons, R.E. 2006. Characterization of c.3.5 billion-year-old organic matter. *Gondwana Research* 10, 393–394, doi: 10.1016/j.gr.2006.07.001.

Marshall, C.P., Love, G.D., Snape, C.E., Hill, A.C., Allwood, A.C., Walter, M.R., Van Kranendonk, M.J., Bowden, S.A., Sylva, S.P., and Summons, R.E. 2007. Structural characterization of kerogen in 3.4Ga Archaean cherts from the Pilbara Craton, Western Australia. *Precambrian Research* 155, 1–23, doi: 10.1016/j.precamres.2006.12.014.

Marynowski, L., Smolarek, J., Bechtel, A., Philippe, M., Kurkiewicz, S., Simoneit, B.R.T. 2013. Perylene as an indicator of conifer fossil wood degradation by wood-degrading fungi. *Org. Geochem*. 59, 143–151, doi: 10.1016/j.orggeochem.2013.04.006

Marynowski, L., Smolarek, J. and Hautevelle, Y. 2015. Perylene degradation during gradual onset of organic matter maturation. *Int J Coal Geol*, 139, 17–25, doi: 10.1016/j.coal.2014.04.013

McCollom, T.M., Seewald, J.S. 2006. Carbon isotopic composition of organic compounds produced by abiotic synthesis under hydrothermal conditions. *Earth and Planetary Science Letters*, 243, 74-84, doi: 10.1016/j.epsl.2006.01.027

McCollom, T.M., Simoneit, B.R.T., A., and Shock, E.L. 1999. Hydrous Pyrolysis of Polycyclic Aromatic Hydrocarbons and Implications for the Origin of PAH in Hydrothermal Petroleum. *Energy & Fuels* 13, 401–410, doi: 10.1021/ef980089i.

McKay, D.S., Gibson, E.K., Thomas-Keprta, K.L., Vali, H., Romanek, C.S., Clemett, S.J., Chillier, X.D.F., Maechling, C.R., and Zare, R.N. 1996. Search for Past Life on Mars: Possible Relic Biogenic Activity in Martian Meteorite ALH84001. *Science,* 273, 924–930, doi: 10.1126/science.273.5277.924.

McKinney, W. 2010. Data structures for statistical computing in python. *Proceedings of the 9th Python in Science Conference*, 445, doi: 10.25080/Majora-92bf1922-00a

McSween, H.Y. 1979. Are carbonaceous chondrites primitive or processed? A review. *Reviews of Geophysics* 17, 1059–1078, doi: 10.1029/RG017i005p01059.

Mißbach, H., Duda, J., Lünsdorf, N., Schmidt, B., & Thiel, V. 2016.. Testing the preservation of biomarkers during experimental maturation of an immature

kerogen. *International Journal of Astrobiology*, 153, 165-175. doi:10.1017/S1473550416000069.

Montgomery, W., Jaramillo, E.A., Royle, S.H., Kounaves, S.P., Schulze-Makuch, D., Sephton, M.A., 2019. Effects of Oxygen-Containing Salts on the Detection of Organic Biomarkers on Mars and in Terrestrial Analog Soils. *Astrobiology*, 19, 711–721, doi: 10.1089/ast.2018.1888

Nabbefeld, B., Grice, K., Schimmelmann, A., Summons, R.E., Troitzsch, U., and Twitchett, R.J. 2010a. A comparison of thermal maturity parameters between freely extracted hydrocarbons (Bitumen I) and a second extract (Bitumen II) from within the kerogen matrix of Permian and Triassic sedimentary rocks. *Organic Geochemistry* 41, 78–87, doi: 10.1016/j.orggeochem.2009.08.004.

Nabbefeld, B., Grice, K., Summons, R.E., Hays, L.E., and Cao, C. 2010b. Significance of polycyclic aromatic hydrocarbons (PAHs) in Permian/Triassic boundary sections. *Applied Geochemistry* 25, 1374–1382, doi: 10.1016/j.apgeochem.2010.06.008.

Nittler, L.R. 2003. Presolar stardust in meteorites: recent advances and scientific frontiers. *Earth and Planetary Science Letters* 209, 259–273, doi: 10.1016/S0012-821X02.01153-6.

Okumura, F., and Mimura, K. 2011. Gradual and stepwise pyrolyses of insoluble organic matter from the Murchison meteorite revealing chemical structure and isotopic distribution. *Geochimica et Cosmochima* 75, 7063–7080, doi: 10.1016/j.gca.2011.09.015.

Ossa Ossa, F., El Albani, A., Hofmann, A., Bekker, A., Gauthier-Lafaye, F., Pambo, F., Meunier, A., Fontaine, C., Boulvais, P., Pierson-Wickmann, A.C., Cavalazzi, B., and Macchiarelli, R. 2013. Exceptional preservation of expandable clay minerals in the ca. 2.1Ga black shales of the Francevillian basin, Gabon and its implication for atmospheric oxygen accumulation. *Chemical Geology* 362, 181–192, doi: 10.1016/j.chemgeo.2013.08.011.

McGrath, T.E., Chan, W.G., Hajaligol, M.R. 2003. Low temperature mechanism for the formation of polycyclic aromatic hydrocarbons from the pyrolysis of cellulose. *Journal of Analytical and Applied* Pyrolysis 66, 51–70, doi: 10.1016/S0165-237002.00105-5

Murray, I.P., Love, G.D., Snape, C.E., Bailey, N.J.L. 1998.. Comparison of covalently-bound aliphatic biomarkers released via hydropyrolysis with their solvent-extractable counterparts for a suite of Kimmeridge clays. *Organic Geochemistry* 29, 1487–1505, doi: 10.1016/s0146-638098.00162-4.

Ossa Ossa, F., Eickmann, B., Hofmann, A., Planavsky, N.J., Asael, D., Pambo, F., and Bekker, A. 2018. Two-step deoxygenation at the end of the Paleoproterozoic Lomagundi Event. *Earth and Planetary Science Letters* 486, 70–83, doi: 10.1016/j.epsl.2018.01.009.

Owens, J.D., Reinhard, C.T., Rohrssen, M., Love, G.D., Lyons, T.W. 2016. Empirical links between trace metal cycling and marine microbial ecology during a large perturbation to Earth's carbon cycle. *Earth and Planetary Science Letters*, 449, 407-417, https://doi.org/10.1016/j.epsl.2016.05.046.

Parnell, J., Cullen, D., Sims, M.R., Bowden, S., Cockell, C.S., Court, R., Ehrenfreund, P., Gaubert, F., Grant, W., Parro, V., Rohmer, M., Sephton, M., Stan-Lotter, H., Steele, A., et al. 2007. Searching for Life on Mars: Selection of Molecular Targets for ESA's Aurora ExoMars Mission. *Astrobiology* 7, 578–604, doi: 10.1089/ast.2006.0110.

Pehr, K., Love, G.D., Kuznetsov, A., Podkovyrov, V., Junium, C. K., Shumlyanskyy, L., Sokur, T., Bekker, A. 2018.. Ediacara biota flourished in oligotrophic and bacterially dominated marine environments across Baltica. *Nature Communications*, 9, 1807, doi:10.1038/s41467-018-04195-8

Pedregosa, F., Varoquaux, G., Gramfort, A., Michel, V., Thirion, B., Grisel, O., Blondel, M., Prettenhofer, P., Weiss, R., Dubourg, V., Vanderplas, J., Passos, A., Cournapeau, D., Brucher, M., et al. 2011. Scikit-learn: Machine Learning in Python. *Journal of Machine Learning Research* 12, 2825–2830.

Peters, K.E., Walters, C.C., Moldowan, J.M. 2005.. The Biomarker Guide. Cambridge University Press, Cambridge, UK.

Peters, K.E. 1986. Guidelines for Evaluating Petroleum Source Rock Using Programmed Pyrolysis. *AAPG Bulletin* 70, 318–329.

Radke, M. 1988. Application of aromatic compounds as maturity indicators in source rocks and crude oils. *Marine and Petroleum Geology* 5, 224–236, doi: 10.1016/0264-817288.90003-7.

Radke, M., Welte, D.H., and Willsch, H. 1986. Maturity parameters based on aromatic hydrocarbons: Influence of the organic matter type. *Organic Geochemistry* 10, 51–63, doi: 10.1016/0146-638086.90008-2.

Remusat, L., Derenne, S., and Robert, F. 2005. New insight on aliphatic linkages in the macromolecular organic fraction of Orgueil and Murchison meteorites through ruthenium tetroxide oxidation. *Geochimica et Cosmochima* 69, 4377–4386, doi: 10.1016/j.gca.2005.05.003.

Remusat, L., Robert, F., Meibom, A., Mostefaoui, S., Delpoux, O., Binet, L., Gourier, D., and Derenne, S. 2009. Proto-Planetary Disk Chemistry Recorded by D-rich Organic Radicals in Carbonaceous Chondrites. *The Astrophysical Journal* 698, 2087–2092, doi: 10.1088/0004-637X/698/2/2087.

Ribeiro, J., Silva, T., Filho, J.G.M., and Flores, D. 2012. Polycyclic aromatic hydrocarbons (PAHs) in burning and non-burning coal waste piles: *Journal of Hazardous Materials* 199-200, 105–110, doi: 10.1016/j.jhazmat.2011.10.076.

Sephton, M.A., Watson, J.S., Meredith, W., Love, G.D., Gilmour, I., Snape, C.E. 2015. Multiple Cosmic Sources for Meteorite Macromolecules? *Astrobiology* 15, 779–786, doi: 10.1089/ast.2015.1331.

Sephton, M.A. 2013. Aromatic units from the macromolecular material in meteorites: Molecular probes of cosmic environments: *Geochimica et Cosmochima* 107, 231–241, doi: 10.1016/j.gca.2012.12.042.

Sephton, M.A., Bland, P.A., Pillinger, C.T., and Gilmour, I. 2010. The preservation state of organic matter in meteorites from Antarctica. *Meteoritics & Planetary Science*. 39, 747–754, doi: 10.1111/j.1945-5100.2004.tb00116.x.

Sephton, M.A. 2005. Organic matter in carbonaceous meteorites: past, present and future research. *Philosophical Transactions of the Royal Society A: Mathematical, Physical and Engineering Sciences*, 363, 2729–2742, doi: 10.1098/rsta.2005.1670.

Sephton, M.A., Love, G.D., Watson, J.S., Verchovsky, A.B., Wright, I.P., Snape, C.E., and Gilmour, I. 2004. Hydropyrolysis of insoluble carbonaceous matter in the Murchison meteorite: new insights into its macromolecular structure. *Geochimica et Cosmochima Acta* 68, 1385–1393, doi: 10.1016/j.gca.2003.08.019.

Sephton, M.A., and Gilmour, I. 2000. Aromatic Moieties in Meteorites: Relics of Interstellar Grain Processes?. *The Astrophysical Journal* 540, 588–591, doi: 10.1086/309296.

Sephton, M.A., Pillinger, C.T., and Gilmour, I. 1998. δ13C of free and macromolecular aromatic structures in the murchison meteorite: *Geochimica et Cosmochima Acta* 62, 1821–1828, doi: 10.1016/S0016-703798.00108-2.

Simmonds, P.G., Bauman, A.J., Bollin, E.M., Gelpi, E., and Oró, J. 1969. The unextractable Organic Fraction of the Pueblito de Allende Meteorite: Evidence for its Indigenous Nature. *Proceedings of the National Academy of Sciences* 64, 1027–1034, doi: 10.1073/pnas.64.3.1027.

Simoneit, B.R.T., 1998. Biomarker PAHs in the Environment in The Handbook of Environmental Chemistry 175–221.

Simoneit, B.R.T., and Fetzer, J.C. 1996. High molecular weight polycyclic aromatic hydrocarbons in hydrothermal petroleums from the Gulf of California and Northeast Pacific Ocean. *Organic Geochemistry* 24, 1065–1077, doi: 10.1016/S0146-638096.00081-2.

Smith, R.E., Perdrix, J.L., Parks, T.C. 1982. Burial metamorphism in the Hamersley basin. *Journal of Petrology* 23, 75-102, doi: 10.1093/petrology/23.1.75

Stein, S. 1978. On the High Temperature Chemical Equilibria of Polycyclic Aromatic Hydrocarbons, *J. Phys. Chem*. 82, 566-571

Sullivan, R.F., Boduszynski, M.M., Fetzer, J.C., 1989. Molecular transformations in hydrotreating and hydrocracking. *Energy & Fuels* 3, 603-612

Suzuki, N., Yessalina, S., and Kikuchi, T. 2010. Probable fungal origin of perylene in Late Cretaceous to Paleogene terrestrial sedimentary rocks of northeastern Japan as indicated from stable carbon isotopes. *Organic Geochemistry* 41, 234–241, doi: 10.1016/j.orggeochem.2009.11.010.

Szopa, C., Freissinet, C., Glavin, D.P., Millan, M., Buch, A., Franz, H.B.., Summons, R.E., Sumner, D., Sutter B., Eigenbrode, J.L., Williams, R., Navarro-González, R., Guzman, R., Malespin, C., Teinturier, S., Mahaffy, P.R., Cabane, M., 2020. First Detections of Dichlorobenzene Isomers and Trichloromethylpropane from Organic Matter Indigenous to Mars Mudstone in Gale Crater, Mars: Results from the Sample Analysis at Mars Instrument Onboard the Curiosity Rover. *Astrobiology* 20, 292-306 doi: 10.1089/ast.2018.1908

van Aarssen, B.G.K., Alexander, R., Kagi, R.I., 2000.. Higher plant biomarkers reflect palaeovegetation changes during Jurassic times. *Geochimica et Cosmochimica Acta* 64, 1417–1424, doi: 10.1016/j.coal.2019.103373

Vuković, N., Životić, D., Mendonça Filho, J.G., Kravić-Stevović, T., Hámor-Vidó, M., Mendonça, J. de O., and Stojanović, K. 2016. The assessment of maturation changes of humic coal organic matter — Insights from closed-system pyrolysis experiments. *International Journal of Coal Geology* 154-155, 213–239, doi: 10.1016/j.coal.2016.01.007.

Wakeham, S.G., Schaffner, C., and Giger, W. 1980. Poly cyclic aromatic hydrocarbons in Recent lake sediments—II. Compounds derived from biogenic precursors during early diagenesis: *Geochimica et Cosmochima Acta* 44, 415–429, doi: 10.1016/0016-703780.90041-1.

Wang, Z., Wang, J., Kouketsu, Y., Bodnar, R.J., Gill, B.C., and Xiao, S. 2017. Raman geothermometry of carbonaceous material in the basal Ediacaran Doushantuo cap dolostone: The thermal history of extremely negative δ13C signatures in the aftermath of the terminal Cryogenian snowball Earth glaciation. *Precambrian Research* 298, 174–186, doi: 10.1016/j.precamres.2017.06.013.

Wickstrom, K., and Tolonen, K. 1987. The history of airborne polycyclic aromatic hydrocarbons PAH. and perylene as recorded in dated lake sediments. *Water, Air, and Soil Pollution* 32, 155–175, doi: 10.1007/BF00227691.

Willacy, K., Alexander, C., Ali-Dib, M., Ceccarelli, C., Charnley, S.B., Doronin, M., Ellinger, Y., Gast, P., Gibb, E., Milam, S.N., Mousis, O., Pauzat, F., Tornow, C., Wirström, E.S., et al. 2015. The Composition of the Protosolar Disk and the Formation Conditions for Comets. *Space Science Reviews* 197, 151-190, doi: 10.1007/s11214-015-0167-6.

Wu, L., Liao, Y., and Geng, A. 2015. Investigation of hydropyrolysis released aromatic hydrocarbons from Permian kerogens at different maturities in the Sichuan Basin, China. *Journal of Analytical and Applied* Pyrolysis 114, 47–59, doi: 10.1016/j.jaap.2015.05.001.

Yabuta, H., Williams, L.B., Cody, G.D., Alexander, C.M.O., Pizzarello, S. 2007. The insoluble carbonaceous material of CM chondrites: A possible source of discrete organic compounds under hydrothermal conditions. *Meteoritics & Planetary Science* 42, 37–48, doi, 10.1111/j.1945-5100.2007.tb00216.x.

Wang, Z., Fingas, M., Shu, Y.Y., Sigouin, L., Landriault, M., Lambert, P., Turpon, R., Campagna, P., and Mullin, J. 1999. Quantitative Characterization of PAHs in Burn Residue and Soot Samples and Differentiation of Pyrogenic PAHs from Petrogenic PAHs−The 1994 Mobile Burn Study. *Environmental Science & Technology* 33, 3100–3109, doi: 10.1021/es990031y.

Waskom, M., Botvinnik, O., O'Kane, D., Hobson, P., Ostblom, J., Lukauskas, S., Gemperline, D.C., Augspurger, T., Halchenko, Y., Cole, J.B., Warmenhoven, J. et al. 2018. mwaskom/seaborn: v0.9.0 (July 2019) (Version v0.9.0). Zenodo. doi: 10.5281/zenodo.1313201

Zumberge, J.A., Rocher, D., Love, G.D. 2019. Free and kerogen-bound biomarkers from late Tonian sedimentary rocks record abundant eukaryotes in mid-Neoproterozoic marine communities. *Geobiology* 18, 326– 347, doi: 10.1111/gbi.12378

CHAPTER FIVE

Conclusions

This dissertation presents detailed compositions of organic matter in both ideally preserved and highly altered ancient sedimentary rocks. The first part of this dissertation focuses on lipid biomarkers and stable carbon isotopic data of exceptionally well preserved samples from Baltica deposited at the end of the Precambrian during the Ediacaran. The low maturity allowed for extensive lipid biomarker analysis despite the relatively low TOC of the samples. Our results show that the biomarker assemblages encompass an exceptionally wide range of hopane/sterane ratios (1.6–119), which represents large contributions by bacteria over eukaryotes (mainly green algae). The highest hopane/sterane ratios (22–119) were measured in samples age equivalent to the peak in diversity and abundance of the Ediacara biota. A high contribution of bacteria to the overall low productivity was most likely the result of persistent oligotrophic conditions and may have bolstered a microbial loop, locally sustaining dissolved organic matter as an important organic nutrient. These oligotrophic, shallow-marine conditions extended over hundreds of kilometers across Baltica and persisted for more than 10 million years.

In addition to the lipid biomarker results, we used the newly developed picomolar-scale compound-specific isotope analyses (pico-CSIA) method to measure compound specific carbon isotopes of the lipid biomarkers reported in Chapter 2. Total organic carbon

(C_{TOC}) isotope values range from –23.0‰ to –33.9‰, with the largest differences observed between the different drill-core locations. The Utkina Zavod samples are unusually enriched in ^{13}C compared to other Ediacaran samples. Pico-CSIA data revealed that this enrichment is also represented within the short-mid chain *n*-alkanes, hopanes, phytane, and C_{29} sterane. Lipid biomarker and iron redox proxies support a brackish, more oxic environment for Utkina Zavod. Utkina Zavod may have had higher pH and bicarbonate concentrations which could result in dissolved CO_2 limitation and may have promoted carbon-concentration mechanisms (CCM) or active bicarbonate uptake by the phototrophs. Bulk carbon isotopes are strongly controlled by local environmental and ecological conditions however, CSIA of our Ediacaran samples from Baltica present a picture of regional environmental heterogeneity during the Kotlin horizon on top of a shift in the microbial populations between the Redkino and Kotlin horizons.

In contrast to the ideally-preserved bitumen-phase lipid biomarkers presented in Chapters 2 and 3, Chapter 4 focused on the range of polycyclic aromatic hydrocarbons (PAH) assemblages bound within kerogen and which are preserved even in highly altered organic matter. A suite of PAH abundance ratios were identified which succeeded in separating biogenic kerogens (including highly overmature samples) versus abiogenic IOM formed from high temperature thermal cracking reactions. The absence of any traces of bound perylene further served as an indicator of organic matter sourced predominantly from hydrocarbon cracking, such as the pyrobitumen concentrates and the coke residue. Bound PAHs of high temperature thermal IOM residues were additionally

characterized by a preponderance of large (6-7 ring) PAHs, especially for the more highly condensed and thermally stable PAH compounds. While not a definitive biosignature, the ability to recognize aromatics formed from low-temperature processing of organic material will aid in the search for past and extant life on extraterrestrial bodies such as Mars, since aromatic-rich macromolecules may comprise the majority of organic matter.